On-line “Organ-in-a-Column” Liquid Chromatography Electrospray Ionization Mass Spectrometry for Drug Metabolism Studies

Stian Kogler

Thesis submitted for the degree of
Master of Science in Chemistry
60 credits

Department of Chemistry
Faculty of Mathematics and Natural Sciences

UNIVERSITY OF OSLO

October / 2019

Stian Kogler

On-line “organ-in-a-column” liquid chromatography electrospray ionization mass spectrometry for drug metabolism studies

2019

On-line “organ-in-a-column” liquid chromatography electrospray ionization mass spectrometry for drug metabolism studies

Stian Kogler

http://www.duo.uio.no/

Print: University of Oslo

Preface

This Master's thesis is as much teamwork as it is my work. A lot of collaborators and brilliant scientists have helped me achieve this work. Without them, none of this would have been possible.

I want to thank the Gadegaard group at the University of Glasgow, especially Neil Convery, for supplying chips and for acting as a sparring partner in all chip related stuff. I also wish to thank the Sullivan group at UiO for supplying the organoids and for all their patience and explanations regarding the biological work. Especially Sean Harrison has been instrumental.

I want to thank the Olav Thon foundation for providing the funding for this work and also for allowing me to present my work and meet great scientists at conferences in Boston, Rotterdam, Milan and Oslo. I sincerely hope you are happy with what I have been able to achieve with the funding.

I also wish to thank the Hybrid technology Hub for providing a great environment with lots of brilliant sparring partners in many fields of science. I am sure that great things will come from the center.

The BACH group has been my daily workplace for the last two years. I want to thank all the students and employees for creating such a great environment that lets people flourish and excel. I want to thank our engineers Inge Mikalsen and Marita Clausen. Without you, none of the technical stuff would work.

I also want to thank all my supervisors, Prof Stefan Krauss, Prof Elsa Lundanes, Prof Ola Nilsen, MSc Frøydis Sved Skottvoll, and Prof Steven Wilson for all their guidance, motivational pep-talks, and expertise. Together with the BACH group, they have guided and supported me during the last two years, and they made all of this possible.

Finally, I want to thank my personal main-sponsors Grete, Gerhard, Bernt and Sabine (parents and bonus parents), and last but not least, my girlfriend Tiril, for encouraging me and motivating me every single day to be the best I can be.

Abstract

Organoids and organ-on-a-chip (OoC) are human-induced pluripotent stem cell-derived miniaturized organs that recapitulate organ specific functions. They open up a plethora of opportunities to change the way we test drugs, research diseases, and treat patients. In this context, liquid chromatography (LC) and mass spectrometry (MS) will have to be used, e.g. for monitoring drug metabolism, toxicity screens and organ function. On-line coupling of these technologies would allow for automatized, high-throughput systems. By downsizing the LC-MS part, low abundant analytes can also be determined.

In this study, an on-line sampling and analysis system for OoC-technology has been developed. The system features hepatic organoids in a flow-through tube with continuous medium flow (organ-in-a-column, OiC), a two-loop valve system for sampling, reverse phase liquid chromatography (LC) analysis, and electrospray ionization mass spectrometry (ESI-MS). Phase 1 metabolism of heroin to its metabolite morphine was successfully measured on-line with the described system. Live/dead double staining revealed the potential of long-term cultivation of organoids in the system.

In parallel, tin oxide coated fused silica nanoelectrospray ionization (nanoESI) emitters suitable for the most narrow bore chromatographic columns have been developed with HF etching and an atomic layer deposition (ALD) approach. The emitters have been tested against commercially available stainless steel (SS) emitters by injections of heroin and showed similar signal-to-noise ratios. These emitters will find a use in a future miniaturized version of the system described herein.

In summary, a proof-of-concept system for on-line measurement of heroin metabolites has successfully been developed for a simple OoC-like device. NanoESI emitters for the most narrow columns have also been developed with a conductive ALD-coating of SnO_2.

Abbreviations

2D	Two dimensional
3D	Three dimensional
6-MAM	6-Monoacetyl morphine
7-HC	7-Hydroxy coumarin
ACN	Acetonitrile
AFFL	Automatic filtration/filter backflushing
ALD	Atomic layer deposition
Calcein-AM	Calcein acetoxymethyl
CVD	Chemical vapour deposition
ECM	Extracellular matrix
ESI	Electrospray ionization
FA	Formic acid
HiPSC	Human induced pluripotent stem cells
HPLC	High performance liquid chromatography
HSA	Human serum albumin
ID	Inner diameter
iPSC	Induced pluripotent stem cell
ITO	Indium tin oxide
LC	Liquid chromatography
LOD	Limit of detection

MeOH	Methanol
MP	Mobile phase
MRM	Multiple reaction monitoring
MS	Mass spectrometry
MS-MS	Tandem mass spectrometry
OD	Outer diameter
OiC	Organ-in-a-column
OoC	Organ-on-a-chip
OTLC	Open tubular liquid chromatography
PBS	Phosphate-buffered saline
PDMS	Polydimethylsiloxane
PEEK	Polyether ether ketone
PI	Propidium iodide
PTFE	Polytetrafluoroethylene, Teflon
Q1-3	Quadrupole 1-3
QCM	Quartz crystal microscale
RNA	Ribonucleic acid
RTP	Rapid thermal processing
RT-qPCR	Reverse transcription-quantitative polymerase chain reaction
SCCM	Standard cubic centimeter per minute
SPE	Solid-phase extraction

SS	Stainless steel
TIC	Total ion current
TMA	Trimethylaluminum

Table of Contents

1 Introduction

1.1 Drug development

Drug development follows a series of stringent steps for finding, optimizing, and assessing drugs. These steps are shown in **figure 1**. Pre-clinical studies are carried out, testing potential new drugs in animal models for efficacy and safety. These studies are required before drugs can be administered to humans in clinical trials. Clinical trials are used to test effectiveness, to find possible side effects and to compare the new drug to conventional treatments that already exist. Clinical trials are divided into three phases: Phase 1 assesses the dose-response in 20-80 healthy volunteers or patients. Most of the data concerning drug metabolism in the human body comes from phase 1 trials. Phase 2 tests the efficacy of drugs in 100-300 people, while phase 3 is carried out with 1000-3000 people [1].

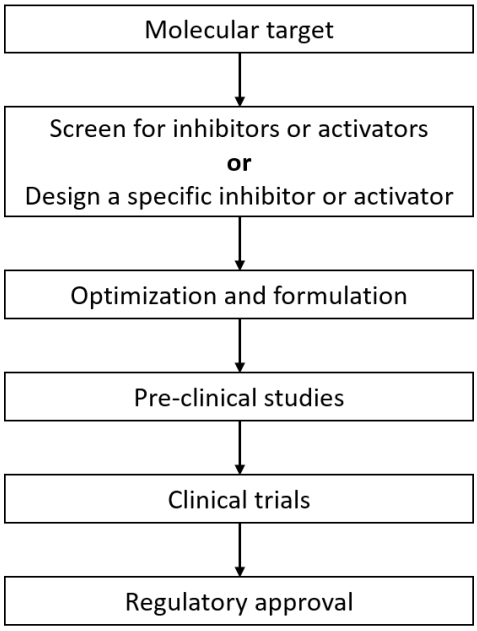

Figure 1 - Steps of the drug development process. First, a molecular target is acquired. Then an inhibitor or activator is found. The molecule is optimized before the drug is tested in pre-clinical and clinical trials prior to regulatory approval. Reproduced from [1].

In current drug development pipelines, significant discrepancies between *in vitro* outcomes of drug screening compared to the performance of a drug during clinical trials are commonly observed [2]. The lack of predictable data that pre-clinical studies provide causes many unsuccessful drugs to move forward in the development pipeline at substantial cost to pharmaceutical companies.

1.2 Liver physiology in light of drug metabolism

The liver is the organ that first meets the toxic effects of most drugs. This makes the liver essential for drug development, as it is the primary drug-metabolizing agent of the body. The liver consists of 1-1.5 million liver lobules and such a lobule is shown in **figure 2**. These lobules are the smallest functioning units of the liver [3]. They are approximately 1 mm in diameter and 1.7 mm long [4]. A lobule has a semi-hexagonal shape with peripheral portal venules and a central vein. Also, arterioles are located at the edges of the lobule. Fenestrated capillaries connect the blood vessels. The portal venules bring nutrient-rich blood from the digestive tract, while the arteries supply the lobules with oxygen-rich blood. Around the fenestrated capillaries, hepatocytes are densely packed and make up the bulk of the liver. A capillary with its surrounding hepatocytes form a cord-like structure called a hepatic sinusoid [5]. The blood from the portal veins and the arteries are mixed at a ratio of about 3+1 [6].

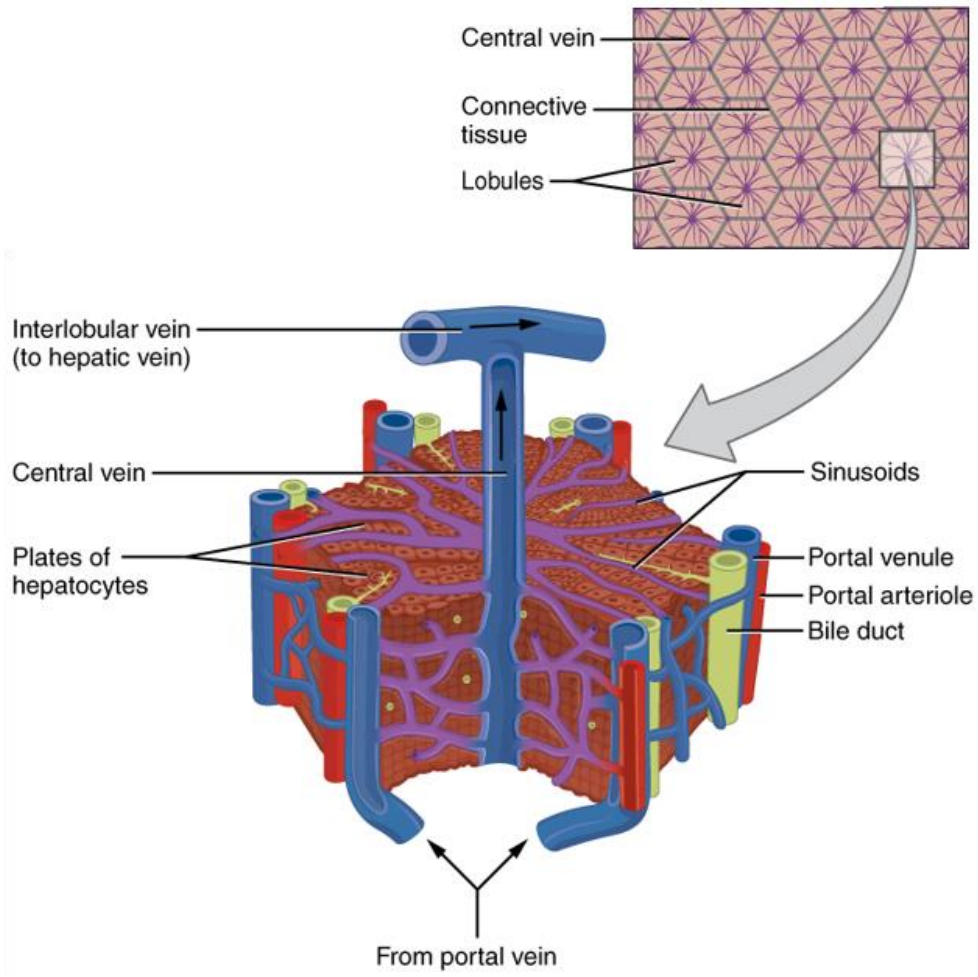

Figure 2 – Liver lobule shown with portal venules, portal arteriole, and central vein. The blood flows from the outer blood vessels through the capillaries into the central vein. Adapted from [5].

The oral route is the most popular way of drug administration because of its non-invasiveness. The mesenteric veins of the gastrointestinal tract collect drugs administered orally and transfer them through the portal vein directly into the liver [7].

Here, the blood flows through the capillaries and is exposed to the hepatocytes, which in turn metabolize the contents. For drugs taken orally, the liver is assumed to be the major site of first-pass metabolism [8].

1.3 From *in vivo* and *in vitro* to *qui vivo*

Conventional two dimensional (2D)-cell cultures have existed for a long time [9]. Despite their profound impact on biomedical research, they lack differentiation and spatial organization and, therefore, cannot support the many specialized functions of a three-dimensional (3D) *in vivo* organ, like the liver. Consequently, 2D-cultures cannot accurately predict tissue functions or drug interactions [10].

Over 50 years ago, 3D-cultures saw the light of day [11], relying on hydrogels of extracellular matrix (ECM) or polymers. These models have vastly increased in complexity, enabling intercellular signaling, cell-cell contact between different cell types, and – to a certain degree – given cells a spatially organized environment to grow in [12-14]. All these factors significantly increased the ability to study biological functions *in vitro*. However, 3D-cultures also have limitations. They usually do not offer tissue-tissue interfaces [15], mechanical stress through blood flow, compression and stretching [16]. It is also difficult to retrieve cells because they are dispersed in a matrix that needs to be removed in order to be studied.

On the other end of the scale for drug testing and biomedical research are animal models. Drug testing in animals is an important step, but can be seen as a legacy from the early days of pharmacological research. In many cases, animal models can show different and even outright wrong predictions of drug interactions and safety [17]. McGonigle *et al.* state, “Animal models are imprecise, empirical, ephemeral and prone to require considerable analysis and debate on their outcomes. Despite concerns regarding the predictive value for safety and efficacy in drug development, they remain a mainstay of preclinical research” [18].

In summary, neither simple *in vitro* models nor complex *in vivo* models satisfy the high standards researchers are looking for in model platforms for drug testing. There is a need for a

new, improved model that satisfies both the scientific and ethical standards of modern science. Such models can include organoids (i.e. lab grown miniature organs) and the Organ-on-a-Chip (OoC, i.e. miniature organs studied on a microfluidic device), as described in **figure 3**.

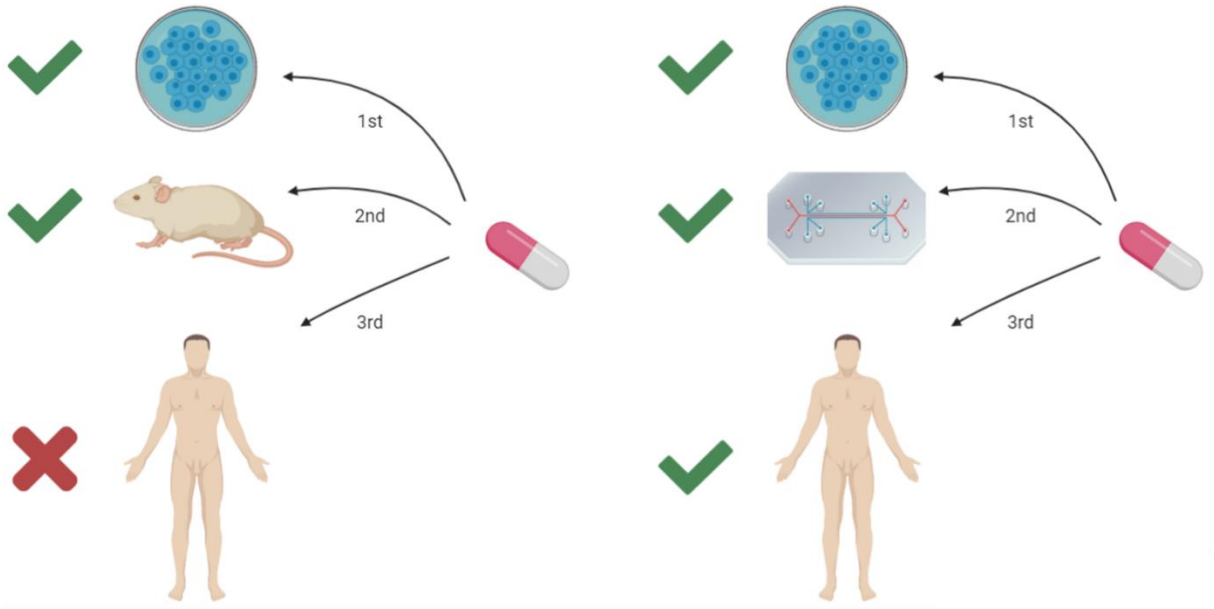

Figure 3 - Simplified overview of drug testing. A drug is tested first in 2D-cell culture and second in an animal model, does not necessarily work in a human (left). By using organ-on-a-chip models or organoids (second), a higher percentage of effective drugs will make it to clinical trials.

1.3.1 Organoids

Organoids are a collection of organ-specific cell types that are differentiated from stem cells or organ progenitors. They must self-organize by sorting out cells, and cells must have lineage commitment similar to *in vivo*. Organoids must be able to recapitulate some organ-specific functions [19]. In this study liver/hepatic organoids are used in a fluidic device.

Existing work on hepatic organoids ranges from early work on reaggregation of primary material [20] to hydrogel based hepatic organoids [21]. Lately, also human-induced pluripotent stem cell (HiPSC) derived organoids have been created [22].

The organoids used in this study differ from traditional 3D-cell cultures. While a traditional 3D-culture may be a mixture of ECM and mature cells, the organoids are self-organizing spheres with many cell types that all differentiated from HiPSCs.

Induced pluripotency

Cellular potency is defined as the potential of a cell to differentiate into a number of daughter cell fates. Cellular potency varies from pluri- to unipotency. Pluripotent stem cells have the highest potency and can differentiate into any of the three germ layers: endoderm, mesoderm, and ectoderm and can form almost any tissue [23].

The discovery that mature adult cells can be reprogrammed to pluripotent stem cells was made in 2006. Four defined factors were found to induce pluripotency in adult mouse fibroblasts, giving induced pluripotent stem cells (iPSC) [24]. The following year the first HiPSC was created [25]. This opened the way to create patient and disease-specific tissues for study and therapy. This work was awarded the Nobel Prize in medicine in 2012 [26].

The authors themselves pointed towards that iPSC derived hepatocytes could be used to predict drug toxicity of drug candidates [25].

1.3.2 Organ-on-a-chip

OoCs are microfluidic devices with micrometer-sized chambers and channels for growing cells in a three-dimensional space to model the functions of organs and tissues. Several of these organs may be connected to simulate interactions between different organs or tissues. One of the first functioning multi-organ-chips was the lung-on-a-chip, which simulated respiration by coupling lung alveolus and a capillary interface [27]. Organs can be connected with microfluidic channels between the chambers they inhabit or through a membrane lined with vascular endothelium to mimic *in vivo* conditions [28-31].

Reflecting the potential of OoCs, the world economic forum listed OoC as one of the top ten emerging technologies in 2016 [32]. As pharmaceutical companies aim to cut costs, there is a clear wish for a “fail early, fail cheaply” approach. This an OoC- or body-on-a-chip-platform could provide [33], as shown in **figure 4**.

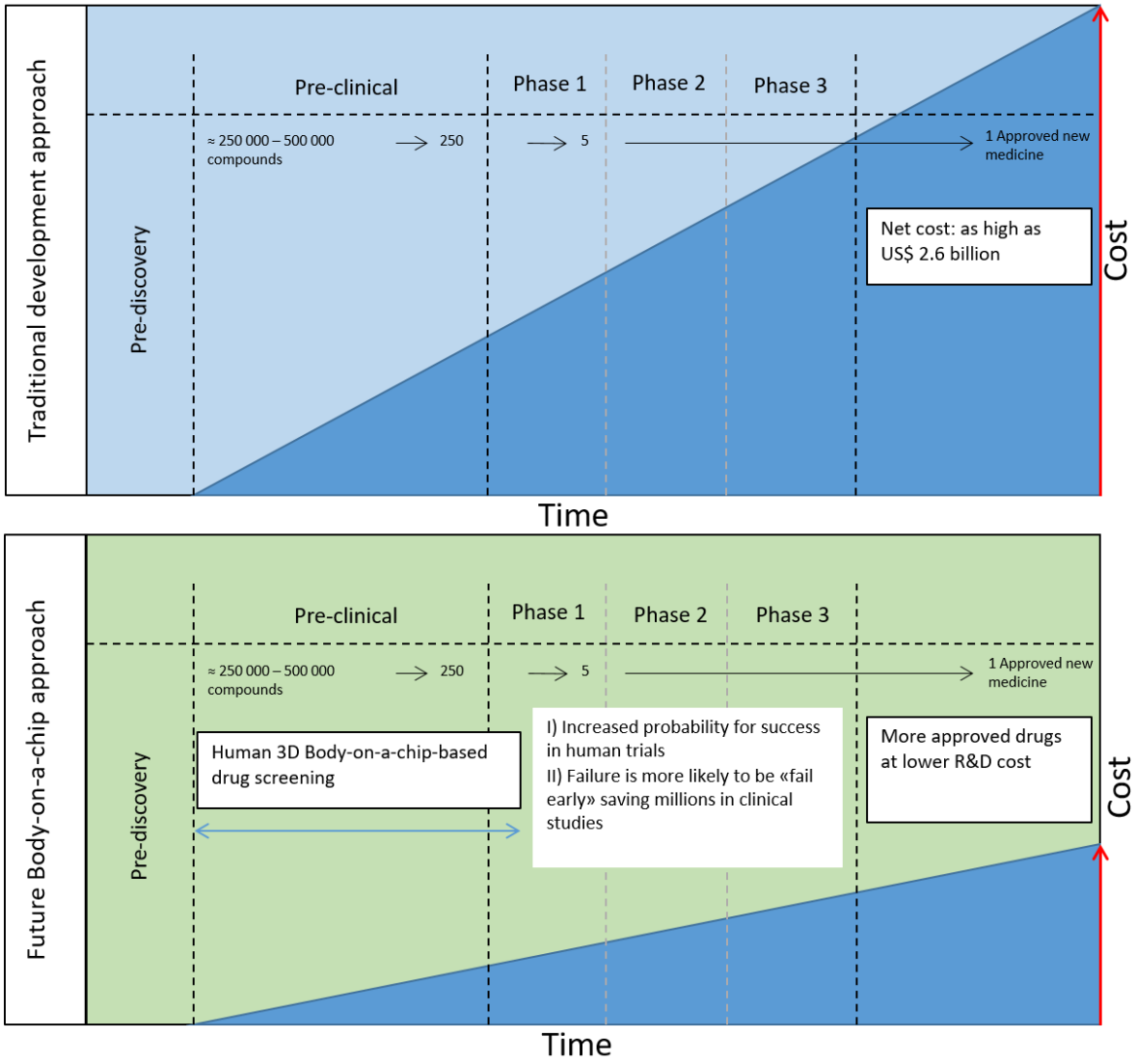

Figure 4 - Top: Traditional drug development pipeline using cell culture and animal models in pre-clinical trials. Unpredictiveness of these models causes large cost during development. Bottom: Using Body-on-a-chip-platform for pre-clinical phases increases the probability of success in later stages. The increased predictiveness of the pre-clinical phase reduces costs and increases the number of approved drugs. Figure adapted from [33].

1.4 On-line analysis of organ-on-a-chip

1.4.1 Analyses of organ-on-a-chip to date

To be able to study the characteristics of biological samples (e.g. organoids/organoid medium), features need to be observable, either through microscopy techniques or through visualization with instrumental analysis. Since the resolution of most methods has increased over time, more and more features have been observable [34].

Such a versatile device as OoC needs precise, accurate, and preferably fast, real-time molecular analysis to both monitor the system on a day-to-day basis and to receive accurate readouts from experiments [35].

A number of molecular and cellular analytical techniques are already applied for OoC platforms. These techniques include reverse transcription-quantitative polymerase chain reaction (RT-qPCR) [36], western blotting [37], different microscopy techniques including confocal [38], spinning disk [39] and light sheet [40], flow cytometry [41] and single-cell RNA sequencing [42].

These techniques are being used to validate the differentiation of cells and to validate the effects of treatments and assays. However, versatile and sensitive bioanalytical tools like liquid chromatography (LC) and mass spectrometry (MS, described in detail in **section 1.5**) are seldom used in the field of OoC. All LC-MS methods are, to the author's knowledge, off-line approaches [43-45] where samples are handled and transferred manually. There are, however, systems to learn from.

On-line analysis of liver slices

Van Midwoud *et al.* have created an on-line LC analysis system for precision-cut liver slices. The slices were placed in a chamber under continuous perfusion of medium. An intricate valve system with five 6-port valves was used for sampling onto loops and in-line addition of substrate or inhibitor. While one loop was being filled, another was sent to analysis, resembling a traditional 2DLC system. An overview of the system is presented in **figure 5**. The liver slices used, were created from rat liver. While Van Midwoud *et al.* used UV as the detection method, a switch to MS could easily be made.

In their study, the metabolism of 7-hydroxycoumarin (7-HC) and diclofenac were examined. By adding an inhibitor, the formation of 7-HC-glucuronide was decreased [46].

This system could serve as a template for an OoC system with MS-detection.

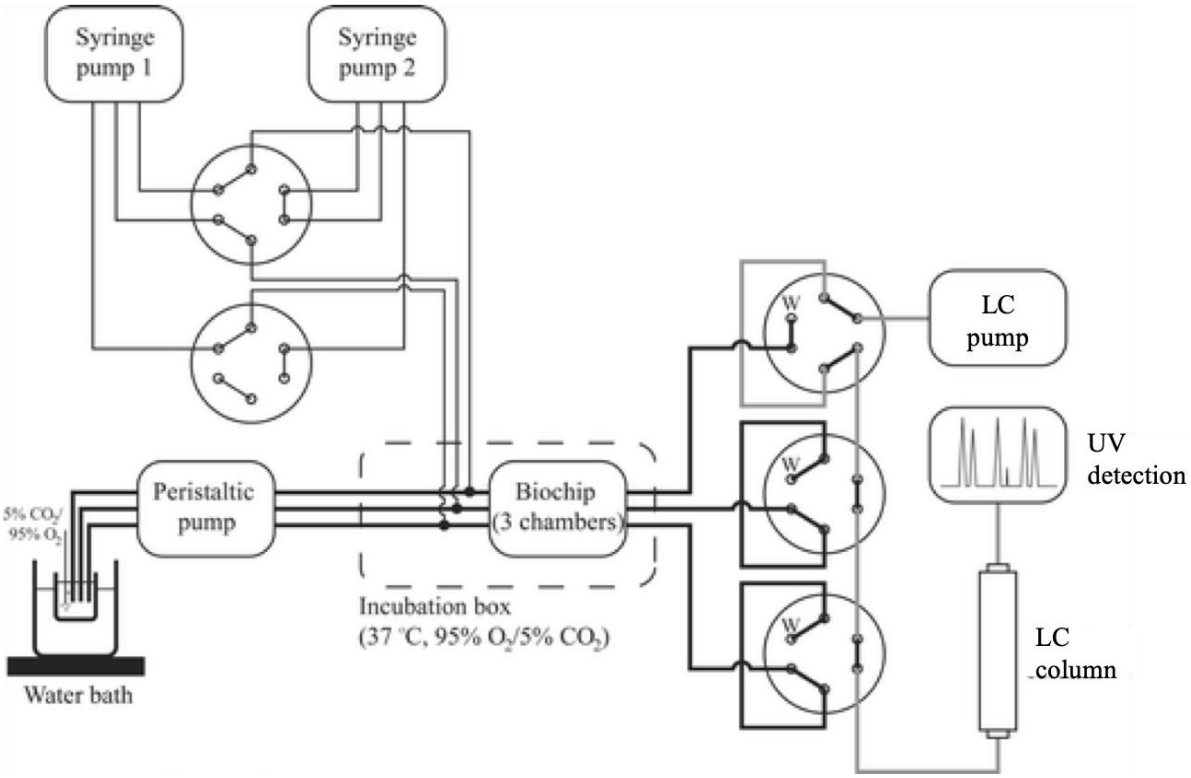

Figure 5 – On-line HPLC-UV system for precision-cut liver slices. Adapted from [46].

1.4.2 The benefits and challenges of on-line systems

On-line systems have advantages like increased precision, reduced time consumption, less chance of outside interference, and are simple to automate. They do, however, suffer from drawbacks like low flexibility, poor robustness due to clogging and incompatibility of different solvents when two or more fluidic systems are connected, e.g. organ-on-a-chip and analytical system [47].

These problems can be addressed, but this often leads to complicated systems. Van Midwoud *et al.* solved this by sampling into loops that can be connected either to the biological side or the analytical side depending on loading or injecting [46].

Solid-phase extraction (SPE) is a method that often is used for on-line sample preparation. Like chromatographic columns, SPE columns also clog with time when crude samples are injected. To prevent this, systems like automatic filtration/filter flush (AFFL)-SPE-LC have been developed. Here, the sample is first filtered to remove particles before it reaches the SPE. During column switching, the filter is back-flushed and particulates flushed away. This allows for thousands of injections without clogging [48].

1.5 Mass spectrometry as a detector

An MS is an instrument used for the detection of compounds. It can be used alone or hyphenated with chromatography techniques, like LC. An MS consists of three parts: An ion source, ionizing compounds before they enter the subsequent parts, a mass analyzer, sorting the ions according to their mass to charge ratio (*m/z*), and finally, an ion detector. Together, these parts form a powerful instrument capable of detecting most ionizable compounds that can be brought into the gas phase [49]. Many different mass spectrometers exist [50-52], and in this thesis, a triple quadrupole mass spectrometer has been used.

1.5.1 Triple quadrupole mass spectrometer

The mass analyzer of the triple quadrupole MS consists of three quadrupoles (denoted as Q1-Q3) in series. A quadrupole is made out of four rod-electrodes, as shown in **figure 6**. They are mounted in a square configuration (XY-direction). The pairs of opposite rods are held at the same potential that consists of a direct current (DC) component and a radio frequency (RF) component. The polarity of the pairs (A and B) is opposite relative to each other. This creates an oscillating electrical field. Mathematically, the potential of the in **Eq. 1 and 2** [49].

$$A = -(U + Vcos(\omega t)) \qquad \textbf{Eq. 1}$$

$$B = +(U + Vcos(\omega t)) \qquad \textbf{Eq. 2}$$

where U is the DC component, and V cos(ωt) is the RF component.

At different values for U and V, ions with different *m/z* have a stable path through the quadrupole and can pass, while instable ions are knocked out. By ramping the U and V, but keeping the ratio at a set level, a scan is performed where ions with one *m/z* can pass at a time [49].

By having three quadrupoles in series that can be operated individually, the MS can be operated in different modes.

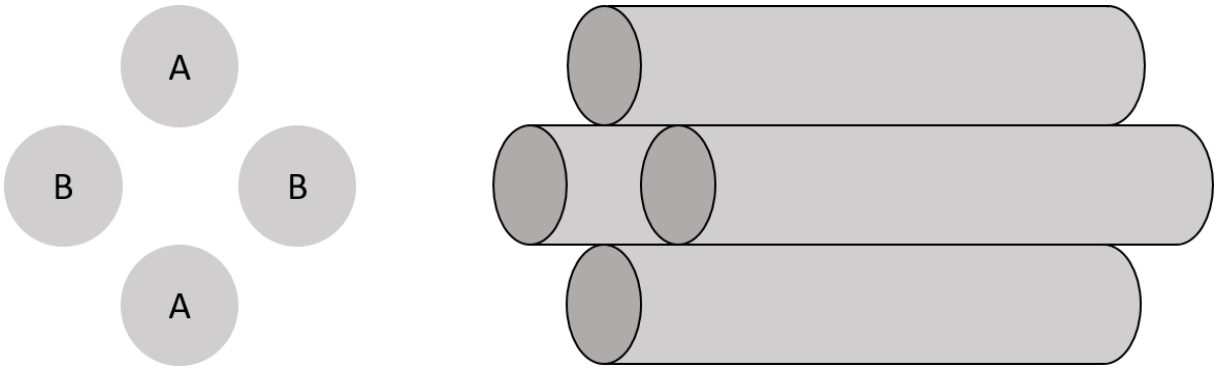

Figure 6 – Illustration of the opposing rod electrodes of a quadrupole mass analyzer which are paired and are held at the same potential. The different rod pairs have opposite polarity. The rods are mounted in the XY-direction and extend into the Z direction. By changing the potential of the rods, specific ions are allowed to pass through. Adapted from [49].

Multiple reaction monitoring

In multiple reaction monitoring (MRM) mode, Q1 is operated by selecting precursor ions with a given/several given *m/z*-values. Q2 is used as a collision-induced dissociation cell (CID-cell) where the selected ions that could pass Q1 collide with an inert gas (usually N_2 or Ar). The collision fragments the ions [53], and Q3 is then used to select specific fragments that then reach the detector. The whole process is shown in **figure 7**. An approach where ions are selected, fragmented and fragments are selected, is often referred to as MRM [54].

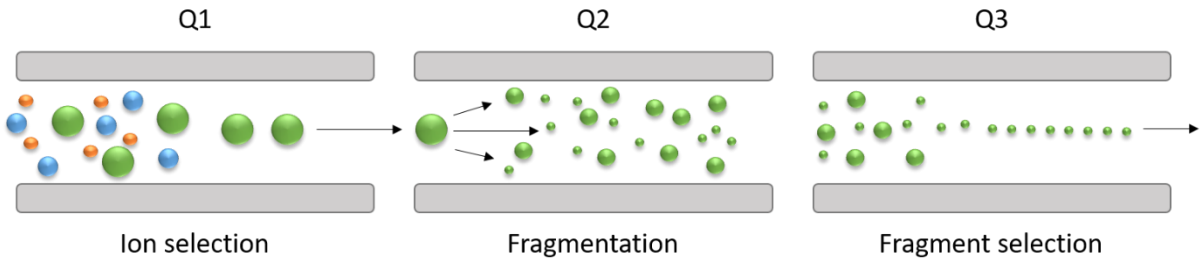

Figure 7 – In multiple reaction monitoring mode, the quadrupoles are operated individually in series. Q1 selects one or more precursor ions that are allowed to pass to Q2, which acts as a collision cell where ions are fragmented. In Q3, one or more fragments are allowed to pass to reach the detector.

To increase the sensitivity and selectivity of an analysis method, a separation step is usually added prior to MS-detection. This reduces matrix effects and the chance of various types of interferences [55].

1.6 Nano liquid chromatography and open tubular liquid chromatography

Conventional packed liquid chromatography columns have an inner diameter (ID) of 3-5 mm (**Table 1**). When compounds of low abundance in limited samples are to be determined, nanoLC with column IDs from 0.01-0.1 mm is the preferred choice [56]. A reduction in ID gives less radial dilution, ensuring that a more concentrated band exits the column, compared to larger ID columns, as shown in **figure 8**. When coupled to a concentration sensitive detector (e.g. electrospray ionization MS (ESI-MS)), these narrow bore columns give higher signal intensity [57].

Table 1 - Classification of LC according to internal diameter (ID) of columns. Adapted from [56].

Column designation	**Typical ID, mm**
Conventional LC	3 – 5
Narrow-bore LC	2
Micro LC	0.5 – 1
Capillary LC	0.1 – 0.5
NanoLC	0.01 – 0.1
Open tubular LC	0.005 – 0.05

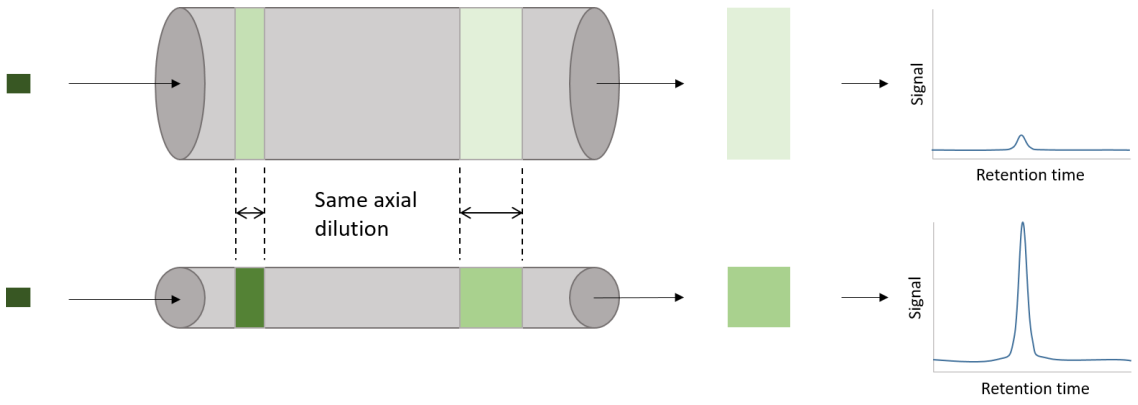

Figure 8 – Illustration of downscaling ID in a tube gives rise to more concentrated bands due to lower radial dilution. Bands that are more concentrated give rise to higher signal intensities when detected by a concentration sensitive detector.

Limit of detection (LOD) is defined as the lowest concentration of an analyte that gives a signal which is significantly different from a blank [58]. Mathematically, the LOD is defined with **Eq. 3** [59].

$$LOD = \frac{3s}{m}$$ **Eq. 3**

where s is the standard deviation of a low concentration of the analyte, and m is the slope of the calibration curve.

Since the intensity of the signal is inversely proportional to the ID of the column, narrow bore columns give lower LOD. This is important, especially in bioanalytics where analytes often are low abundant proteins, hormones, metabolites, etc. [49]. There is an everlasting quest for lower LOD [34], therefor many researchers look towards open tubular LC (OTLC) [60-62]. A scanning electron microscope image of a 10 µm ID column with a porous layer coating the inside of the column wall is shown in **figure 9**.

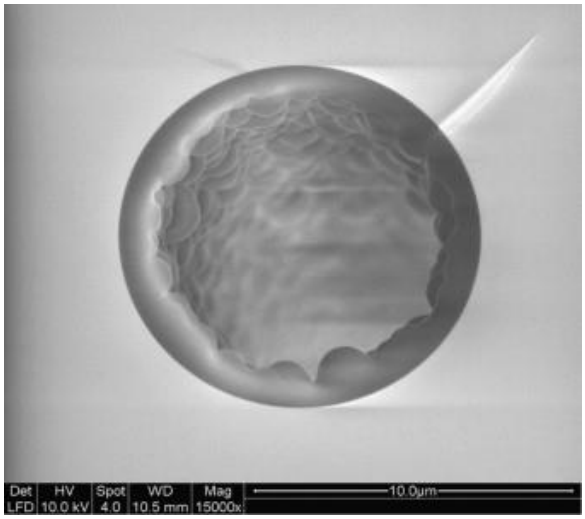

Figure 9 – Scanning electron microscope image of a 10 µm ID OTLC column with a porous layer coating the inside of the column wall. Image reproduced from [63].

The effect of downscaling can be calculated using the theoretical downscale factor given in **Eq. 4** [64].

$$downscale\ factor = \frac{d_{c1}^2}{d_{c2}^2}$$ **Eq. 4**

where d_{c1} and d_{c2} are the diameters of the two columns.

1.6.1 Band broadening

Band broadening occurs both inside and outside the chromatographic column, but pre-column band broadening is easily corrected by refocusing on the chromatographic column. By injecting

the sample in a solvent that has a lower elution strength than the mobile phase (MP), the analytes can be focused as a very narrow band at the column entrance [49].

Post-column band broadening, on the other hand, is a problem due to the lack of possibility for refocusing without interfering with the separation. Therefore, several measures can be made to ensure that post-column band broadening remains at an absolute minimum. One of these measures is ensuring that the ID of components and tubing after the column is equal to or smaller than that of the column. If components of various IDs are used, they should be smaller towards the end of the system, and none should be larger than the ID of the column [65, 66].

1.7 Electrospray ionization and nanoelectrospray ionization emitters

ESI is widely used because it is a versatile, soft ionization method that also allows large ions (e.g., proteins) to enter the gas phase before MS-detection [67]. Also, ESI-MS is a concentration sensitive detector, where the analyte response is directly proportional to the analyte concentration [64].

The sample is introduced to the MS in a solvent through typically a stainless steel (SS) needle. In nanoESI, the emitter is a more narrow hollow needle, made either from a conductive material or from an insulating material with a conductive coating. When potential is applied in positive mode, the emitter becomes the positive electrode, while the MS inlet becomes the negative electrode. Positive ions are drawn towards the surface of the liquid and towards the MS inlet, while negative ions are drawn towards the emitter tip. Once enough positive ions have conjugated on the surface that the repulsion between the ions becomes larger than the surface tension, a Taylor cone is formed. This allows the solvent (containing the ions) to move downfield. If the applied field is large enough, a jet is formed that culminates in the ejection of tiny droplets, packed with ions. The positive ions in the droplets again conjugate on the surface [68]. The whole process is shown in **figure 10**.

As the solvent evaporates from the bubbles, the repulsion between the ions increases. Once the repulsion becomes larger than the surface tension, bubbles explode into smaller bubbles. This is called a Coulomb fission. The newly formed droplets undergo more evaporation of solvent and several fissions until there are only free ions left in the gas phase [69].

Since the surface at the emitter tip becomes smaller with decreasing emitter size, also the Taylor cone becomes narrower, resulting in smaller droplets and more efficient ionization. This can increase the sensitivity as more ions are able to enter the gas phase before reaching the MS inlet [70].

Conventional ESI is used for larger ID columns with a flow rate in the µL/min range and follows the same principle, but a nebulizing gas (usually N_2) is added coaxially at the emitter tip to help with droplet formation. In addition, a drying gas may be added in the opposite direction of the flow, flowing from the MS-inlet towards the emitter. The source can also be heated to help with evaporation of solvents [49]. ESI-MS is a concentration sensitive detector, where the analyte response is directly proportional to the analyte concentration [64].

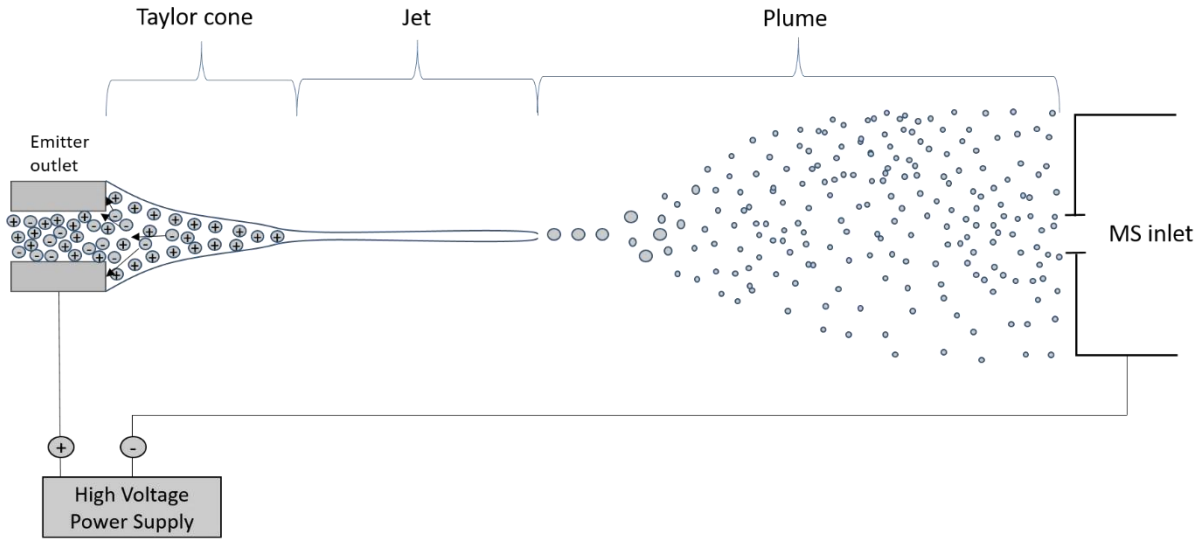

Figure 10 – ESI process in positive mode showing the formation of Taylor cone, the jet, and the charged droplets in the plume. Negatively charged ions in the solvent move towards the emitter tip, while positive ions are drawn towards the MS inlet (arrows in Taylor cone). Adapted from [68].

1.7.1 Challenges associated with commercial emitters

Commercially available emitters come, to the author's knowledge, mainly in two forms: SS emitters and fused silica emitters. Thermo Fisher Scientific produces SS emitters with ID of 30 µm [71]. New Objective produce emitters with a tip ID down to 5 µm, but since these emitters are pulled, both the OD and ID decrease towards the tip, and the back end of the smallest pulled emitters is as large as 50 µm [72]. New Objective also produce emitters with a constant ID, but only down to 20 µm [73].

As described in section 1.3, nanoLC columns and OTLC columns have an ID of 10-100 µm and 5 – 50 µm, respectively. The smallest IDs of these two column formats are considerably smaller than the smallest commercially available emitters. The use of these emitters in combination with narrow columns, would result in radial dilution and thus decreased sensitivity. Also, such coupling would lead to post-column band broadening.

Because of the lack of commercial alternatives, researchers are looking for approaches to fabricate nanoESI emitters in-house.

1.7.2 Existing work on fabrication of emitters

The general trend for nanoESI emitters is to use a single emitter, either in fused silica or SS. Many different coating and tapering approaches have been tried. An alternative to coating, is having a liquid junction where the potential can be applied directly to the solvent, but researchers seem inclined to use emitters with coaxial coating. Multi-emitter arrays also exist, but are used less because of tedious production and no commercial availability. They are also costly and require modification of the MS-inlet [74].

Since commercial emitters do not exist for the most narrow columns, some researches have created approaches to make narrow ID emitters in-house [75-77]. To the author's knowledge, all these emitters are fabricated from fused silica capillaries, which are available in many IDs. A taper is made on one end of a fused silica capillary to reduce the surface area of the tip.

In all subsequent examples, the taper of the fused silica emitter is achieved through etching with HF. HF reacts with SiO_2. The reactions involve several steps, but the net reactions can be written, as shown in **Eq. 5** [78-80].

$$4H^+(aq) + 6F^-(aq) + SiO_2(\mathrm{s}) \rightarrow SiF_6^{2-}(\mathrm{aq}) + 2H_2O(l) \qquad \textbf{Eq. 5}$$

Since fused silica is an insulating material, the resulting fused capillary needs to be coated with an electronic conducting material to function as an emitter.

No significant breakthroughs or changes in the technology exist to the author's knowledge in recent years. However, novel methods for fabrication of emitters have been examined that possibly make fabrication simpler.

Arnesen developed an approach based on Kelly *et al.* [81] where fused silica capillaries were immersed in HF. The immersed part was etched away, but because of the surface tension, some HF also climbed up the walls of the capillary, resulting in a tapered tip. The main problem with this approach was that HF also would enter the capillary from the bottom, widening the ID. To prevent this, flow was put on through the capillary. This diluted the HF and made the process slower. In addition, to immerse the capillaries, larger amounts of HF were needed. The etched emitters were then coated with TiC with atomic layer deposition (ALD, see **section 1.8**) [77].

Zhu *et al.* developed an etching method where only a few µL of HF were needed. The approach was titled "Gravity assisted etching self-termination". The capillary would be passed through a small cup with an orifice at the bottom. With the cup in place, the capillary was hung vertically. The cup was then filled with HF. With this approach, very little HF was used, and the etching would end as soon as the walls of the capillary became so thin that they broke, resulting in a falling HF-reservoir. After etching, the emitters were gold-coated by an electroless deposition approach [76].

Kogler further developed the approach of Zhu *et al.* by using cups with a rounded bottom to ensure contact between the capillary and the HF after some of the acid had evaporated. The cups were fabricated by cutting the bottom off Eppendorf tubes and drilling a hole in the center. Further, many different coatings were examined, both ALD and dipping methods, but Zhu *et al*'s gold coating yielded the best results in terms of longevity and stability of spray [75].

1.8 Atomic layer deposition

ALD is a method for controlled deposition of monolayers. The deposited film is grown one atomic layer at a time as shown in **figure 11**. This is achieved by pulsing one precursor at a time into a vacuum chamber where the substrate is kept. Each pulse is separated by a purging step to remove excess reactants and by-products from the previous pulse. The growth of the film is based on the alternating chemisorption of the different precursors. Repetition of the cycle produces film growth, layer by layer, in a very controlled manner.

When carried out within certain temperature limits, ALD is a self-limiting process where only available chemisorption sites react. ALD has the potential to grow homogenous crystalline films with control of the atomic layer. The main drawback, compared to other methods like

chemical vapor deposition (CVD), is the time consumption. Sequential pulsing and purging takes a few seconds and limits the growth rate [82].

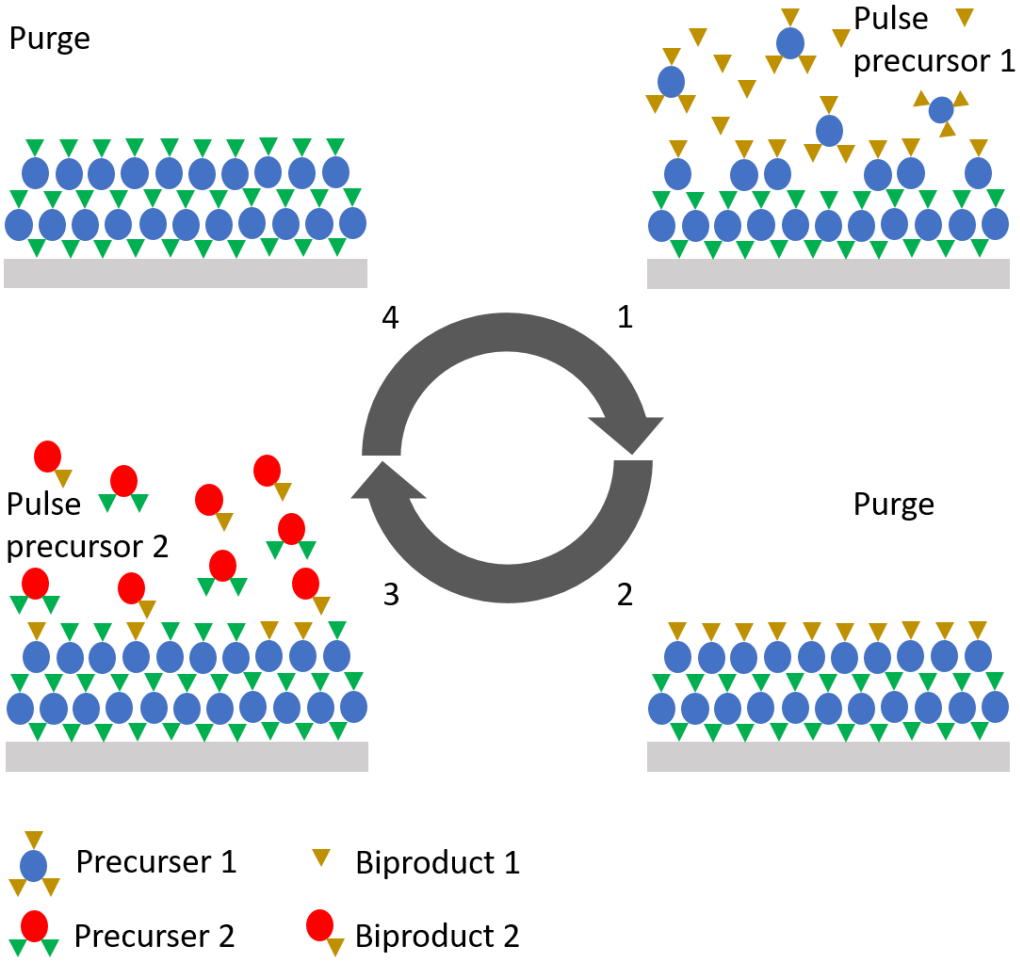

Figure 11 – Illustration of one ALD cycle. The process can be broken down into four steps: The first pulse (1) introduces one precursor to the vacuum chamber. Some of the precursor reacts with the surface. The remains and byproducts are purged out of the chamber (2). In the second pulse, a different precursor is introduced into the reaction chamber (3). This precursor reacts with the previous layer. Byproducts are removed again, and what is left is a uniform atomic layer of the end product (4).

1.8.1 Atomic layer deposition coated electrospray emitters

To the author's knowledge, no scientific articles on ESI-emitters coated by ALD exist. Nevertheless, both Arnesen [77] and Kogler [75] have used ALD to coat etched emitters with different coatings. Arnesen coated emitters with TiC. This coating was by Kogler found to work, but only for a limited time (≤ 200 min). Kogler also attempted TiN deposited by ALD as a coating, but the film was thicker than expected and was cracking and flaking off. The longevity of the emitters also was only ≤ 120 min. Although both TiC and TiN coated emitters

stopped working after a relatively short time, they could be reconditioned by moving them slightly on the electrode. Likely, emitters ceased to function due to degradation around the contact point to the electrode.

Ti-Nb-O thin film

In the last decade, transparent conductive films have seen a large increase in industrial use. In 2005, Furubayashi *et al.* reported the discovery of a conductive form of TiO_2, Nb-doped anatase, with excellent transparency and high conductivity [83].

Niemelä *et al.* [84] and Pore *et al*. [85] both reported approaches for ALD of amorphous Ti-Nb-O thin film, which post-deposition is annealed/crystallized in reductive atmosphere (5% H_2 in inert gas). The annealing step created cross-like patterns after explosive crystallization [85]. The resulting material was reported to have excellent conductivity by both groups when using $TiCl_4$ and $Nb_2(OEt)_5$ and H_2O as precursors.

SnO_2

Tin dioxide is reported to have high conductivity and excellent stability and durability [86, 87]. Tin dioxide can be deposited in several ways, but ALD can give a dense film with a low density of defects.

A review from 2014 thoroughly describes ALD of tin dioxide [88] and concludes that the choice of precursors is crucial for achieving various film properties. While metal-organic precursors significantly reduce the synthesis temperature, the use of inorganic precursors is far more common.

Cheng *et al.* have examined SnO_2 films grown at temperature ranging from 300-450 °C with $SnCl_4$ and H_2O as precursors. They found that the growth rate per cycle increased with increasing temperature up to 400 °C and decreased after that. The same pattern was shown for film resistivity. The deposited film was polycrystalline [89].

1.8.2 Quartz crystal microscale for *in situ* measurement of growth rate

A QCM sensor is a highly sensitive device capable of detecting mass changes down to the sub-picogram level. It functions by applying an AC current to a quartz crystal that is sandwiched between two electrodes. The applied current causes the crystal to oscillate at a characteristic frequency. The deposition of mass to the crystal changes its frequency [90]. The change in frequency is proportional to the change in mass, as described in the Sauerbrey equation [91].

1.9 Summary of knowledge of methods available

On-line systems that include LC and ESI-MS detection are suitable systems for the detection and measurement of many biological compounds. Downscaling these systems with narrow columns, tubing and emitters, improves LOD and makes the analysis of small samples with low abundant analytes possible. In other words, such systems are beneficial for work with organoids, where little metabolic tissue is responsible for the production of low abundant analytes.

1.10 Heroin: a model compound for hepatic organoid systems

Heroin is a semi-synthetic, highly addictive morphine derivative. The pathway for metabolism is well established, and extensive research on the metabolism of heroin has been conducted since the 1930s [92]. Since heroin has a high first-pass effect (rapid metabolism) in the liver, heroin is either smoked or injected intravenously to circumvent metabolism before reaching systemic circulation [93].

Heroin is metabolized mainly by carboxylesterases in the blood and the liver. Heroin is quickly converted to 6-monoacetyl morphine (6-MAM). This process can happen spontaneously or be facilitated enzymatically [94]. 6-MAM is further metabolized to morphine. This step happens only through enzymatic activity [95]. These steps of metabolism are called phase 1 metabolism. Phase 2 metabolism consists of glucuronidation of morphine to morphine-3- or morphine-6-glucuronide [96]. The metabolism is shown in **figure 12**.

The high first-pass effect of heroin, combined with a step in its metabolism that only happens through enzymatic activity, makes heroin a well-suited model compound for experiments with hepatic organoids. If morphine is detected, functioning metabolism is confirmed.

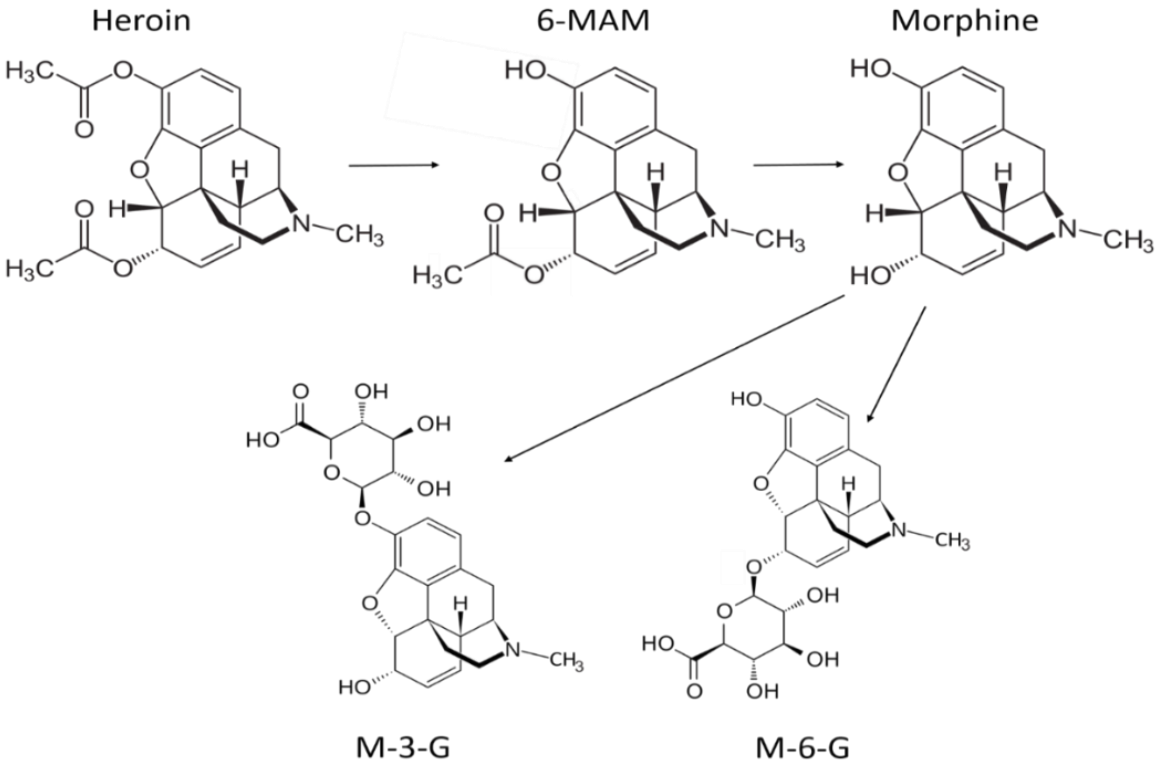

Figure 12 – Pathway for metabolism of heroin. Heroin to 6-MAM happens both enzymatically and spontaneously. 6-MAM to morphine happens only through enzymatic activity. These two steps are phase 1 metabolism of heroin. Phase 2 metabolism consists of glucuronidation of morphine to M-3-G and M-6-G.

2 Aim of study

As previously described, neither simple cell cultures, nor complex animal models satisfy the high standards scientists are looking for in modern drug development. A new advanced 3D culture called organoids, that mimics organs, has been developed together with advanced fluidic chip designs to recapitulate organ functions for biomedical research and drug development.

Although these emerging technologies seem promising, the use of bioanalytical tools like LC and MS seem completely absent. To give scientists an analytical platform to work on, this study aims to hyphenate organ-on-a-chip technology with LC-MS. The idea was to demonstrate metabolism of heroin in organoids by the detection of morphine as proof-of-concept. To do this, an on-line system was to be developed.

It was believed that nanoLC columns were necessary to provide detection of low abundant analytes. Since commercial tapered ID nanoESI emitters perform suboptimal, etched, ALD coated emitters were to be developed for use in the OoC-LC-ESI-MS-system.

Based on that, the aim of this study was divided into two parts:

1) To develop ALD-coated fused silica emitters for ESI-MS hyphenated with nanoLC columns intended for OoC systems.
2) To develop an on-line OoC-LC-ESI-MS-system for proof-of-concept testing with heroin.

A graphical overview of the workflow in this study is given in **figure 13**.

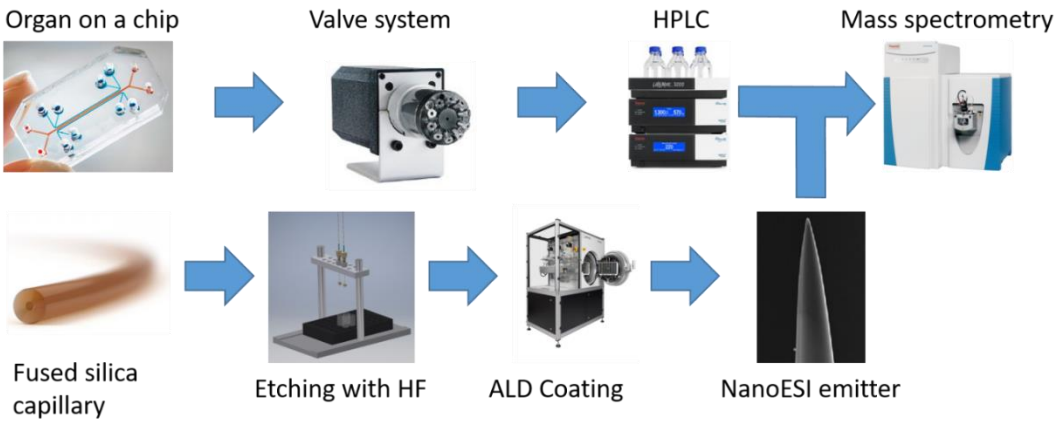

Figure 13 – Graphical overview of the workflow in this study. An on-line OoC-LC-ESI-MS system with in-house made nanoESI emitters was to be developed for proof of concept testing.

3 Experimental

3.1 Reagents and solutions

Sodium hydroxide (pure pellets), hydrofluoric acid (HF/H_2O, 49/51%, w/w), calcium carbonate (≥ 99.9%) formic acid (FA, ≥ 98%), caffeine (analytical grade) and titanium(IV) chloride (≥ 99.9%) were purchased from Merck (Darmstadt, Germany). Niobium(V) ethoxide (≥ 99.95%), tin(IV) chloride (≥ 99.995%), uracil (≥ 99.0%), human serum albumin (≥ 99%), fluorescein (free acid), live/dead cell double staining kit and trimethylaluminum (TMA) (97%) were purchased from Sigma-Aldrich (St. Louis, MO, USA).

A gas mixture of 10% hydrogen in nitrogen gas (Formier 10) and nitrogen (≥ 99.999%) were purchased from Praxair Norge AS (Oslo, Norway). Type 1 water was produced with a Milli-Q ultrapure water purification system from Millipore (Bedford, MA, USA). Water (LC-MS grade) and acetonitrile (ACN, LC-MS grade) and methanol (MeOH, LC-MS grade) were purchased from VWR International (Oslo, Norway).

PhD Inger Lise Bogen at the research group on drugs of abuse at the Oslo University Hospital supplied solutions of heroin, 6-MAM, morphine, morphine-3-glucuronate, and morphine-6-glucuronate. Fetal bovine serum-free medium, L15 base medium (prepared according to [97], hereafter referred to as organoid medium), and phosphate-buffered saline (PBS, pH 7.4) were supplied by the Sullivan group (Faculty of Medicine, University of Oslo).

3.2 Consumables and hardware

Polyimide coated fused silica capillaries (360 µm OD, 10 µm and 150 µm ID) were purchased from Polymicro Technologies (Phoenix, AZ, USA). Polyether ether ketone (PEEK) unions, PEEK nuts (for 1/16” tubing), SS unions, reducing unions (1/16” to 1/32”), ferrules and screws/nuts (all for 1/16” tubing and for 1/32” tubing), an easy-flange flanging tool kit, graphite/vespel ferrules (ID 300 µm), SS tubing (1/32” OD, 0.020” ID and 0.005” ID), 1/16” SS screens (1 µm pores), 2-position 10-port valves (for 1/32”, C82X-6670ED) tubing and 2-position 6-port injection valves (for 1/16” tubing) were purchased from VICI Valco (Schenkon, Switzerland).

PEEK sleeves (ID 360 µm) and PEEK tubings (1/32" OD and 1/16" OD, both with ID 0.015" and 0.005") were purchased from IDEX (Erlangen, Germany). Eppendorf Safe-Lock Tubes (1.5 mL) were purchased from Eppendorf AG (Hamburg, Germany). SS emitters (OD 150 µm, ID 30 µm), SST Vipers (130 µm x 650 mm), and polystyrene beads (150 µm) were purchased from Thermo Fisher Scientific (Waltham, MA, USA). Polytetrafluoroethylene (PTFE, Teflon) tubing (1/16" OD, 1/32" ID) and 1/4"-28 microfluidic fittings kit were purchased from Darwin microfluidics (Paris, France). Quartz crystal microscale sensors (QCM-sensors) were purchased from Inficon (Bad Ragaz, Switzerland). Silicon wafers were purchased from UniversityWafer, Inc. (Boston, MA, USA). A microfluidic organ-on-a-chip platform was purchased from BIOND Solutions B.V. (Delft, the Netherlands). A chromatographic column (1 mm x 5 cm) packed with Kromasil C4 (3.5 µm, 100 Å) was purchased from Teknolab (Ski, Norway).

A chromatographic silica monolith column (75 µm x 12 cm) and a silica monolith pre-column (75 µm x 4 cm), both functionalized with C18, were fabricated in-house by BSc Tao McQuade. MSc Neil Convery, at the Gadegaard group (Biomedical Engineering laboratory, School of Engineering, University of Glasgow), produced injection-molded polystyrene fluidic chips. Hepatic organoids were supplied by PhD Sean Harrison (Sullivan group, University of Oslo).

3.3 Instruments

The TSQ Quantiva triple quadrupole MS with the Nanoflex II ion source, The Easy-nLC 1200 pump, the Dionex Ultimate 3000 RS UV-detector (7 mm flow cell, 2.5 µL volume), the Dionex UltiMate 3000 UHPLC system and the TSQ Vantage MS with the HESI-II ion source were all purchased from Thermo Fisher Scientific.

A MP-degasser (G1379A), an LC-pump (G1376A), and a multiple wavelength detector (G1365D) with a 2 µL, 3 mm path flow cell were purchased from Waters (Milford, MA, USA). The light microscope (W10x/20) was purchased from Motic (Hong Kong, China) while the syringe pump (AL-1000) was bought from World Precision Instruments (Sarasota, FL, USA).

The Beneq TFS 500 reactor was purchased from Beneq (Espoo, Finland) and the Rapid Thermal Processing oven (RTP-oven, OTF-1200X) was purchased from MTI Corporation (Richmond, CA, USA). The α-SE ellipsometer was purchased from J.A. Woollam Co., Inc. (Lincoln, NE, USA). Two multimeters were used: A digital multimeter from Keithly, Tektronix (Bracknell,

UK), and a Fluke 8846A precision multimeter (Everett, WA, USA). A SUB Aqua 5 Plus water bath was purchased from Grant Instruments (Cambridge, UK).

3.4 Preparation of etched open emitters

The procedure for etching used in this thesis is an improved version of the etching procedure from Zhu *et al*. [76]. This approach was improved in earlier work with a round bottom etching cup [75], and the improved version has been used in this study.

3.4.1 Etching apparatus and cups

An apparatus for etching, depicted in **figure 14A**, was designed and produced in-house by Principal Engineer Inge Mikalsen after a figure from Zhu *et al*. [76]. The base of the etching apparatus consisted of a steel plate with tracks for a stand for various plastic ware for collection of debris. On the base, two steel poles were mounted that held a movable plate. To this plate, SS unions holding capillaries could be fixed.

The etching cups were prepared from standard Eppendorf tubes. The lids of the tubes were cut off with a knife, and the etching cup itself was prepared in the following way: The tube was mounted to a drill so that the bottom 0.5 cm stuck out of the chuck of the drill [98]. The drill was used to spin the tube, removing the bottom 0.5 cm creating the cup. Next, a hole was drilled in the center of the cup with a 0.380 mm drill. An etching cup created in this way is shown in **figure 14B** with an Eppendorf tube for reference.

3.4.2 Gravity assisted etching self-termination

For the etching itself, 1-2 cm of the polyimide layer of an approximately 10 cm long fused silica capillary (10 µm ID) was burned off, 1 cm above the capillary end, with a lighter to create a window for etching. This window was cleaned with a tissue paper soaked in methanol to remove the remainder of burnt polyimide. The capillaries were passed through the orifices of the etching cups so that the cup would sit on top of the polyimide layer at the bottom of the window, as seen in **figure 14C**. A container was filled with a saturated NaOH solution, into which the falling etching could fall. Aliquots of 25 µL of HF were pipetted into the cups. The etching took approximately 6 hours, creating an emitter of approximately 9 cm in length.

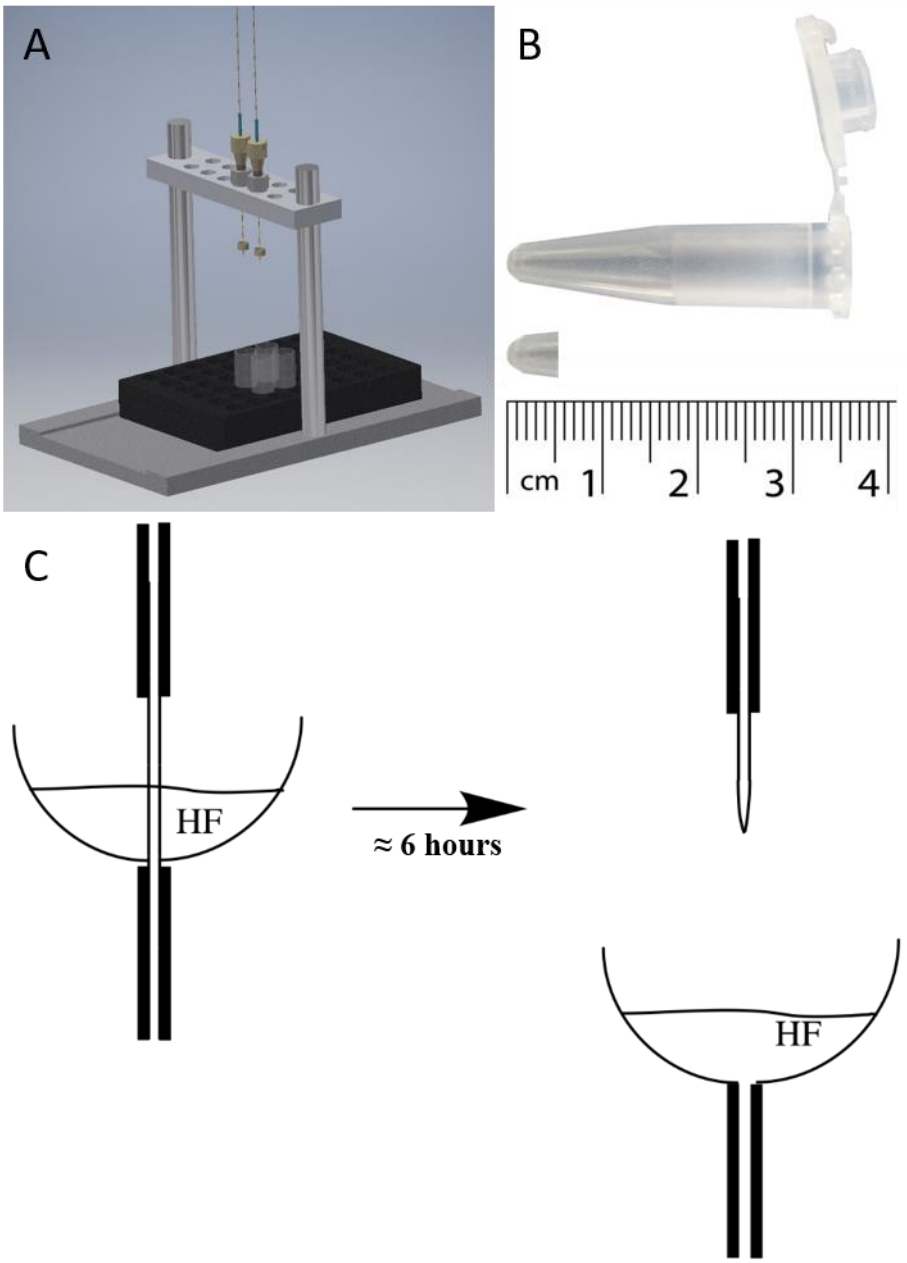

Figure 14 – A: Illustration of etching stand with two capillaries mounted during etching. B: Illustration of etching cup fabricated by cutting off the bottom of an Eppendorf tube. C: Illustration of etching cup with HF creating a needle over six hours. Once the etching is finished, the reservoir falls away and stops etching the needle. Polyimide layer shown in black.

3.5 Deposition of Nb-doped TiO_2

Deposition of TiO_2, Nb_2O_5, and Nb-doped TiO_2 was performed on the Beneq TFS500 reactor. The QCM-sensor was used as the substrate during optimization.

3.5.1 Optimization of deposition of TiO_2 thin-film

For optimization of deposition, a sequence with set parameters was used as a starting point for deposition. The standard sequence is shown in **table 2**. By varying the parameters, one at a time, the deposition could be optimized. Every sequence was run 30 times before making changes. All depositions were performed at 200˚C.

Table 2 - Standard deposition sequence used as a starting point for the optimization of deposition. The sequence describes the timings for the valves. All purging was done with nitrogen.

$TiCl_4$ pulse	Line-purge	$TiCl_4$-purge	H_2O pulse	Line-purge	H_2O-purge	Purge
0.5 s	0.25 s	1 s	0.5 s	0.25 s	3 s	40 s

Before any variations in parameters, the standard sequence was deposited 80 times to create a nucleation layer. This was repeated at the start of every deposition.

The signal (Hz) from the QCM was plotted against time (ms) in Origin 2017 (from OriginLab Corp., Northampton, MA, USA). The slope of each sequence was calculated. The slope of each sequence was inversely proportional to the growth rate of that specific sequence.

3.5.2 Optimization of deposition of Nb_2O_5 thin film

Quartz crystal microbalance testing

In the same way as with $TiCl_4$, a standard sequence was used for the optimization of deposition of Nb_2O_5. This standard sequence is shown in **table 3**.

Table 3 - Standard deposition sequence used as a starting point for the optimization of deposition. The sequence describes the timings for the valves. All purging was done with nitrogen.

$Nb_2(OEt)_5$ pulse	Lpurge	$Nb_2(OEt)_5$-purge	H_2O pulse	Lpurge	H_2O-purge	Purge
0.5 s	0 s	3 s	0.5 s	0.25 s	3 s	40 s

Initially, a test-deposition was performed by depositing with the standard sequence 80 times. This procedure was used for all the depositions to create a nucleation layer. One parameter of the standard sequence was varied at a time, for optimization of the deposition.

The data resulting from the QCM-measurements was analyzed in the same way as for TiO_2.

Deposition on substrates

Silicon wafers were cut into approximately 1 cm^2 pieces and placed in the chamber of the reactor. Five substrates were placed in the chamber at positions north, east, south, west, and in the center (see **figure 15**), so that gradient monitoring was possible.

The cylindrical reactor chamber consisted of two pieces: A horizontally compartmentalized bottom piece with a gas inlet in the bottom compartment and a deposition platform in the top compartment, connected to the bottom through a perforated outer section is shown in **figure 15**. The second piece was a metal lid, closing the reactor chamber.

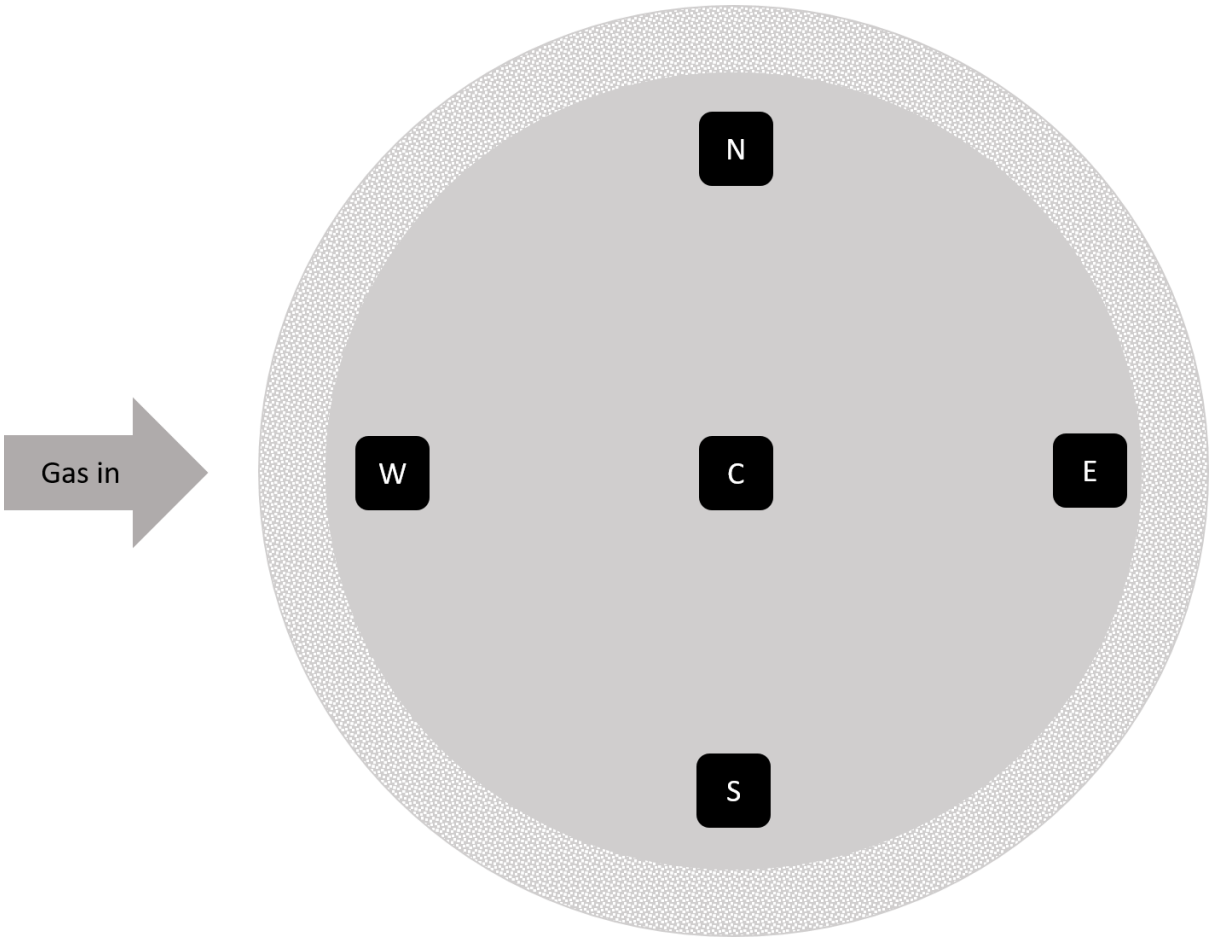

Figure 15 - Schematic drawing of the chamber of the reactor with silicon substrates (black) placed in the north, east, west, south, and center of the chamber. During pulsing, gas flows into the bottom of the chamber, and up through the holes in the perforated outer section of the reactor before evacuation on the opposite side through the perforated section shown.

Nb_2O_5 was deposited onto the substrates using the sequence, shown in **table 4**, 750 times at 200 ˚C.

Table 4 - Deposition sequence for $Nb_2(OEt)_5$ onto silicon substrates.

Valve	**Time, s**
$Nb_2(OEt)_5$	4
Purge	1
H_2O	0.5
Line purge	0.25
Purge	3

3.5.3 Deposition of Ti-Nb-O film

Deposition of Ti-Nb-O film was done by running a sequencing program with two sequences for Ti, one for Nb and one Ti. The sequences are shown in **table 5**. This was repeated 250 times. Before deposition, in addition to the five silicon substrates, also two glass slides were put into the reaction chamber between west and center and center and east substrates (see **figure 15**).

Table 5 - Sequences for deposition of Ti-Nb-O-film. Ti sequence to the left, Nb sequence to the right.

Ti-sequence		**Nb-sequence**	
Valve	**Time, s**	**Valve**	**Time, s**
$TiCl_4$	0.5	$Nb_2(OEt)_5$	4
Purge	2	Purge	1
H_2O	0.5	H_2O	0.5
Lpurge	0.5	Lpurge	0.25
Purge	3	Purge	3

3.5.4 Crystallization of Ti-Nb-O

The procedure for crystallization of Ti-Nb-O thin film was adapted from Pore *et al.* [85] and Niemelä *et al.* [84]. A tube furnace was loaded with glass slides with deposited Ti-Nb-O-thin film. The tube in the furnace then was closed and evacuated by a pump. Formier 10 was flushed through the chamber for 20 minutes. The oven was then turned on and set to 475 ˚C. Once the temperature was reached, it was kept at the same temperature for 30 minutes before cooling. The gas flow was shut off when room temperature was reached.

After the initial experiment, the furnace was replaced with a RTP-oven. Substrates of coated glass were loaded into the oven, evacuated and flushed with Formier 10. The oven was set to 500 ˚C. Samples were left for 10 or 30 minutes. Two coated slide samples were left for 30 minutes at 600 ˚C.

3.6 SnO_2

3.6.1 Optimization of deposition of SnO_2

Preliminary deposition of SnO_2 was performed on the Beneq TSF500-ALD reactor. The chamber was loaded with silicon substrates in the same positions as with the other methods (N, W, S, E, C), and the additional two glass slides were placed in the chamber between W and C, and C and E.

The deposition consisted of 750 cycles at 350 ˚C with the setup described in **table 6**.

Table 6 - Sequence used for deposition of SnO_2 using the Beneq TSF500-reactor.

$SnCl_4$	Purge	$H_2O + O_3$	Line purge	Purge	Purge
0.5 s	2 s	2 s	0.5 s	3 s	40 s

Optimization of deposition of SnO_2 and deposition on fused silica emitters was performed in an in-house built ALD reactor based on a tubular furnace and inert gas valves with injections extending into the hot zone. The precursors were kept in containers outside the reactor at room temperature.

Approximately 1 cm^2 pieces of silicon wafers were placed on a ≈ 50 cm long, ≈ 8 cm wide aluminum plate covered with aluminum foil acting as a platform for deposition in the reactor. Three silicon pieces were placed on the aluminum platform. One in the front (closest to the gas inlet), one in the middle, and one in the back. In between, two pieces of microscopy glass slides were placed for measurement of conductivity as seen in **figure 16**. The silicon substrates were marked Front (F), Center (C), and Back (B).

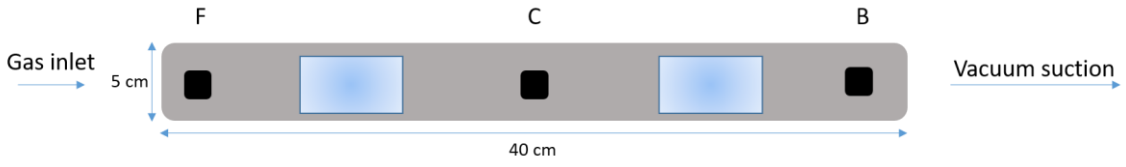

Figure 16 – Illustration of aluminum platform with silicon substrates (black) and glass substrates (light blue) used during deposition as a base for substrates and to easily load and unload the reactor.

The loaded aluminum platform was placed in the reactor chamber at the vacuum suction end, which, in turn, was placed in the furnace. The reactor was evacuated before a deposition program was run.

For optimization of deposition, one parameter was changed at a time. In addition to pulse times and purge times, the flow of nitrogen (purging agent) was changed, and a needle valve was fitted to the $SnCl_4$ flask so that also the availability of the precursor could be changed.

The final deposition program used for deposition on substrates consisted of 300 cycles at 400 ˚C. The direct flow into the reactor was set to 300 standard cubic centimeters per minute (SCCM). The skirt gas flow that goes around the reactor chamber from the back-end towards the gas inlet and through the chamber was set to 150 SCCM. The needle valve on the $SnCl_4$ was opened two full rounds. The remaining parameters of the deposition program are shown in **table 7**.

Table 7 - Final deposition program for deposition of SnO_2 using the in-house built ALD reactor.

$SnCl_4$, ms	Line purge, ms	Purge, ms	H_2O, ms	Line purge, ms	Purge, ms
500	500	2000	2000	500	2000

3.6.2 Gradient test

The aluminum platform was loaded with 23 silicon substrates, covering the entire platform (see **figure 17**). Then, the platform was placed towards the vacuum suction end of the chamber and placed in the furnace for deposition. The optimized program, shown in table 6, was used for deposition with 300 cycles at 400 ˚C.

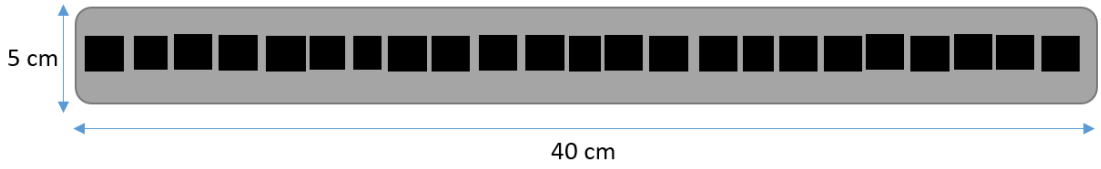

Figure 17 – Illustration of the aluminum platform covered with 23 silicon substrates (≈ 1 cm^2 each) used to test for longitudinal gradients in the reactor.

After deposition, the film thickness on the different substrates was measured with the α-SE ellipsometer (see **section 3.7.1**).

3.6.3 Deposition of SnO_2 on fused silica emitters

For deposition of SnO_2 on etched fused silica emitters, principal engineer Inge Mikalsen created an aluminum stand. The stand consisted of two walls with five holes drilled in them for placement of five capillaries at a time. Capillaries were passed through the holes so that the back end of the capillaries was held by the two walls, letting most of the emitter, including the tip, stand in mid-air for deposition, as shown in **figure 18**. A photograph of the aluminum deposition stand can be seen in **figure 19**.

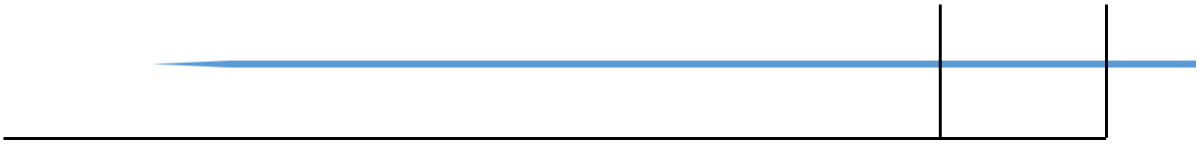

Figure 18 – Cross-section of deposition stand with etched fused silica capillary (blue) mounted.

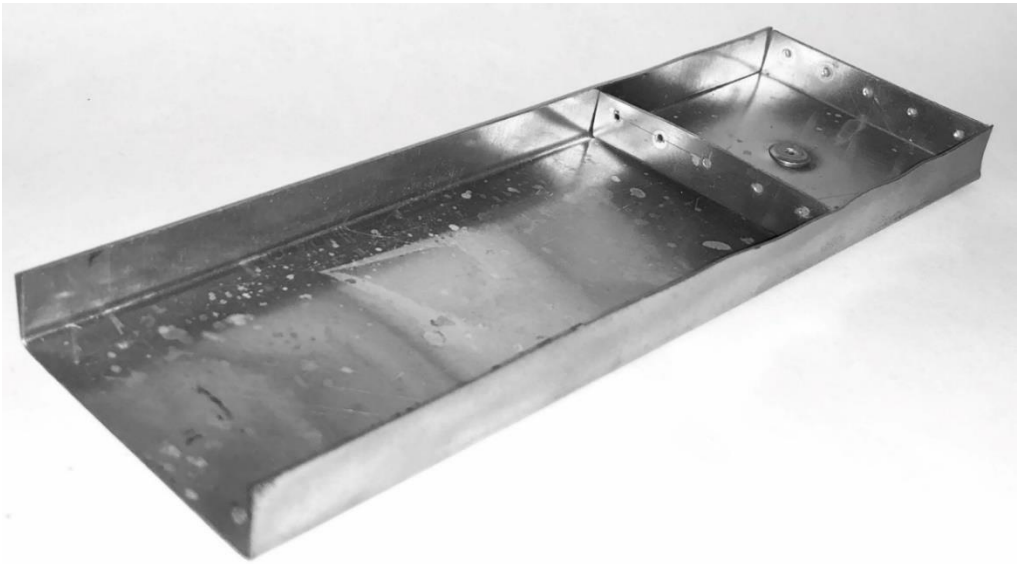

Figure 19 - Photograph of deposition stand for emitters.

Below the emitter tips, a cut piece of microscopy slide glass was placed. On top of the glass, two silicon substrates were placed, as shown in **figure 20**. The glass slide was used for measuring conductivity, while the silicon substrates were used for measurement of film thickness.

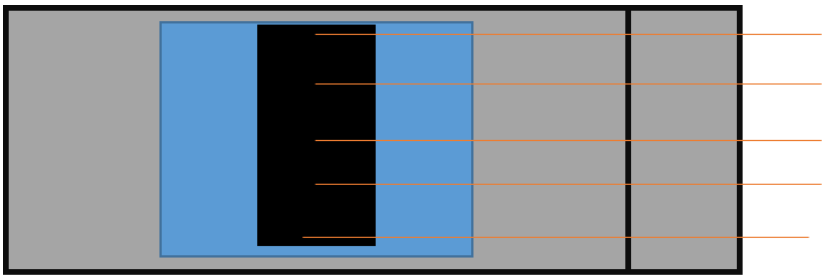

Figure 20 – Illustration of the deposition hardware showing emitters (orange) in the stand, above silicon substrates (black) on a glass substrate (blue).

Deposition on emitters was performed using the same program, with the same parameters, as the optimized deposition shown in **table 7**. The program was run for 1500 cycles to begin with, but this was increased to 6000 cycles in the finalized method.

3.7 Characterization of conductivity and film thickness

3.7.1 Measurement of film thickness

Film thickness was measured using the Woollam α-SE ellipsometer. Coated silicon substrates were placed with the coated side up, so that the measurement area was in the middle of the substrate. For each measurement, a mathematical model for transparent films on Si (Cauchy's equation [99]) was used and fitted to the acquired data.

3.7.2 Measurement of conductivity

Conductivity was measured using the 4-point probe method and the Keithly, Tektronix digital multimeter. Coated microscopy slides (glass substrates) were put into the measuring box, and the 4-point probe was lowered onto the substrate. The current was slowly increased, and the resistance was measured. If the plot of the measured data was linear, the film was considered conductive.

3.7.3 *In situ* measurement of conductivity

A microscope glass slide was roughened with sandblasting/abrasive blasting, so that the center of the slide had a rough surface. Copper threads were then fixed to the edges of the rough field with silver paint so that the distance between the two fields was approximately 1 cm. The setup

is shown in **figure 21**. Once dried, the copper threads were connected to cables insulated in glass tubes to withstand the applied temperature. The slide was then placed in the reactor chamber in the same spot as the emitters. The cables were connected to a Fluke 8846A precision multimeter. The final deposition sequence shown in **table 7** was then deposited with 600 cycles. The measured conductivity data (Ohm) was plotted in Origin 2017 against time.

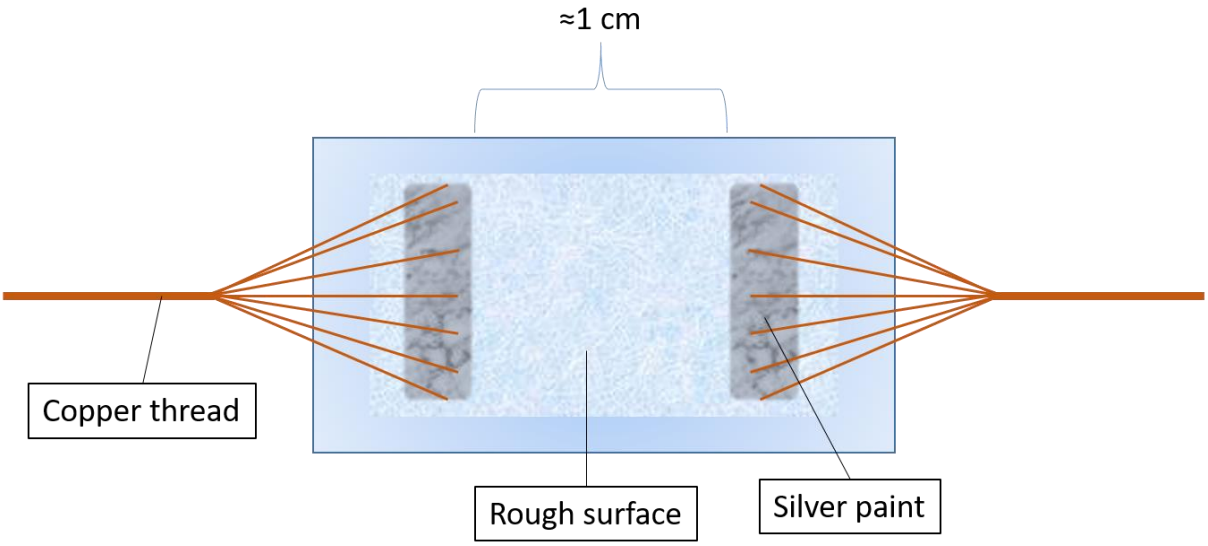

Figure 21 – Illustration of setup of glass slide with copper threads fixed by silver paint for *in situ* conductivity measurement.

3.8 Nano electrospray ionization test systems

3.8.1 Preparation of mobile phase

Three MP components were made. MP reservoir A contained 0.1% formic acid in HPLC water (*v/v*). MP reservoir B contained acetonitrile/HPLC water/FA (90/10/0.1%, *v/v/v*). MP reservoir C contained MeOH/HPLC water/FA (90/10/0.1%, *v/v/v*).

3.8.2 Testing of emitters

Flow injection testing system

Coated emitters were tested using the TSQ Quantiva Trippel Quadrupole MS equipped with the nanoflex II nano-ESI ion source. An EASY-nLC 1200 pump was used to deliver the solvent. The emitters were connected to an approximately 1 meter long fused silica capillary (150 µm

ID) using a PEEK union, PEEK screws, and PEEK sleeves. The fused silica capillary was connected to the pump using SS unions and screws and graphite/vespel ferrules. The flow rate was set to 300 nL/min with 95% MP A and 5% MP B. The MS was run in continuous full scan mode with positive ionization at 3 kV. The resulting total ion current (TIC) was recorded.

Nano liquid chromatography mass spectrometry testing system

The in-house made emitters and commercial SS emitters were tested. The emitters were connected using PEEK screws, a PEEK union, and PEEK sleeves with corresponding IDs to the emitters ODs. Emitters were placed in the Nanoflex II nano-ESI source. An in-house fabricated silica based monolith column (75 µm x 12 cm) functionalized with C18 with a pre-column fabricated in the same way (75 µm x 4 cm) was used. The gradient program described in **table 8** was used with a flow rate of 400 nL/min. Positive spray voltage was set to 2.2 kV and negative spray voltage to 0.6 kV. MRM-parameters are shown in **table 9**.

Emitters were compared based on the resulting chromatographic peaks from 2 µL injections of 50 pM heroin in H_2O. To compare the performance (signal to noise ratio) of the emitters an F-test and two-tailed t-test were used.

Table 8 – Gradient program used for comparison of SS emitters with in-house fabricated fused silica emitters.

Minutes	**% MP B**
0-20	0-50
20-22	50-100
22-27	100

Table 9 – MRM parameters used on the TSQ Quantiva for detection of heroin.

Parent ion, *m/z*	**Product ion, *m/z***	**Collision energy, eV**
370	328	28
370	268	30
370	165	54

3.9 Development of an on-line analysis system for Organ-on-a-Chip

3.9.1 Preliminary testing with a commercial organ-on-a-chip platform

Preliminary testing was performed using the commercially available OoC platform by BIOND Solutions B.V. The chip was connected using PTFE tubing and Teflon end fittings with ferules for 1/16" OD tubing. A syringe pump was used for pumping solutions (solvents, medium) through the chip system at flow rates between 20 – 200 µL/min.

A 6-port 2-position valve was added between the chip and the pump. A schematic drawing of the setup (setup 1) is shown in **figure 22**.

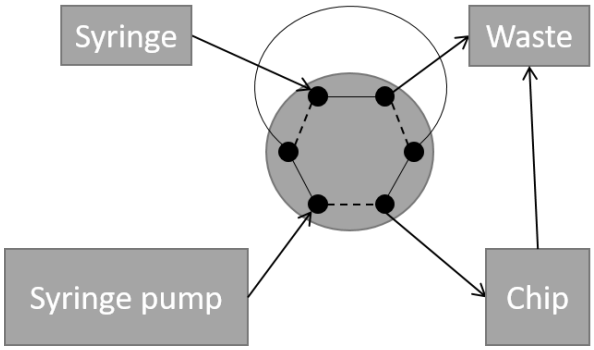

Figure 22 – Schematic of setup 1 used during testing of the commercial OoC platform.

In setup 2, a UV-detector (Dionex Ultimate 3000 RS) with a flow cell of 7 mm in length and 2.5 µL volume was used. The system (setup 2) is shown in **figure 23**.

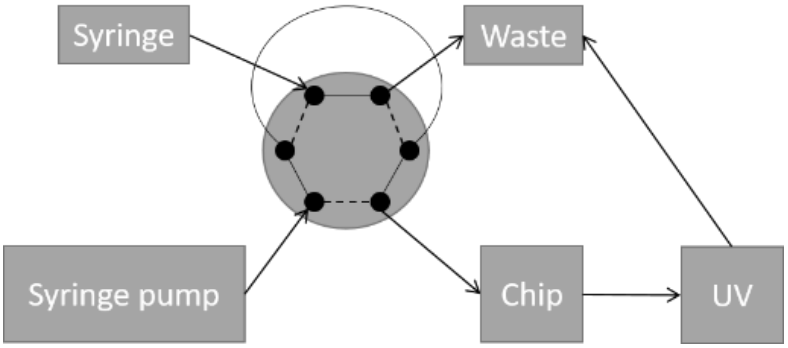

Figure 23 - Schematic of setup 2. A UV-detector was used.

For some experiments, the chip was replaced with a union compatible with the connections to the chip (1/4”, butt-to-butt). A 2 µL injection of 40 µg/mL Fluorescein in type 1 water was performed.

In setup 3, the 6-port injection valve was placed behind the chip and water was switched with organoid medium. The medium was run through the chip and loop overnight. The experimental setup (setup 3) is shown in **figure 24**.

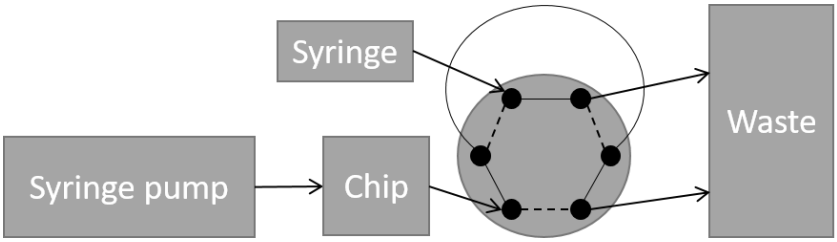

Figure 24 – Schematic of setup 3 for test with medium.

3.9.2 Connectors for chips

The microfluidic chips, supplied by the Gadegaard group (University of Glasgow), are injection molded polystyrene chips. The chips have an inlet and outlet connected by a narrow passage. In the passage, a step acts as a trap for particles. Organoids can be injected through the inlet and then are trapped and stay in the channel under perfusion. In the inlet and outlet wells, a 1 mm hole was drilled. See **figure 25** for an image of such a chip.

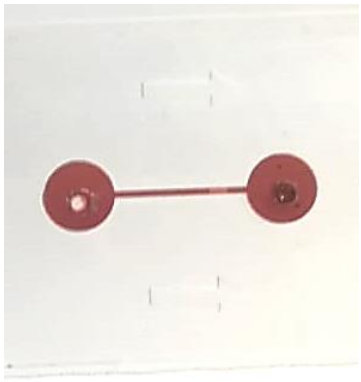

Figure 25 – Chip designed and fabricated by the Gadegaard group at the University of Glasgow. The trap is visible at the right end of the connecting channel. The flow direction through this chip would be from the left port, towards the right port. Picture by Neil Convery.

To connect the chips with tubing, a connector was designed together with principal engineer Inge Mikalsen. The connectors consisted of a U-shaped piece of aluminum. Through one side

of the metal U, a PEEK nut could clamp down on the chip. On the other side of the clamp, a small hole was used for aiming at the entry port. Through the screw, a PTFE tubing was passed. The end of the tubing was flanged with the Easy-Flange Flanging Tool Kit. By screwing the flanged tubing, centered against the hole, a seal was formed. A 3D rendering of the connectors is shown in **figure 26**.

The seal was tested with medium with flow rates up to 10 mL/min overnight.

To test the trapping of spheres on the chip (e.g. organoids), 150 µm polystyrene beads were loaded into a syringe and solvated in 5 mL type 1 water. A syringe pump, pumping at 100 µL/min, was used. The Motic light microscope was used for visual inspection of the trapping.

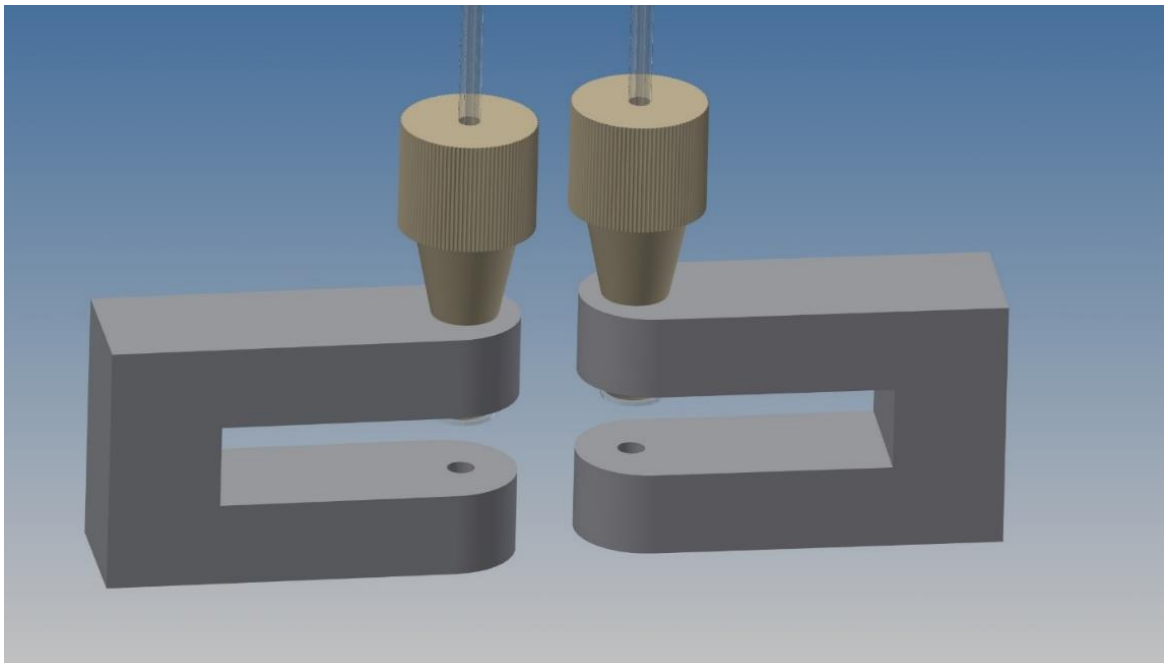

Figure 26 – Assembled connector with U-shaped aluminum, PEEK nut, PTFE tubing with flange, and aiming hole used for connecting the chips to fluidics. By tightening the screw, the tubing is pressed against the chip, creating a seal. Connectors were designed in cooperation with principal engineer Inge Mikalsen.

3.9.3 Liquid chromatography-UV system for testing of fluidics

The fluidic valve system consisted of a 10-port 2-position valve from VICI Valco. 20 µL loops of 1/32" OD, 0.015" ID PEEK tubing were made. All other tubings were cut from 1/32" OD, 0.005" ID PEEK tubing. The tubings were assembled according to **figure 27** with SS ferrules and screws. A reducing union was used to go from 1/16" format to 1/32" format in the valve. A short column with Kromasil C4 was used as chromatographic column. For perfusion of the

chip, a syringe pump was used. The LC setup consisted of a degasser (G1379A), a pump (G1376A), and a multiple wavelength detector (G1365D) with a 2 µL, 3 mm path flow cell.

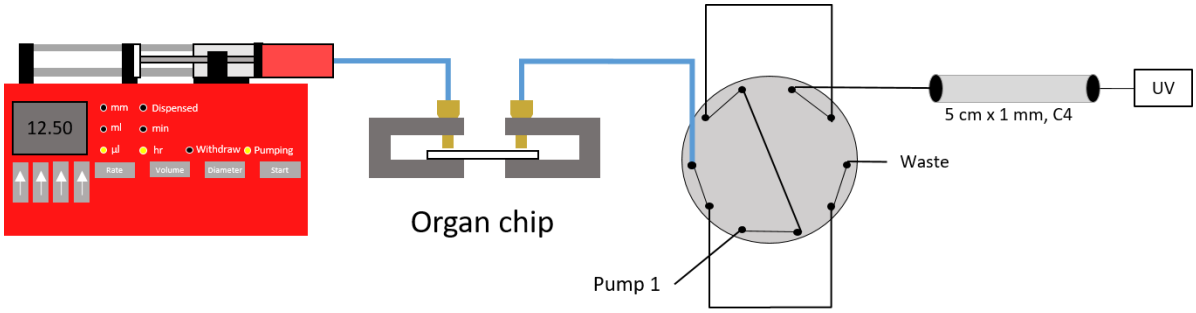

Figure 27 – Illustration of Chip-LC-UV test system. The syringe pump provides a steady flow of solution to the chip. The loops on the valve sample fractions of the solution. LC-UV provides the analytical part. Reducing union converting from blue 1/16" to black 1/32" is not show. 20 µL loops were used in this setup.

Solutions of caffeine, uracil, and human serum albumin (HSA) were prepared according to **table 10**. The solutions were injected through the syringe pump and loop system, to ensure that the performance of the fluidics and the chromatography were satisfactory and to develop a method.

Table 10 – Solutions for testing of fluidics and chromatography. All solutions were prepared in type 1 water, except media.

Solution	**Contents**
1	50 µg/mL uracil
2	25 µg/mL uracil
3	50 µg/mL caffeine
4	25 µg/mL uracil, 25 µg/mL caffeine
5	0.1 mg/mL HAS
6	1 mg/mL HAS
7	5 mL 50 µg/mL uracil, 5 mL 50 µg/mL caffeine, 1 mL 1 mg/mL HSA
8	50 µg/mL caffeine, 1 mg/mL HSA
9	50 µg/mL caffeine, 0.1 mg/mL HSA
10	Fetal Bovine Serum (FBS) free cell growth medium
11	Organoid medium containing heroin (1µM)
12	100 µM heroin
13	18 µM 6-MAM, morphine, M3G and M6G

The finalized method was a gradient method with 3-20% MP B from 0-8 min and a re-equilibration step with 3% MP B from 8-10 min. The remaining part of the MP consisted of MP A. The flow rate was held constant at 100 µL/min.

3.9.4 Fabrication of organ-in-a-column

For fabrication of the organ-in-a-column (OiC), an approximately 5 cm long piece of PTFE tubing was cut and assembled with SS nuts and ferrules and one SS union with a 1 µm SS screen connected to one of the sides of the tube.

1-22 mL of medium containing organoids were then filled into a Luer-lock syringe. The open side of the OiC was connected to the syringe, and with a syringe pump, the medium was pumped through the PTFE tube at a rate of 100 µL/min. Once the entire content of the syringe was passed through the tubing, the backside was fitted with a screen and a union. A schematic of an organ-in-a-column housing is shown in **figure 28**.

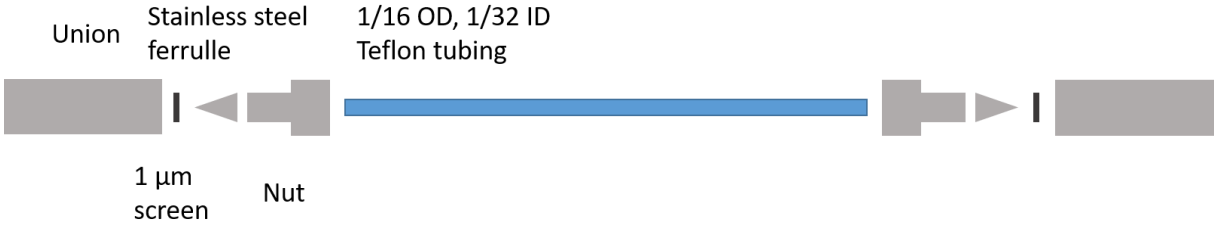

Figure 28 – Schematic of the different parts used to make the organ-in-a-column housing.

Subsequently, a new syringe was filled with fresh organoid medium and connected to the OiC, so that the flow was the opposite way as during filling. The pump was set to 10 µL/h, and the OiC was placed in a water bath at 37 ˚C.

Robustness testing of organ-in-a-column

1µM heroin in organoid medium was prepared and loaded into a syringe. The previously described Chip-LC-UV system was modified and set up as shown in **figure 29**. The syringe pump was run at a flow rate of 2.5 µL/min. The finalized gradient program described in the previous section was used (see end of **section 3.9.3**).

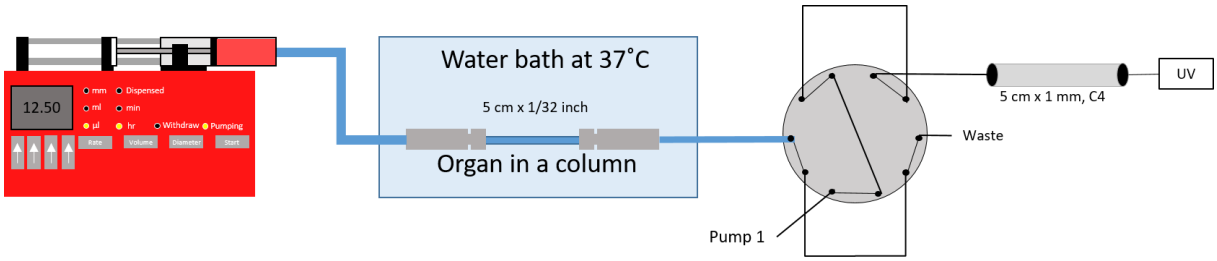

Figure 29 – Illustration of the OiC-LC-UV test system used to verify the columns robustness. 20 µL loops were used in this setup.

After ten injections, the column was disassembled, and the contents, including the filters examined with a light microscope.

3.9.5 Test system for organ-in-a-column

For testing with the MS, the tubings in the high-pressure part of the system (on the valve) were changed to SS tubings of the same dimensions. The LC-MS part of the system consisted of the Dionex UltiMate 3000 UHPLC system coupled to a TSQ Vantage MS.

The functionality of the system and MS parameters for MRM were verified by injecting several different solutions with the syringe pump through the loop system. The different solutions are shown in **table 11**.

Table 11 – Solutions used for verifying system and MS parameters

Solution	**Contents**
1	25 µg/mL caffeine
2	1µM heroin
3	1µM 6-MAM and morphine
4	0.2 mL organoid medium and 1.8 ml 1µM 6-MAM and morphine
5	0,3 mL organoid medium and 0.4 mL 1 µM 6-MAM and morphine
6	200µL 50 µM 6-MAM and morphine in 9800 µL organoid medium

The final MRM parameters are shown in **table 12**, while general MS parameters are shown in **table 13**.

Table 12 – MRM parameters used for detection of heroin and its phase 1 metabolites.

Molecule	**Parent ion, *m/z***	**Product ion, *m/z***	**Collision energy, eV**
Heroin	370	272	30
6-MAM	328	211	25
Morphine	286	201	20

Table 13 – General MS parameters for detection of heroin, 6-MAM and morphine.

Parameter	**Value**
Capillary temperature	300.0 ˚C
Vaporizer temperature	200.0 ˚C
Sheath gas pressure	20.0
Ion sweep gas pressure	0.0
Auxiliary valve flow	5.0
Spray voltage	Pos: 3000.0 V Neg: 0.0 V
Collision gas pressure	1.0 mTorr

3.9.6 Retention time test

100 injections of solution 6 described in **table 11** were performed. The solution was loaded into a 10 mL syringe. A syringe pump was used to continuously load sample at a flow rate of 25 µL/min. The test system described in figure 29 was used for this experiment, but with an empty organ-in-a-column housing.

3.9.7 On-line liquid chromatography-mass spectrometry with heroin-containing medium

Three on-line experiments with organoids and heroin-containing medium were performed.

In the first experiment, a 1 µM solution of heroin in organoid medium was used. 2 mL of dispersed organoids were loaded into the organ-in-a-column manually. After 0.5 mL of solution had passed through, the remaining organoids in solution were loaded by letting them sink into the column through gravity before closing the column off. The column was turned around, so that the flow through the column was reversed. The column was taped into the water bath vertically.

In the second experiment, the same OiC was used. After 10 minutes of flow, the flow over the organ-in-a-column was shut off for 2 hours. After the two hours had passed, the contents of the column were transferred to the loops and injected.

In the third experiment, suspended organoids (47 days old) were used. 22 mL were loaded into the organ-in-a-column housing with a syringe pump. This column was left under organoid medium flow overnight at a rate of 12.5 µL/h. A 100 µM solution of heroin in organoid medium was made, replacing the "overnight"-medium. A final LC-gradient program was made and is shown in **table 14**. Once the pure organoid medium was flushed off, injections were made.

Table 14 – Final gradient program used for final on-line OoC-LC-ESI-MS experiment. The purpose of the different steps is described.

Time, min	Flow, µL/min	%B	Purpose
0	50	3	Separation
20	50	20	
20	50	80	Wash
60	50	80	
60	50	3	Re-equilibration
70	50	3	
70	0	3	Save MP
110	0	3	
110	50	3	Re-equilibration
120	50	3	

The experimental setup is shown in **figure 30**. After the experiment, the medium was switched back to pure organoid medium, and the organ-in-a-column was left perfused.

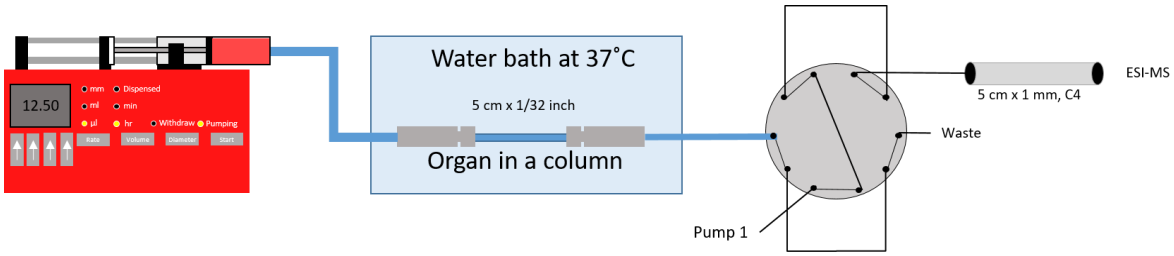

Figure 30 – Illustration of the OiC-LC-MS test system for on-line sampling and analysis of organoid medium containing heroin. 20 µL loops were used on this system.

3.9.8 Live/dead staining for viability testing

Seven days after the preparation, the organ-in-a-column was flushed with phosphate-buffered saline (PBS) pH 7.4 to remove the medium. Then, the column was dismantled, and the content was collected. Organoids that were stuck to the filters were scraped off. The organoids were transferred to a glass slide, and excess PBS was removed. The organoids were then stained with

Live/Dead Cell Double Staining Kit suitable for fluorescence from Sigma Aldrich in the following manner:

100 µL of the staining solution (5 mL PBS, 10 µL solution A and 5 µL solution B) were pipetted onto the organoids. A cover slide was placed on top, and the organoids were then incubated at 37 ˚C for 15 minutes. Dr. Khulbhushan Sharma (Faculty of Medicine, University of Oslo) carried out the fluorescence microscopy experiments.

3.10 Safety considerations

HF is extremely hazardous, classified as very toxic, and corrosive. Extreme care must be taken when handling HF. Always operate in a closed fume hood. Protective equipment must be worn at all times. If the skin is exposed to HF, immediately rinse with running water. HF-antidote gel (gel containing calcium gluconate) must be applied after that and massaged into the exposed areas while the exposed person is being rushed to a hospital. For large exposures, at least a liter of saturated calcium carbonate solution should be at hand to rinse the exposed areas.

In this study, HF-antidote gel and one liter of saturated calcium carbonate solution was at hand in the fume hood. For disposal of HF and NaOH containing HF, calcium carbonate solution was added to the solution in excess, neutralizing the fluorine.

4 Results and discussion

The aim of this study was to 1) develop ALD-coated fused silica ESI-emitters hyphenated with nanoLC columns intended for OoC systems and 2) to develop an on-line OoC-HPLC-ESI-MS-system for proof-of-concept testing with heroin. Because this is a proof-of-concept study, a larger ID column was chosen to avoid possible problems with robustness (e.g. clogging) which are associated with nanoLC columns. Subsequently, the developed ESI-emitters have not been used in the on-line system, but have been tested separately in a nanoLC system. Consequently, the following Results and discussion part is divided into two, where the development of ESI emitters is discussed in **sections 4.1-4.3** and the development of an on-line analysis system is discussed in **sections 4.4-4.6**.

4.1 Nb-doped TiO_2 thin film

Nb-doped TiO_2 is a relatively newly discovered material reported to have excellent conductive properties [83], making it a suitable material for deposition on emitters.

4.1.1 Optimization of deposition

Since deposition of Nb-doped TiO_2 consists of sequences of TiO_2 and Nb_2O_5. Consequently, the deposition of these sequences was optimized before depositing them together.

QCM-sensors constitute a versatile tool and make *in situ* growth rate measurements possible. In this study, they were used to optimize ALD conditions for deposition of Nb-doped TiO_2 thin film. By changing one parameter at a time, changes in signal could be plotted against time. The slope of each sequence was calculated and by comparing the change in Hz/cycle, growth rates can be compared.

TiO_2

TiO_2 was deposited by pulsing $TiCl_4$ and water sequentially.

First, the pulse time of $TiCl_4$ was examined, as shown in **figure 31**, and as expected, the growth rate decreased towards zero when the pulse time went towards zero. Surprisingly, when H_2O pulse time was examined, changes in pulse time only meant insignificant changes in growth

rate. However, the pulse time was not lowered to zero because of restraints for the size of the deposition program. Therefore, another examination of the growth rate as a function of water pulse duration was performed (see **figure 32**). As the pulse time of water decreased to zero, growth was still observed, indicating a fault with the reactor, probably moisture leaking into the reactor chamber.

Purge times after $TiCl_4$ and H_2O pulses were also examined without giving substantial changes to growth rates and were therefore held constant. Diagrams of growth rates as a function of various parameters can be seen in **Appendix figure 1-3**.

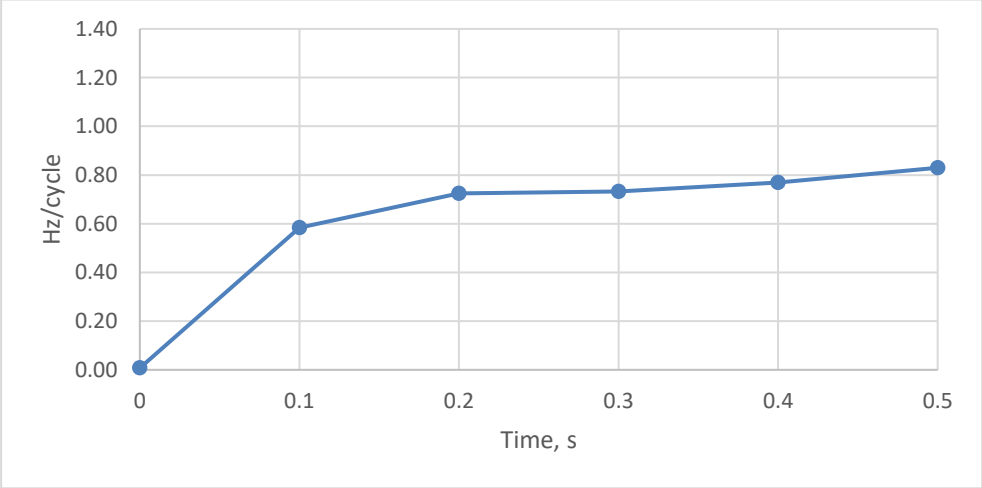

Figure 31 – Growth rate, measured as Hz/cycle, as a function of pulse time of $TiCl_4$.

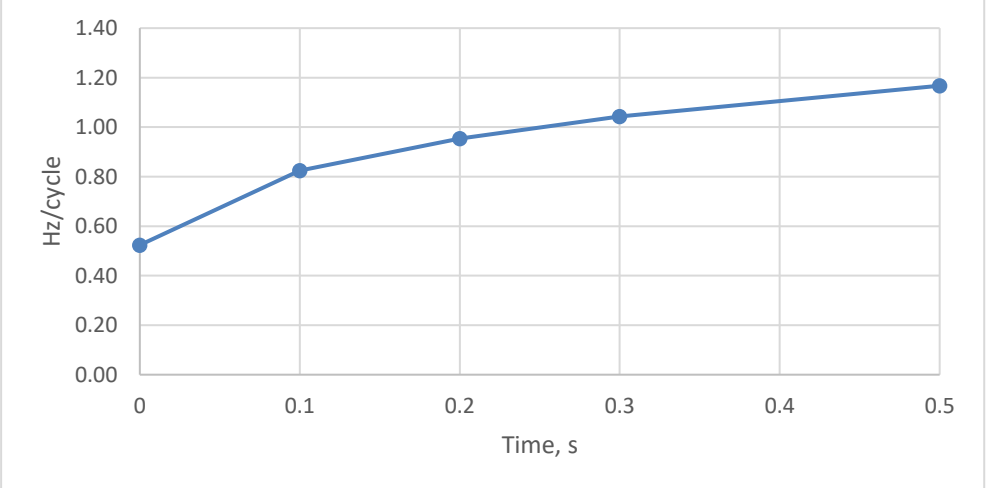

Figure 32 - Growth rate, measured as Hz/cycle, as a function of pulse time of H_2O.

Due to the uncertainty with respect to growth at zero pulse of water, the H_2O part of the sequence was further examined. First, the line-purge for the waterline was removed, and the

water pulse time was varied. Still, growth was observed when the water pulse was removed. Because it was believed that too short purge time after the water pulse could be responsible for the growth, the water pulse was varied with purge times of both 3 and 5 seconds. All of the tests showed growth when no water was actively pulsed (**Appendix figure 4-6**), indicating that neither the line purge, nor the purge after water pulse was responsible for the growth.

Leak search was performed, and several gaskets were changed. To reduce sample use, the $TiCl_4$ pulse was reduced to 0.3 s since that should not have reduced growth rates, as shown in **figure 31**, but no growth was observed. Hence, the pulse time was increased back to 0.5 s.

As the experiment was repeated, the water pulse, $TiCl_4$ pulse, water purge, and $TiCl_4$ purge were varied. The 0-water pulse sequence showed significantly lower growth than the other water pulses (**figure 33C**), but still growth was observed similar to earlier experiments (**figure 32**). When no $TiCl_4$ was actively pulsed, very low growth was observed (**figure 33A**) as expected. The tests regarding purge times (**figure 33B and 33D**) showed little variance between the different times.

Further leak testing was performed, but no leak was found and it was decided to move forward to optimization of Nb_2O_5.

Deposition of TiO_2 was optimized by examining various parameters like pulsing time and purging time through deposition on a QCM. When no water was pulsed, growth was still observed. Leak search lead to a thorough examination of the reactor and a few gaskets were changed. Growth was still observed, but since no further leak was found, the decision to move forward was made regardless.

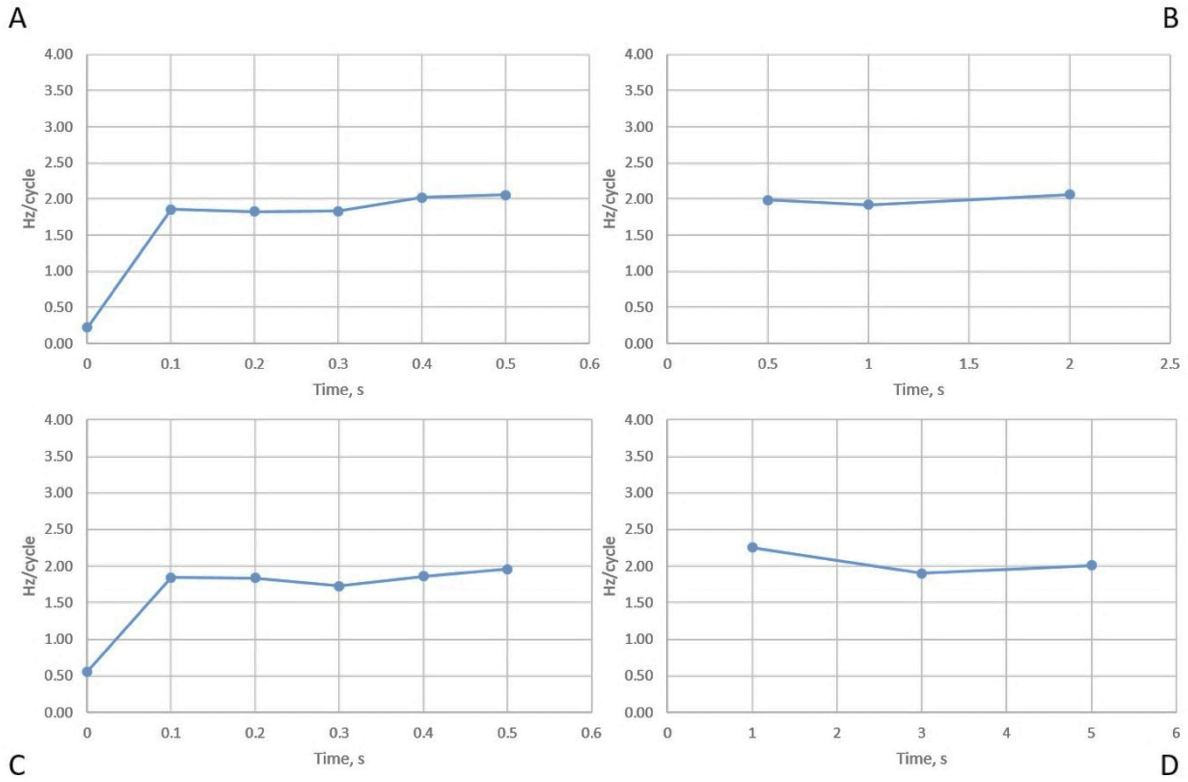

Figure 33 - A: Growth rate, measured as Hz/cycle, plotted as a function of $TiCl_4$ pulse time. B: Growth rate, measured as Hz/cycle, plotted as a function of $TiCl_4$ purge time. C: Growth rate, measured as Hz/cycle, plotted as a function of H_2O pulse time. D: Growth rate, measured as Hz/cycle, plotted as a function of H_2O purge time.

Nb_2O_5

For the first test deposition of Nb_2O_5, the Nb-source was heated to 85 ˚C, but no growth was observed. The Nb-source was then set to 67 ˚C with a pulse time of 4 seconds, but no growth was observed. The temperature, therefore, was set to 110 ˚C for the source. Finally, growth was observed, but all Nb-precursor was used up quite fast.

The glass precursor boat that held the Nb-precursor was then carefully washed and refilled with $Nb(OEt)_5$. As the water pulse was decreased, the growth rate only slightly decreased (**figure 34C**), indicating that the leak possibly was not fixed after all, or that a new leak had arisen.

As the Nb-pulse decreased, the growth rate rapidly sunk towards zero, showing that a time around 4 seconds might be necessary (**figure 34A**).

Nb purge and water purge showed stable growth rates over the entire range investigated (**figure 34B and 34D**), and their durations were thus believed to not be of utmost importance.

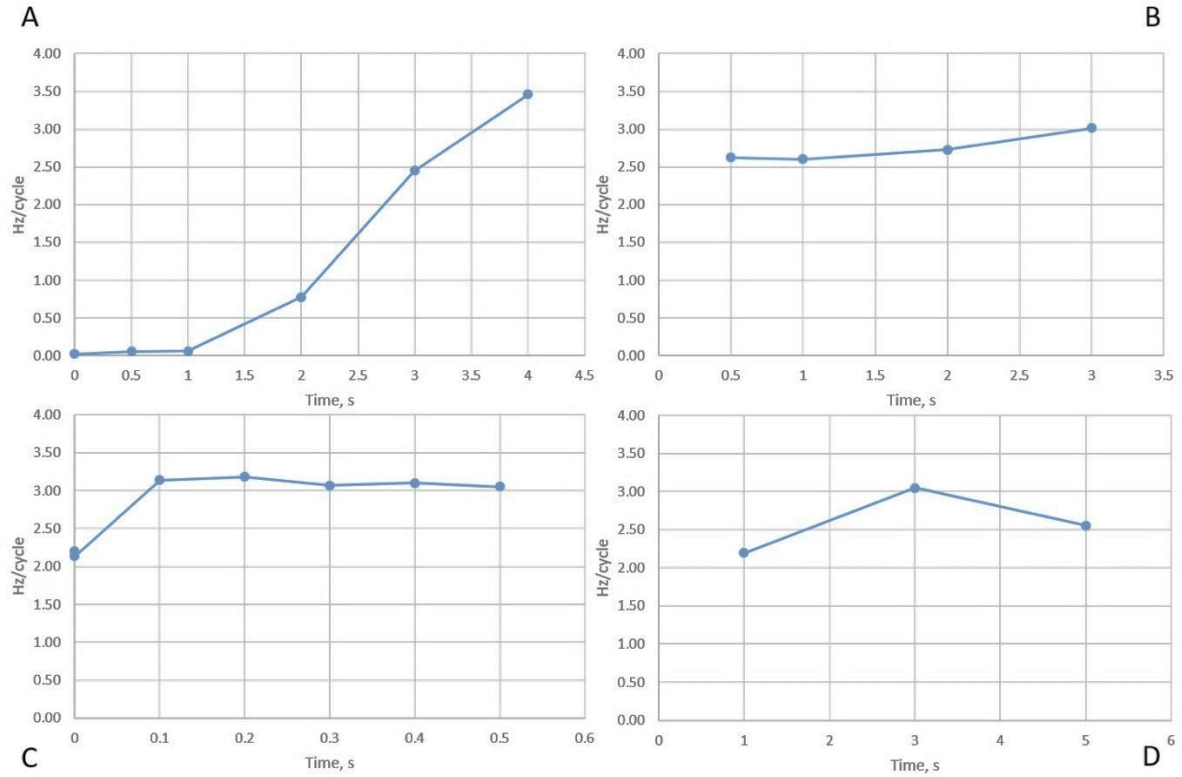

Figure 34 - A: Growth rate plotted as a function of $Nb(OEt)_5$ pulse time. B: Growth rate plotted as a function of $Nb(OEt)_5$ purge time. C: Growth rate plotted as a function of H_2O pulse time. D: Growth rate plotted as a function of H_2O purge time.

After optimization of the individual sequences, TiO_2, Nb_2O_5 and Ti-Nb-O-film were deposited on glass and silicon substrates.

The deposition of Nb_2O_5 was optimized by varying pulsing times and purging times. As during deposition of titanium dioxide, growth was measured without pulsing water, indicating that the leak was not fixed, or that a new leak had arisen. As previously described, no leak was found. After optimization, deposition on substrates was performed.

Film thickness

Film thickness was measured for all TiO_2, Nb_2O_5 and Ti-Nb-O-coated silicon substrates, and the results are compiled in **table 15**, ranging from 50 nm to 108 nm. This corresponds to growth rates from 0.050 nm – 0.143 nm per cycle.

Table 15 - Thin-film thickness measured with an ellipsometer. The deposition parameters can be found in appendix table 1, for deposition parameters. N, W, S, E, C describe the position of the substrates in the reaction chamber, as describes in **figure 15**.

	Thickness of films on substrates, nm					
Deposition	**Material**	**N**	**W**	**S**	**E**	**C**
2018041001	Nb_2O_5	60.9	56.5	53.0	54.4	55.8
2018041101	Ti-Nb-O	57.9	55.1	50.5	51.1	52.6
2018052801	Ti-Nb-O	81.1	94.8	94.9	75.2	86.2
2018052901	TiO_2	107.5	81.6	72.7	82.6	78.3

A corroded hole between the outer cooling jacket and the inner vacuum chamber was found a year after the work was carried out. This hole allowed moisture to leak into the chamber when the reactor was heated. Since this is a leakage on the inside of the reactor, it was not discovered during leak testing.

4.1.2 Crystallization and conductivity

The deposited Ti-Nb-O thin films were not conductive. As reported in the literature [83, 84], crystallization of the material is necessary to achieve the conductive properties of the material.

For the initial crystallization experiment of Ti-Nb-O thin films, a tubular furnace was used. The main issue with this method was that it was too time-consuming with a total time consumption of at least 5 hours, since both heating and cooling took a long time. The films that were attempted crystalized did not conduct electricity.

Instead, an RTP-oven, heating up to 600 ˚C in a matter of seconds, was used. The same gas mixture (Formier 10) was used with the RTP-oven. Here it is important to note that too quick heating can cause glass substrates to break.

Different approaches of crystallization were attempted. First, substrates were heated to 500 ˚C for 10 minutes. Other substrates were left at 500 ˚C for 30 minutes, before additional substrates were left for 30 minutes at 600 ˚C. In all cases the films did not conduct electricity, and the results found in the literature [84, 85] could not be reproduced.

It is unknown what caused the lack of conductivity, but several reasons could be responsible. The stoichiometry of Ti, Nb, and O could have been incorrect. Another possibility was the leaking into the reactor, causing a different film than desired. Other explanations might be failing crystallization either due to wrong oxidation state of the metals or that the substrates, being transparent, were not sufficiently heated with a lamp-based oven such as the RTP-oven. To ensure that heating occurred, a piece of silicon (being black) was placed beneath the coated glass substrate. Whether this approach ensured sufficient heating is unknown.

Hence, further work on Nb-doped TiO_2 films was put aside since the SnO_2-films were found to conduct without any tedious crystallization process. In addition, the deposition seemed simpler with only two reactants/precursors, although a higher deposition temperature was required.

4.2 SnO_2

In earlier studies [75], a coating of indium tin oxide (ITO) was pursued for nano-ESI emitters through a sol-gel approach without giving rise to conductive films. Due to high chemical stability and reports of simple deposition schemes by ALD [88], SnO_2 seemed like a suitable choice of coating material, and it was decided to pursue this material further.

4.2.1 Optimization of deposition

An initial test-deposition of SnO_2 was performed using the Beneq TSF500-reactor. Conductivity and film thickness were measured, and both glass substrates conducted electricity. Measurements of film thickness are reported in **table 16**.

Table 16 – Film thickness from test-deposition of SnO_2 using the Beneq TSF500 reactor.

	Thickness of films on substrates, nm				
Deposition	**N**	**W**	**S**	**E**	**C**
2018060401	14.1	19.8	14.0	12.2	13.5

Since deposition-temperatures for SnO_2 reported in the literature are generally above or very near, the upper temperature limit of the Beneq TSF500-reactor at 450 ˚C, the decision to move to a high-temperature ALD-reactor was made.

Initially, TMA and water were used to deposit Al_2O_3. This was used to find the basic settings of the reactor, like gas flows, before optimization of deposition of SnO_2. First, the gas flow around the reactor chamber was increased to push the pulsed gas further into the chamber to create a larger area of relatively high growth of film (2018090702). The vacuum pump was changed to a larger, stronger pump to increase the internal pressure difference further (2018091101). Finally, TMA-pulse time was doubled to 600 ms giving rise to growth rates up to 0.25 nm/cycle (2018091201). This was considered sufficient, and a flask containing $SnCl_4$ was prepared inertly for deposition. The growth rate per cycle on the three substrates coated with Al_2O_3 is shown in **figure 35**. All parameters for the different depositions of Al_2O_3 are shown in **appendix table 3**.

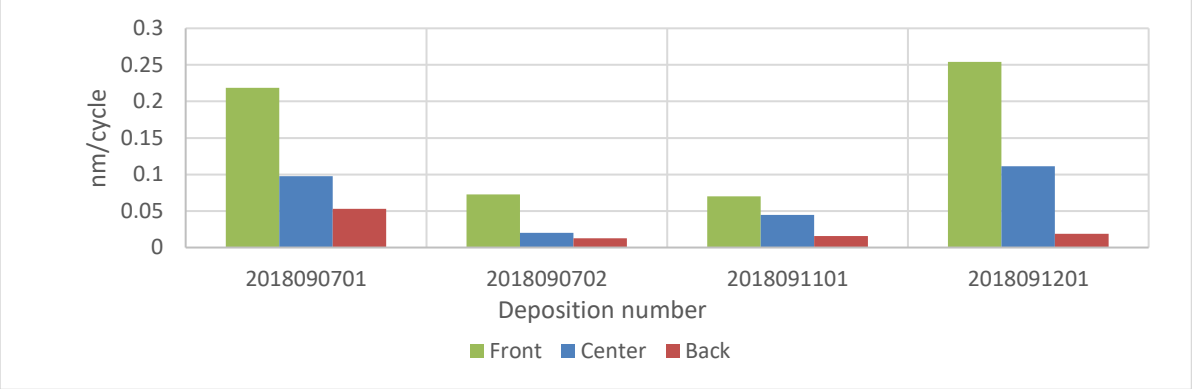

Figure 35 - nm/cycle development for Al_2O_3. All the parameters for each deposition can be seen in appendix table 2.

The line holding the Sn-precursor was fitted with a needle valve to give the possibility of restraining access. In the first deposition of SnO_2, growth rates of only 0.03 nm/cycle were obtained (2019092001). During the deposition, gas flows and pulsing times were optimized. Finally, a deposition rate of 0.05 nm/cycle were obtained on both the front and center substrate, ideal for covering entire emitters (2018101201). An in depth description of the optimization is giving in **section 7.2.1**. The final deposition parameters are shown in **table 17.**

Table 17 – Finalized deposition parameters achieved through optimization.

In-line flow, SCCM	**Flow around, SCCM**	**Valve opening**	**$SnCl_4$ pulse**	**Line purge**	**Purge**	**H_2O pulse**	**Line purge**	**Purge**
300	150	2 rounds	0.5 s	0.5 s	2.0 s	2.0 s	0.5 s	2.0 s

The entire optimization is shown in **figure 36**. For an overview of all the deposition parameters, see **appendix table 4**.

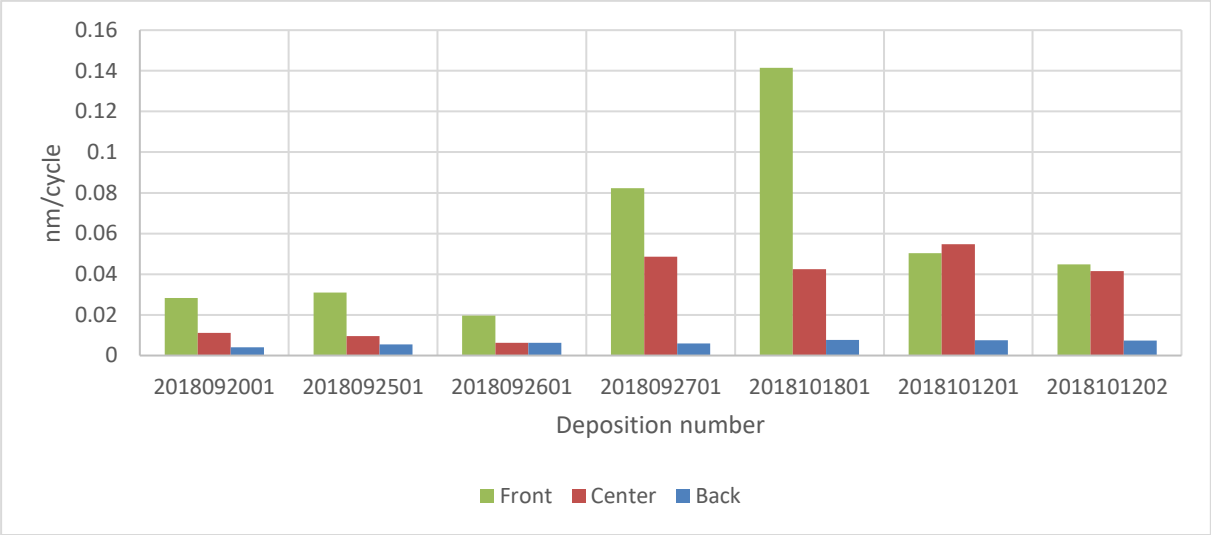

Figure 36 - Development of nm/cycle through the optimization of deposition of SnO_2. All parameters for the different depositions are shown in appendix table 3.

In the literature, growth rates of up to 0.50 nm/cycle are reported at 400 ˚C [89]. The question remains if the optimization for deposition of SnO_2 was sufficient. Several simple measures could be initiated. For example, the pulse length of $SnCl_4$ could be increased together with an increase in the opening of the $SnCl_4$-needle valve. An increase in growth rates up to 0.50 nm/cycle would yield faster deposition, lower consumption of precursor, and overall, be more economical and practical. Although these are reasonable arguments for a commercial production, here the focus was on the development of working emitters with narrow ID. Since this project has a finite deadline, time was deemed more valuable than the increased cost, and it was decided to move forward.

In an examination of the deposition temperatures influence on film resistivity for SnO_2, the resistivity increased up to 400 ˚C and decreased thereafter [89]. Deposition temperature has not been examined in this study, but if this trend applies to the high-temperature ALD-reactor used in this study, 400 ˚C may not be the ideal temperature for the deposition on emitters, as the conductive properties are those of interest.

Pulsing and purging times were varied to find a deposition program that would yield high growth rates. Gas flows into the reactor were varied to increase the area where growth was the highest. After optimization growth, rates of 0.05 nm/cycle were obtained on both the front and center substrate giving a large enough area to cover an entire emitter (in length).

4.2.2 Gradient test

Theoretically, the growth rate is affected by deposition temperature and should be highest at the warmest area in the oven, which should be in the center of the oven. The oven in the in-house built ALD-reactor used for this deposition was not optimized to deliver even temperature along the reactor. Subsequently, gradients of growth rate were expected as a function of temperature.

Additionally, turbulence in the pulsed gas could have altered the temperature gradient in the oven and is not easily controlled. Since correct simulations of fluid dynamics are challenging to achieve, an experimental approach was chosen.

As shown in **figure 37**, the deposed film was thickest on the left-hand side of the center of the oven, possibly due to higher relative concentrations during pulsing of precursors.

This indicated that the best position for the stand containing emitters is a little to the left of the center during deposition.

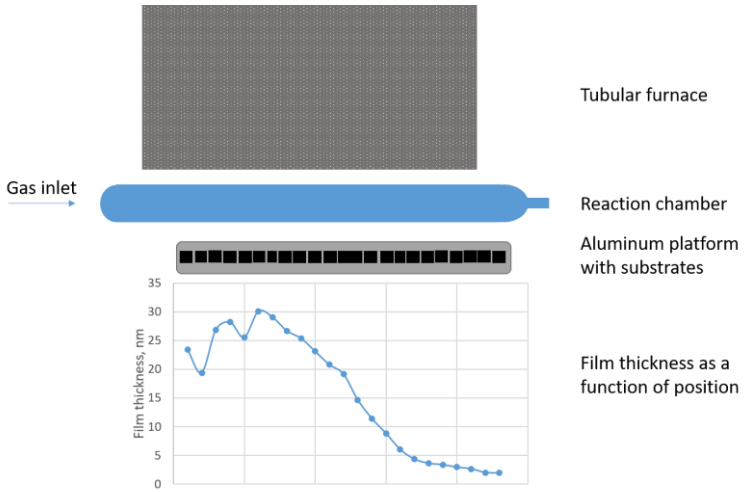

Figure 37 – Illustration of the setup during gradient test, shown with graph for film thickness as a function of position. All the different parts of the illustration are placed in the correct position relative to each other (along the x-axis). The points in the graph reflect the position of the Si-substrates.

4.2.3 Conductivity

Conductivity was measured because it is the most interesting property of a coating material for emitters. Conductivity was measured as current-voltage characteristics with a 4-point probe and a multimeter to log the data. A well conductive material gives a constant resistance

(voltage/current) as the voltage is varied. The method was only used to verify that the deposited materials were, in fact, conductive as this was considered the only relevant aspect regarding emitter fabrication. Subsequently, data from the measurements are not reported.

In situ measurement of conductivity

The *in situ* measurement of conductivity was especially interesting as it gave real-time data during a deposition, which otherwise is a largely "unseen" process. The intention was to shed light on how the film thickness would affected the resistance of the material.

As shown in **figure 38**, the resistivity decreases rapidly in the beginning and is inversely proportional to the film thickness. The gain in conductivity decreases throughout the experiment. The small bulge between 200 kohm and 100 kohm is believed to arise when the multimeter in use switches its range. The actual average trend was believed to follow a hyperbolic pattern, as if the bulge was not there.

The *in situ* experiment was believed to give reasonably accurate insight into what is happening during deposition. There are however two main differences from the glass slide to the emitters.

The deposition during the *in situ* measurement consisted of 600 cycles, while the deposition on emitters in the finalized method was 6000 cycles. In other words, the *in situ* measurement only covers a tenth of the entire deposition. Although the decrease in resistivity becomes smaller towards the end in the *in situ* measurement, an increase in number of cycles to a tenfold will significantly increase conductivity.

Film adhesion to borosilicate glass (slide) and fused silica is assumed different, but no flaking of the film has been observed, indicating that the adhesion is sufficient on both.

The smaller zoomed-in graphs in **figure 38** show an entirely different response to pulses and purges at the beginning of deposition and middle and end. It is important to note that the scale on the y-axis in the three graphs is not the same. The largest decrease in resistivity occurs in the beginning as the first layers of conductive material are deposited. Subsequently, as the last layers are deposited, the added conductive material is much smaller relative to the already present material. Hence, a much smaller response to pulses and an altered shape in the diagram.

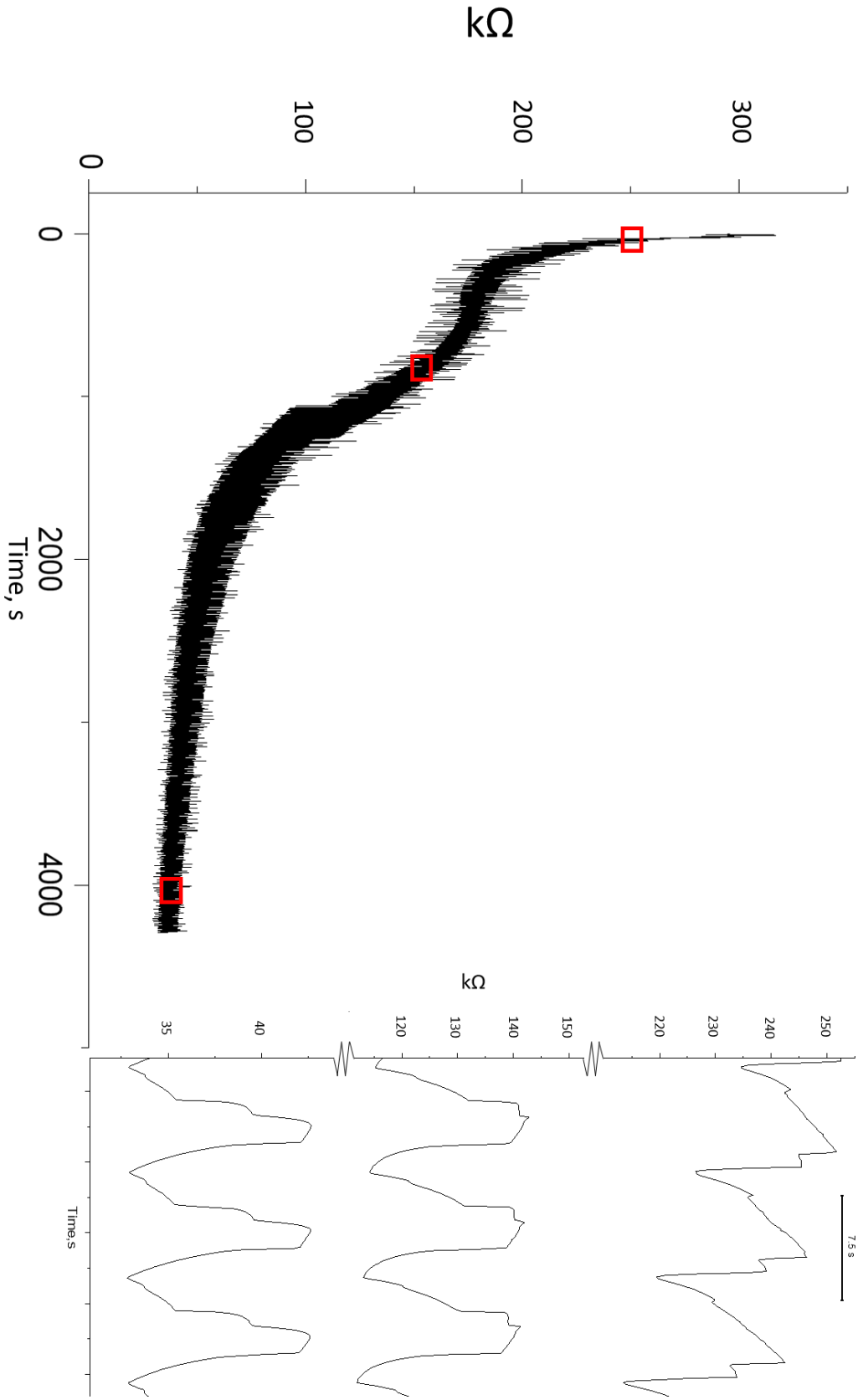

Figure 38 – Function of resistance (ohm) plotted against time. The red boxes indicate where a zoom has been made to closely analyze the response to each step in the cycle at the beginning, middle and end of deposition. Note that the intervals on y-axis in the last zoom are smaller than in the previous zooms.

The response to one sequence is shown in **figure 39** where also the instances of the individual pulses and purges are noted. The overall resistivity of the film increases upon pulsing of tin chloride, while it is notably reduced during pulsing of water. However, the resistivity is also increased during the subsequent purging of water. The net decrease in resistivity is slightly larger than the net increase, resulting in decreased resistivity as the film grows.

The response to pulsing and purging follows this pattern in the middle and bottom zoom in **figure 38**, but cannot be fitted to the top zoom. This indicates that a different mechanism of conductivity may be active at the beginning of the *in situ* measurement than later, when a thicker film is present.

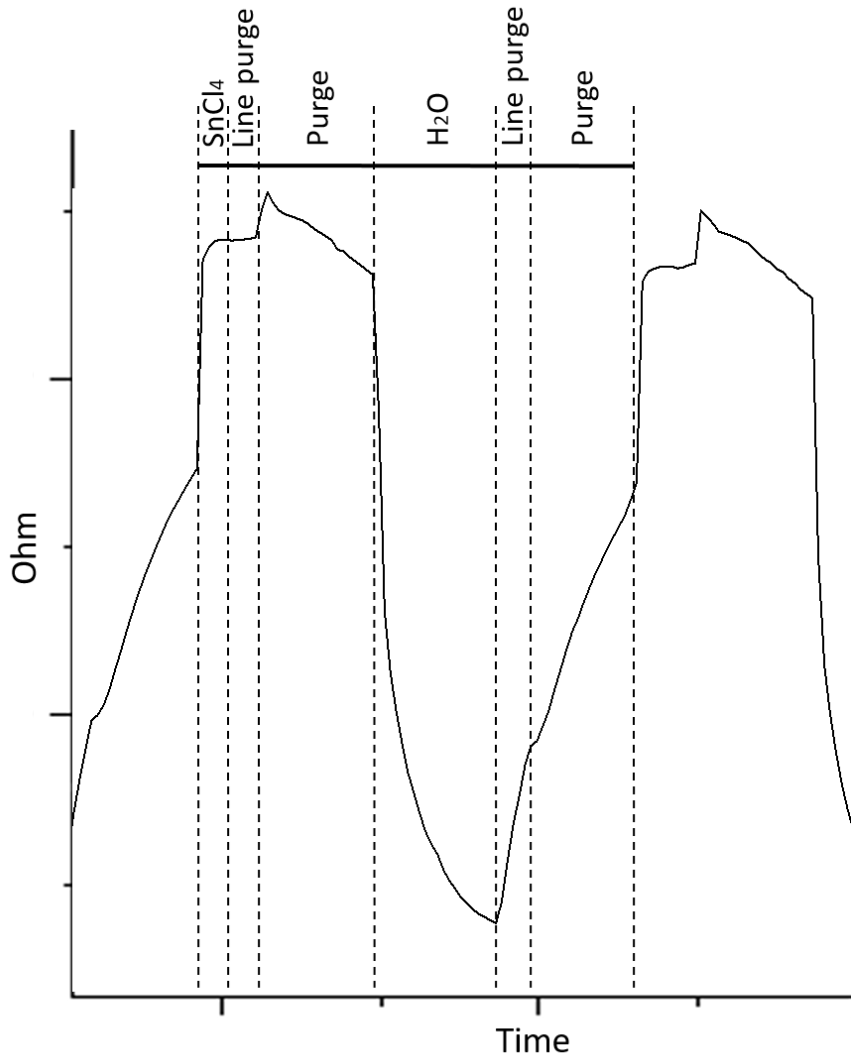

Figure 39 – Pulsing sequence with recorded response. The SnCl4-pulse increases the resistivity of the film, but once it reacts with the water to form SnO2, the resistivity decreases below the lowest previous point.

To sum up: *Two different coatings have been examined. A Nb-doped TiO_2 coating was first attempted, but no conductivity was achieved and results found in the litterature could not be replicated, likely due to a leak in the reactor chamber where moisture was leaking in. Further work on this coating was therefor set aside in favor of a SnO_2-coating. Because higher temperatures were needed for proper growth of this coating, a high-temperature ALD reactor was used.*

After an optimization, a gradient test along the axis of the reactor was carried out to determine the best location for emitter coating. An in situ measurment of conductivity revealed real-time data on film properties and the response to the different pulses and purges.

4.2.4 Emitters

Successful, etching of fused silica capillaries was performed as described in previous work [75].

After deposition of the coating using the optimized method, a few visual changes could be seen. The polyimide coating on the fused silica had changed color from amber to a dark brown-blackish color due to high temperature (400 ˚C in the furnace).

Characterization of deposition using substrates

During deposition, a glass substrate and two silicon substrates were placed below the emitter tips for accurate measurement of film thickness and conductivity of the film because these parameters are difficult to measure on very narrow (OD 360 µm) cylinders.

Variance between the batches was observed. Three batches with 1500 cycles were made. The top and bottom substrate of the first batch (2018112601) had films with thicknesses of 76 ± 6 nm and 95 ± 3 nm, respectively. The second batch (2018121401), in comparison had average thicknesses of 89 ± 3 nm and 86 ± 3 nm for top and bottom substrates, respectively. The third batch (2018121701) had film thicknesses of 80 ± 8 nm and 80 ± 4 nm for top and bottom substrates, respectively. The measured resistance for all these batches varied between ≈ 3-16 kΩ, depending on the measuring point. No pattern or trend was observed in regards to measuring point.

The number of cycles was increased to 6000 because a thicker film theoretically would give higher conductivity because there is more material to conduct electrons. Another reason is that it was believed that a thicker film would give more physically robust emitters.

Two batches of ALD-coated emitters with 6000 cycles were made (2019021901 and 2019022001). The measured film thicknesses were 293 ± 32 nm (top) and 365 ± 12 nm (bottom) for the first batch and 266 ± 38 nm (top) and 333 ± 35 nm (bottom) for the second batch. The measured resistance was 771 Ω and 101 Ω for the first and second batch, respectively, an apparent reduction from the depositions with only 1500 cycles. The resistance was measured in approximately the same spot.

The variation in thickness and resistance was caused either by poor repeatability or by varying position of substrates in the stand or varying placement of the stand in the reactor chamber. The addition of an aluminum piece/rod attached to the back end of the stand could function as a spacer to ensure fixed placement of the stand in the chamber, but this was not done in this study. Gradients have been observed in every deposition both across and along the axis of the reactor. It is likely that this, in addition to the varying placement, causes the variations.

With 1500 cycles, film thicknesses from 76-95 nm were obtained on the substrates. Measured resistance varied from 3-16 kΩ. By increasing the number of cycles to 6000, the resistivity decreased to 0.1-0.7 kΩ with film thicknesses of 266-365 nm. Both radial and longitudinal gradients have been observed, meaning that variations could have arisen due to varying placement of substrates in the reactor.

4.3 Testing of emitters using mass spectrometry

4.3.1 Testing with flow injection

Coated emitters were tested using the method described in **section 3.8.2**. Many of the emitters broke upon placement and during handling. This could have been minimized by making the etching window on the capillary smaller, resulting in less fragile emitters. However, this is not easily achieved. One of the problems with removing parts of the polyimide coating was that although the entire emitter was coated, an edge was still visible where the polyimide ends. At this edge, the coating is the most fragile, and the emitter broke easily in this spot.

Where on the emitter the electrode providing the current should be placed is debatable. While contact with the polyimide-coated part would need the current to flow over the edge, it provides a robust section where the emitter will not break. Contact at tin oxide coated fused silica would provide the best properties for the flow of electricity, and also ensuring that the distance the current has to travel in the material is minimized, but the electrode would be placed at an extremely fragile section, and the placement itself can break the emitter.

Issues with the fragility could perhaps be overcome by placing the emitters into a conductive tube (e.g. steel tubing), slightly larger than the emitters OD, so that only the tapered tip sticks out. A conductive gel inside the tube could ensure contact. Another option could be to deposit a soft, conductive metal directly on the capillaries, like the gold coating developed by Zhu *et al.* [76].

During testing, emitters were left for up to around 2500 min or until they stopped working. All emitters that delivered spray worked for a minimum of 1000 min. Because many emitters broke during handling, no clear pattern to the function with regard to placement in the deposition stand was observed.

Out of the ten emitters that were coated with 6000 cycles, six broke. The remaining emitters were functional.

Figure 40 shows the TIC of an emitter providing stable spray for 2700 min. The TIC of two more emitters is shown in **appendix figure 7**.

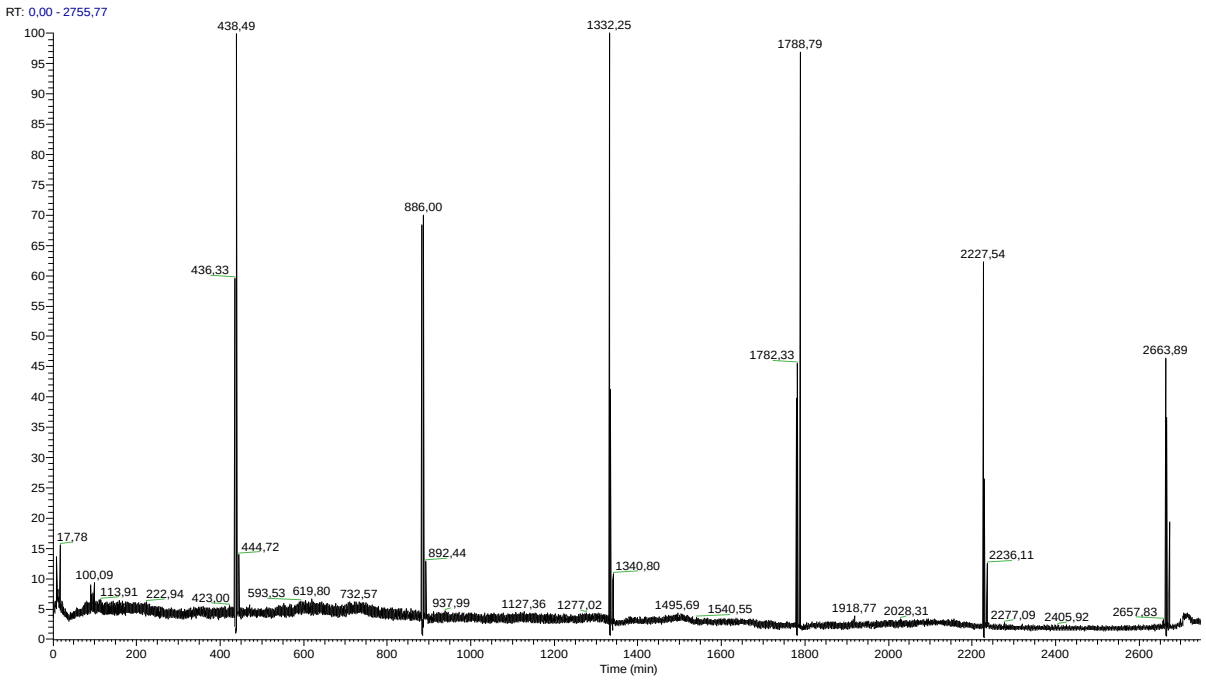

Figure 40 – Recorded TIC of an emitter providing stable spray for over 2700 min using the flow injection testing system. The periodical spikes were caused by the syringe pump stopping to refill.

4.3.2 Comparison between commercial steel emitters and in-house prepared emitters

Emitters were tested in a nanoLC-system with a 4 cm pre-column and a 12 cm long separation column, (both with 75 µm ID) consisting of a silica monolith with a C18 stationary phase. Injections of 2 µL 50 pM heroin were used, and the flow rate was 0.40 µL/min.

The performance of in-house made fused silica emitters was compared to that of commercial SS emitters. An attempt to test against commercially available fused silica emitters was also made, but the entire package, which was opened two years before the experiment, was not functional anymore. Overlayed chromatograms obtained with an in-house fabricated emitter and a commercial SS emitter are shown in **figure 41**.

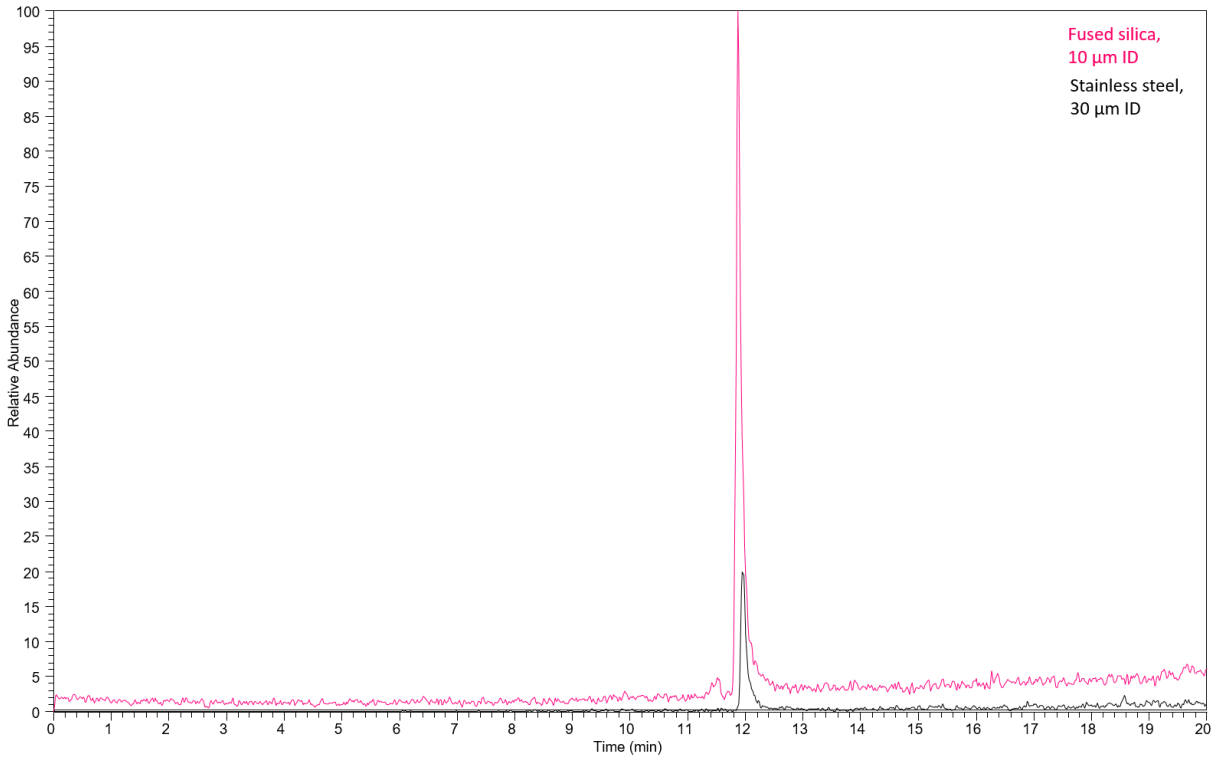

Figure 41 – Overlay MRM of chromatograms from 2 µL injections of 50 pM heroin using in-house prepared fused silica emitter (pink) and commercial SS emitter (black). The flow rate was 0.40 µL/min.

The commercial SS emitter shows much lower peak intensity than the in-house fabricated fused silica emitter, but the noise scales in the same manner. To compare the performance of the two emitters, the signal to noise ratio was calculated. Data from the emitter that was placed in the middle of the deposition stand was used. For the SS emitters, only one emitter was tested with three replicates. For comparison, only chromatograms from the middle (in the deposition stand) in-house made emitter were used. Because of the tedious manual calculation of signal-to-noise (s/n) ratio, only the last three replicates (8-10) were used. The rest were just visually checked to determine that the noise level and peak height were similar, which they were.

The average s/n was calculated to be 48 ± 6 and 36 ± 3 for SS and in-house prepared SnO_2-coated fused silica, respectively. The average noise was calculated by measuring the minimum and maximum 1 minute before and after the peak. For the fused silica emitters a small peak, which is also visible in **figure 41**, seemed to elute right before the heroin peak at ≈ 11.5 min. This peak was excluded from the measurement of noise maximum and minimum.

An F-test was performed in Excel and revealed that the variations were unequal. Subsequently, a two-tailed t-test was performed. The two-tailed t-test revealed that the two data sets were significantly different.

The peak area of the heroin peak differs quite a lot between the emitters. The simplest explanation for this is that with a smaller ID emitter, smaller primary droplets are formed in the electrospray process. This leads to higher ionization efficiency as less solvent needs to evaporate from each droplet before only free ions in the gas phase are left. The area of the peaks in **figure 42** was calculated with Xcalibur. The in-house prepared SnO_2 coated fused silica emitter (area=7670) gives more than six times larger peak area than the SS emitter (area=1243). The peaks with their respective areas are shown in **figure 42**.

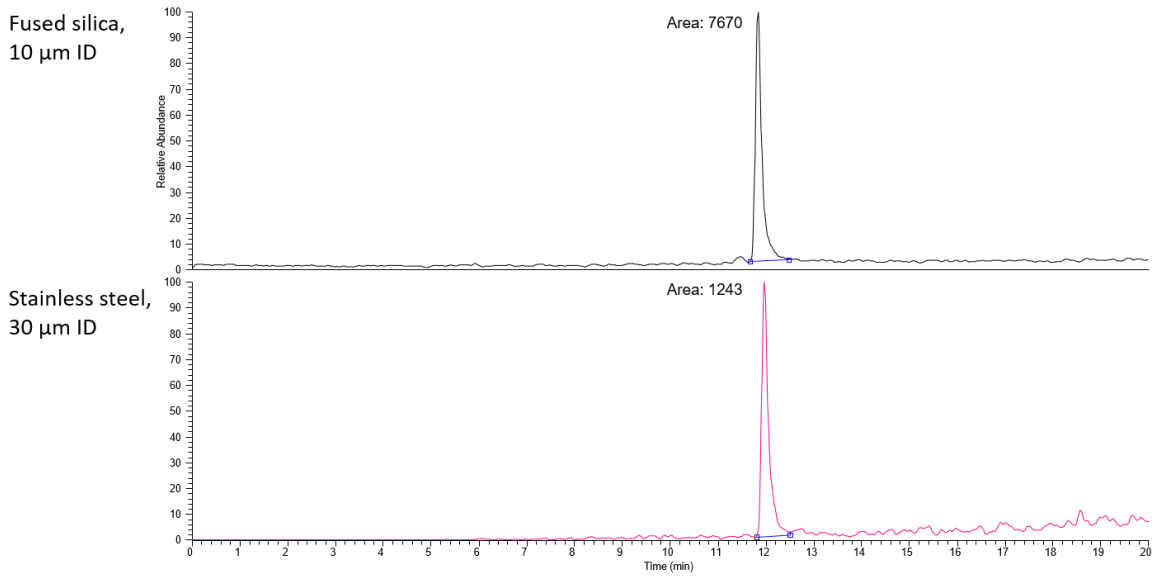

Figure 42 – Comparison of peak area of heroin obtained with an in-house fabricated fused silica emitter and commercial SS emitter. The fused silica emitter shows more than six times larger peak area. The nanoLC testing system was used.

One of the significant critiques against this comparison of emitters is that the size of the column does not dictate the use of a different emitter than the conventional SS emitter. They have a large advantage in terms of robustness and ease of handling as they do not break but rather bend without breaking.

The in-house prepared fused silica emitters coated with tin dioxide should be tested against both commercially available fused silica emitters and SS emitters using nano- or OT-columns ≤ 30 µm ID to ensure conditions where they are needed. The SnO_2 coated emitters should also be tested against previously made gold-coated emitters [75].

***In summary**: The SnO_2-coated in-house fabricated fused silica emitters seemed to perform well under the conditions tested, but should be tested with sub-30 µm ID columns. The work with*

the smallest narrow columns is difficult, but necessary for ultra-low sample sizes. These emitters, together with the previously developed gold-coated emitters give scientists who need them an improved tool, as commercially available emitters are not available at the preferred ID.

The etching approach is suitable for all capillaries with 360 µm OD. This means that emitters of any size ID can be produced as long as capillaries exist with 360 µm OD. The etching method should also function with other ODs, but this has not been tested. The ALD-coating procedure also fits all sizes and is not limited to capillaries, but for example, chip-designs or channels could also be coated.

4.4 Preliminary testing with a commercial chip platform

The goal of this part of the study was to develop an on-line OoC-LC-MS platform. A simple commercial chip was purchased to see if such a simple device could be used until platforms that were more sophisticated became available.

Initial testing revealed problems with leakage from the organoid well of the BIOND-chip (see **figure 43**). After closer examination, the flow rate used (up to 200 µL/min) was too large, forcing a lot of the medium through the PDMS membrane up through the organoid well, overflowing it. As the flow was lowered towards and below 20 µL/min, the well was still overflowing. This problem was solved by placing a piece of tape above the well for sealing (as indicated in **figure 43**).

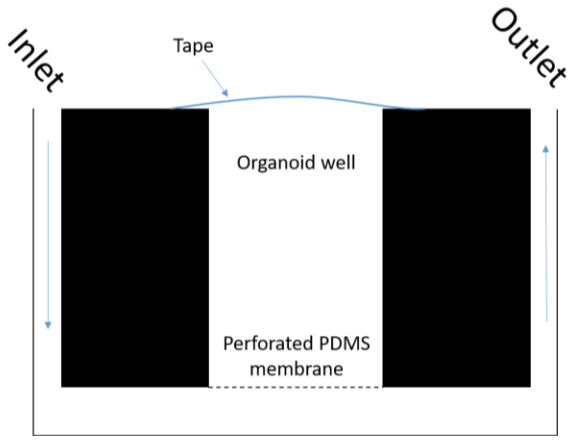

Figure 43 - Simplified drawing of a cross-section of the commercial chip.

With the tape in place, with flow rates of 20 – 70 µL/min, no leakage was observed as setup 1 was used.

The pressure arising from either the outlet tubing from the UV-flow cell or the UV-flow cell itself caused the PDMS-membrane to break in setup 2. In order to be able to test the other parts of the system, the chip was removed and replaced with a plastic union. This chip-less system did not show leakage and 2 µL of a fluorescein solution was injected twice. Unstable pressure due to the lack of sufficient backpressure for the pump caused much drifting of the flow rate and UV-signal. The resulting signal as a function of time is shown in **figure 44**.

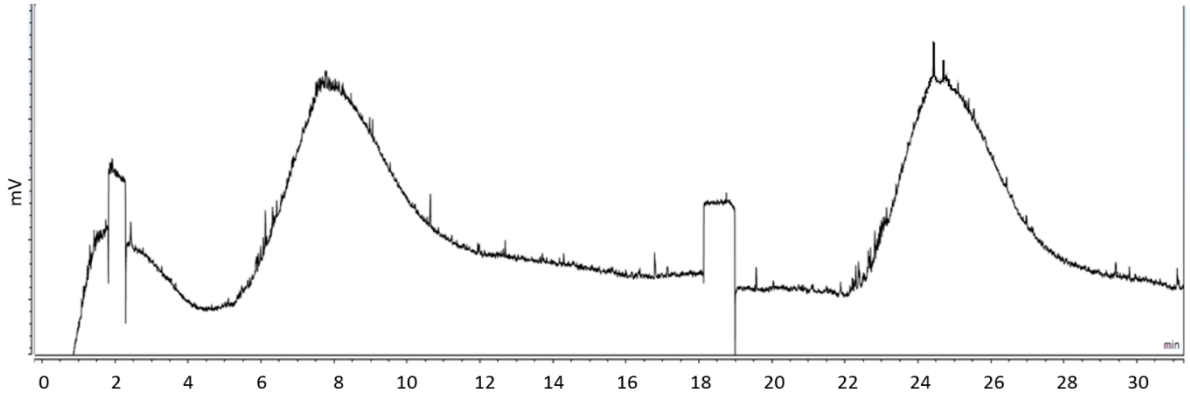

Figure 44 – UV absorption at 230 nm as a function of time for two injections (2 min and 18 min) of fluorescein. The switching of the injection valve can be seen as the two plateaus.

The injected band was only 2 µL (corresponding to ≈ 2.4 s at 50 µL/min), but the peaks were much broader (≈ 6 min), indicating that considerable band broadening had occurred. This is not ideal for drug measurement in an OoC-system where very low concentrations will be present.

In setup 3, a new PDMS membrane was fitted to the chip, and the 6-port injection valve was placed behind the chip. The UV-detector was removed. The reason for moving the valve behind the chip was that for sampling in the complete system, a loop was going to be used. The chip needed to be able to withstand pressures arising from such a setup. The flow rate was set to 20 µL/min, and the chip, still with tape over the well, did not leak at the arising pressures.

The flowing medium was subsequently changed to the organoid medium (from the Sullivan lab) to see if a change in viscosity would affect pressure, but the chip did not break or leak, when using medium. Although the chip did not break or leak, keeping biological material in an open well, with a piece of tape preventing it from overflowing was not providing the robustness such a system demands. A flow through approach where organoids are kept in a closed tube or

chip where medium flows through seemed like a better option. Further work on the commercial chips was therefor put aside.

A commercial chip with an open well to culture organoids was tested at various flow rates. The chip overflowed easily, but this was solved by placing a piece of tape over the well. The chip had a flexible PDMS membrane that broke upon being subjected to back pressure from a UV-detector. Since cultivating biological material in an open well is not ideal, the work on thus chip was put aside in favor of closed alternatives.

4.5 Glasgow chip in an on-line fluidic platform

The LC-UV studies performed are to be regarded as preliminary experiments as the goal, from the beginning, was to move to a LC-MS system. Early during the study, it was understood that a valve system would be necessary to combine the biological low-pressure side, with the high-pressure side of LC. It was clear that the organoids should not be subjected to high pressures at any time, and sampling onto a loop, which further could be a part of the high-pressure side utilizing a valve seemed ideal. To avoid loss of metabolized medium, a second loop could be filled while the first was sent to analysis. This loop switching system resembles a traditional 2D-LC setup, and is shown in **figures 27, 29 and 30**.

For connection of OoCs to the fluidic system (chip-LC-UV system), in-house made connectors, shown in **figure 26**, were used. Solutions of uracil and caffeine were used initially to establish the chromatographic performance of the short C4 column. HSA was used to resemble the albumin content present in the organoid medium. A mixture of the three was used to verify and develop the method. In **appendix figure 8**, one of the resulting chromatograms from injection of an 18 µM heroin, 6-MAM, M3G and M6G solution is shown. This solution was used to verify that the developed method could separate the metabolites. Only two peaks were observed, most likely due to non-optimized wavelength for the metabolites.

A 1 mm ID column was used to ensure higher robustness compared to more narrow formats. Because most proteins are larger than the pore size of the column particles used (100 Å), it was believed that proteins would be excluded from the particles and go through the column outside the particles, similar to size exclusion chromatography. By choosing a low hydrophobicity stationary phase like C4, proteins would not get significant retention on the outside of the particles. The low hydrophobicity of the stationary phase would also affect the chromatographic

performance for the metabolites of interest, but proteins were seen as the main problem because they would give large ion suppression and also clog the column. Since the main goal was to couple the chip to MS, which is mass selective, lower performance chromatography was acceptable as long as most proteins could be separated from the analytes.

Restricted access medium columns have existed for quite some time [100, 101]. These only have stationary phase on the inside the pores. In theory, they would be ideal for a task like this, as the size exclusion functionality would remove most of the larger proteins from the metabolites of interest, but it was difficult to find an appropriate column material commercially.

The chromatograms of the FBS-free medium and organoid medium containing heroin, using the chip-LC-UV system, showed low repeatability, and pressure issues arose quickly, indicating clogging of the column. Since the pump had an upper-pressure limit of 400 bars, many runs had to be stopped, and much time was used for washing with gradients and high organic content mobile phase. One major problem with samples with very complex matrices like organoid medium is that the UV-detector does not have any possibilities for sorting out certain substances, and it does not either give any information about what elutes from the column. Since these were preliminary experiments to get experience with the chip system, this was thought to be a temporary problem until using MS for detection.

4.5.1 Organoid trapping and alternatives to using a chip

Since making organoids is a time-consuming task, loading the "Glasgow-chips" was first attempted with 150 µm polystyrene beads at various flow rates. The beads were dispersed in PBS and water. The loading of the beads was monitored visually through a microscope. No trapping of beads was observed.

The same was attempted with hepatic organoids from the Sullivan group. Like the beads, the organoids moved through the chip without being trapped. Although some organoids got stuck at the entrance and exit ports of the chip, this was deemed insufficient.

Since the simplest OoCs consist of just a channel that can contain a population of perfused tissue, no reason was found why this should not be possible to do in a tube without the surrounding chip. Separation scientists have long experience of packing chromatographic

columns with particles. A similar but modified approach was therefor used to pack the organoids into such a column housing. Organoids are after all circular living particles.

A sampling and injection valve system was developed for on-line analysis of medium from an OoC. The "Glasgow chip" was connected to the fluidic system using in-house made connectors. Through coupling this setup to a chromatographic column with C4 stationary phase, the possibility of separation was achieved. Injections of various samples were used to develop a chromatographic method.

The trapping of organoids was tested first with polystyrene beads and with organoids. In both cases, the particles were not retained on the chip as intended.

4.6 Organ-in-a-column as an alternative to organ-on-a-chip

4.6.1 Packing an organ-in-a-column

The housing consists of PTFE tubing (1/32" x 5 cm), SS nuts, unions, ferrules and 1 µm filters. To prevent clogging and pressure build-up, a loose packing of organoids was preferred. After trying to push dispersed large organoids into the tube with a syringe and doing the same with a syringe pump at relatively low flow rates (5 µL/min), it was discovered that the number and size of organoids was crucial for the packing. Large organoids (visible and > 300 µm in diameter) would easily cause clogging and backpressures, but they sank in solution and could easily be packed even without flow. As long as the column and connection to the syringe were filled with medium, the organoids could sink into the column.

Columns with smaller organoids seemed to be less prone to clogging and the organoids could be loaded with a syringe pump at flow rates of around 100 µL/min without clogging. Another critical factor was to use the column with the flow in opposite direction to that during packing. The idea was that this would push organoids stuck to the filter out into the solution. Placing the column in vertical position so that the flow would go against gravity was also attempted. It was believed that this could keep the organoids suspended, flowing up and down in the tube. Organoids flowing up and down along the column was observed for a short time and seemed to function, but how long this effect lasts and at which flow rates is unknown.

The main problem regarding packing an OiC is that the amount of biological material is challenging to measure as organoids differ in size and concentration. The best way is probably to count organoids in solution. As long as organoids in solution are created from a fixed amount of cells, the total cell amount in 1 mL should be the same every time. It is important to note that the number of organoids and their size are inversely proportional, since large organoids consist of more cells and smaller organoids of fewer cells.

4.6.2 On-line liquid chromatography UV detection with organ-in-a-column

To test the OiC, it was coupled into the OiC-LC-UV system described in **figure 29** instead of the chip with its connectors. In this system, the syringe pump delivered the organoid medium at 2.5 µL/min and the LC pump was run at 100 µL/min with a gradient program. The main goal of this experiment was not the separation and detection itself, but to test the viability of the organoids at operational conditions (37 ˚C in water bath, syringe pump flow, retainment of organoids in the housing, etc.). The medium is such a complicated matrix that UV detection is not suited without any sample cleanup.

One of the resulting chromatograms from an injection of organoid medium containing heroin is shown in **figure 45**. It looks incredibly messy and does not give much information other than that there was some separation accruing. Ten injections were made. The repeatability was low, probably due to carry-over/too-short run time.

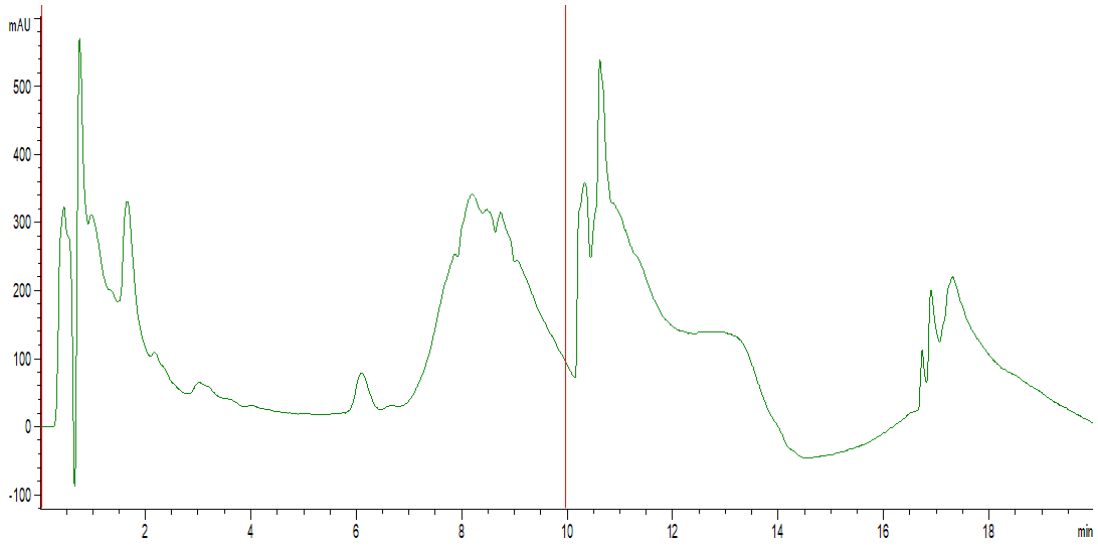

Figure 45 – UV-Chromatogram (210 nm) of two injections (indicated by red line) of organoid medium containing 1 µM heroin.

As the column was flushed with 100% MP B, after the ten injections, something eluted, indicating that a strong wash step should be added to the method.

The OiC was then disassembled, and its content and filters were examined with a light microscope. As shown in **figure 46**, organoids had been retained by the filters and held their shape throughout the experiments indicating that they might survive the treatment.

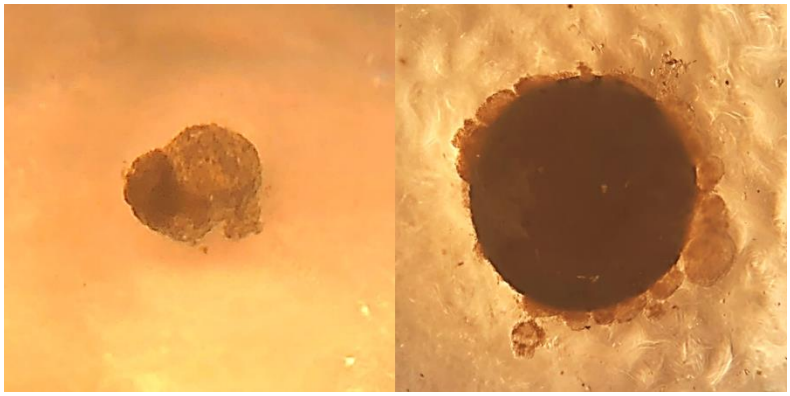

Figure 46 – Pictures of organoids after use in an OiC. Left: Single organoid from inside the column, held its circular shape throughout the experiment. Right: Filter (1/16” diameter) with many retained organoids, with circular shape still intact.

4.6.3 On-line measurement of heroin metabolites with liquid chromatography mass spectrometry

During optimization on the MS, the most crucial factor was considered the ability to separate heroin, 6-MAM, and morphine from other compounds like proteins to avoid ion suppression. Injections of samples with increasing complexity were therefore thought to reveal problems at an early stage.

A chromatogram (using the OiC-LC-MS system, with an empty OiC) from two injections of 1 µM 6-MAM and morphine in organoid medium is shown in **figure 47**. Elution of 6-MAM and morphine occurred approximately 1 minute after injection. Most notable is that the intensity of the 6-MAM peak was more than six times greater than that of morphine. Part of this problem could be solved by separating the two compounds from each other.

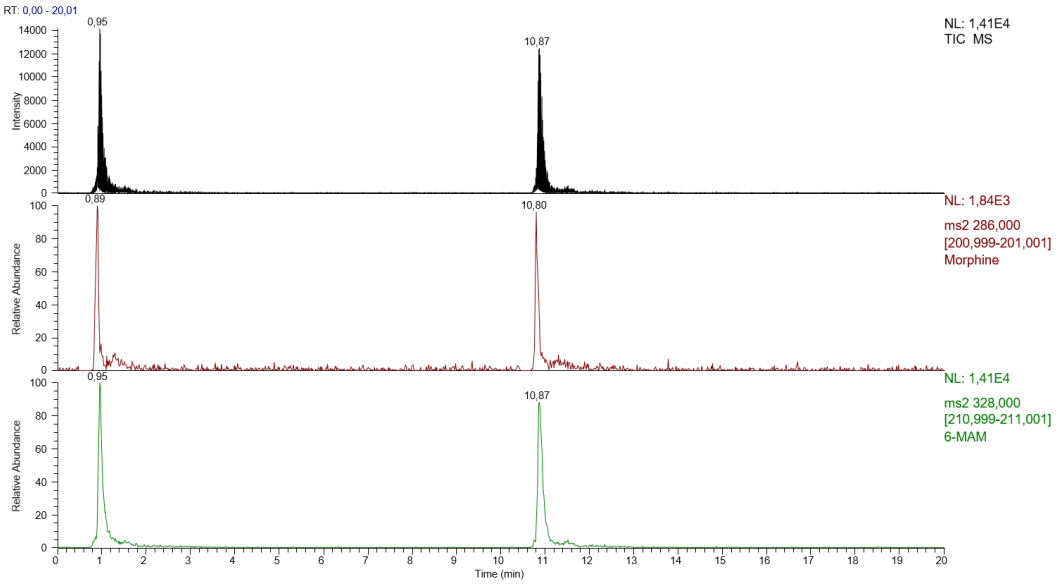

Figure 47 – MRM chromatograms of organoid medium containing 1 µM 6-MAM and morphine using an empty OiC-LC-MS system (without organoids). The extracted chromatogram for morphine is shown in red (middle), while the extracted chromatogram for 6-MAM is shown in green (bottom). Note that the intensity of the 6-MAM peaks is more than six times greater than that of morphine. Sample was injected at 0 min and 10 min.

The main goal of this study was to develop a proof-of-concept system for on-line analysis of organ-on-a-chip. Chromatographic issues as co-elution could, therefore largely be overlooked as long as the MS could measure the analytes. The chromatography then serves its purpose mostly as a way of separating the analytes from the main part of the matrix, while the MS separates the analytes from each other based on mass-to-charge ratio.

Robustness - retention time and peak area of 1 µM morphine

To test the robustness of the system, 96 injections (48 runs) of 1µM 6-MAM and morphine in medium was performed. The retention times were plotted as a function of injection number. As shown in **figure 48**, the retention time of the compounds remained relatively stable over 96 injections with an average of 0.88 ± 0.04 min and 0.96 ± 0.06 for morphine and 6-MAM, respectively. The difference in retention time between the two compounds was measured to be only 0.09 ± 0.03 seconds on average. The chromatographic method should be altered to facilitate baseline separation to avoid inter-analyte ion suppression. The zigzag pattern that is observed when plotting the retention time is due to a longer way from one loop to the MS than from the other.

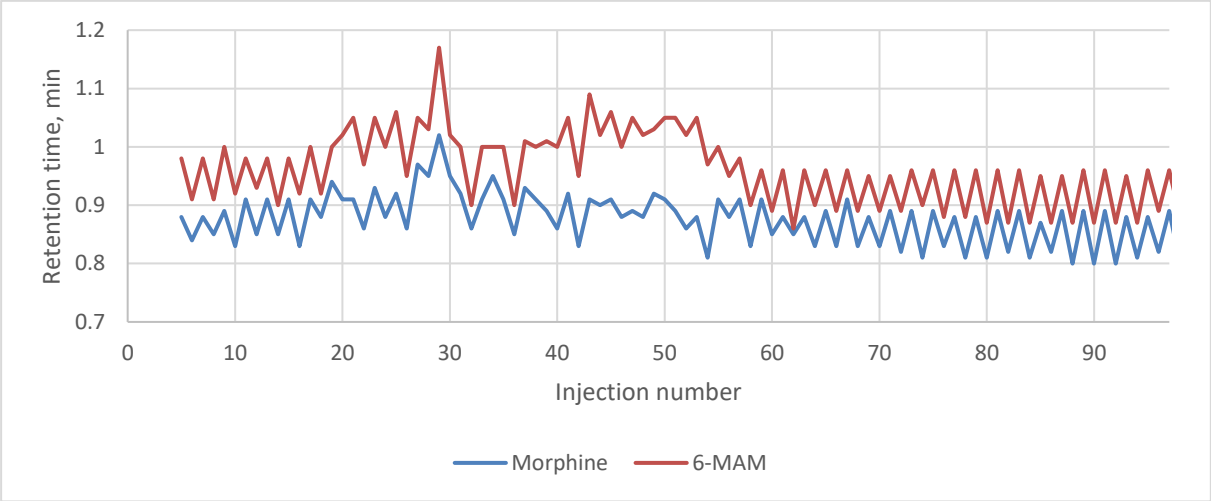

Figure 48 – Plot of retention times of morphine and 6-mam as a function of injection number. The retention time varied little throughout 96 injections, but the compounds themselves should ideally be further apart. The zigzag pattern is because one loop has a slightly longer way to the MS than the other does.

When peak areas were plotted as a function of injection number, a steady decline was observed, as shown in **figure 49**. Because the organoid medium is such a complex sample packed with proteins and nutrients, it easily leaves deposits in the ion transfer tube. After the 96 injections, the orifice in the tube was almost entirely clogged by burnt medium residue.

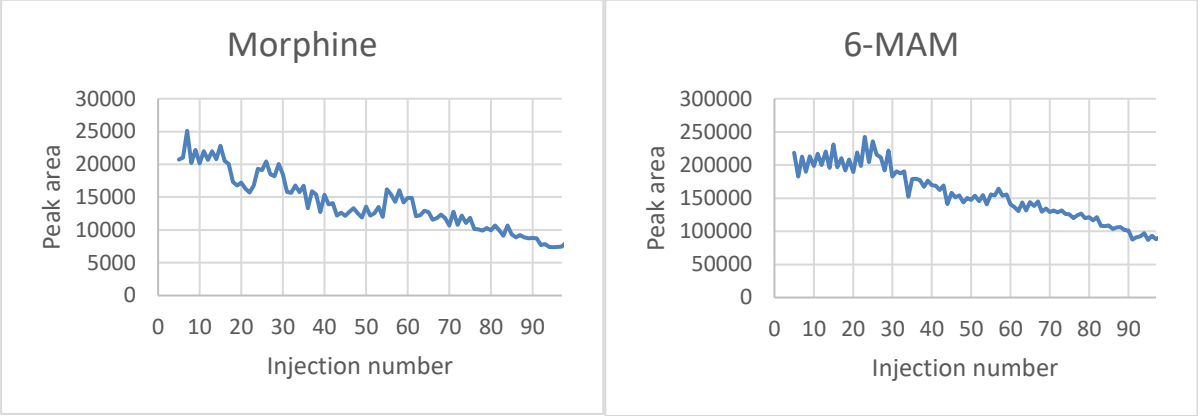

Figure 49 – Peak areas of morphine plotted against injection number.

A replication of the experiment with MeOH as the organic modifier instead of ACN was attempted, but the pump stalled every time due to pressure. Something likely precipitated in the MP with MeOH that was soluble in the ACN containing MP, as clogging also happened when the flow rate was lowered. This was the only experiment conducted with MP C. In all subsequent experiments, MP B (ACN) is used.

On-line experiments with organoids

Three experiments were performed using the complete OiC-LC-MS system with organoids. In the first experiment, a syringe pump flow rate of 1 µL/min of organoid medium (containing heroin at a concentration of 1 µM) was used. No morphine was detected, but both heroin and 6-MAM were detected. This is likely due to spontaneous decomposition of heroin to 6-MAM as the syringe with medium was subjected to room temperature during the experiment. The flow rate of the LC-pump was reduced to 50 µL/min because of pressure issues after the above-mentioned previous experiment with MeOH in the MP.

Too high flow rate over the organoids was believed to be the reason for no detectable morphine. An approach where the syringe pump was turned off for two hours to allow enrichment of morphine was tried, but no morphine was detected.

In the final experiment, a flow rate of 12.5 µL/h was used for the syringe pump supplying medium. The heroin concentration in the medium was increased to 100 µM. Since the flow rate of the syringe pump, filling the loops, was decreased substantially, the gradient program had to be changed as well. To avoid excessive consumption of MP, the LC-pump was turned off for 40 minutes. A total time of 120 minutes per injection was used. To prevent further clogging, a 40 min wash step was also added.

This final experiment was promising, showing considerable concentrations of morphine in every injection of metabolized medium. An MRM chromatogram of morphine is shown in **figure 50**. The peak height and area increased substantially throughout 22 injections, as shown in **figure 51**, for both 6-MAM and morphine. There are two possible explanations for this phenomenon. The increase in morphine is due to either slow kinetics or upregulation of metabolizing enzymes. Due to messy chromatograms with low signal for heroin, no peak was distinguishable from the noise. The increase of 6-MAM likely is due to the metabolism and spontaneous degradation of heroin. Perhaps the transport of heroin and 6-MAM into the cells and morphine out of them is slow. The other option is that the hepatocytes upregulate the expression of the enzymes responsible for the metabolism of heroin and 6-MAM. As the concentration of these enzymes increases, the metabolism also increases. A qPCR-analysis or targeted proteomics of the organoids could reveal this. A combination of the two mechanisms is also possible.

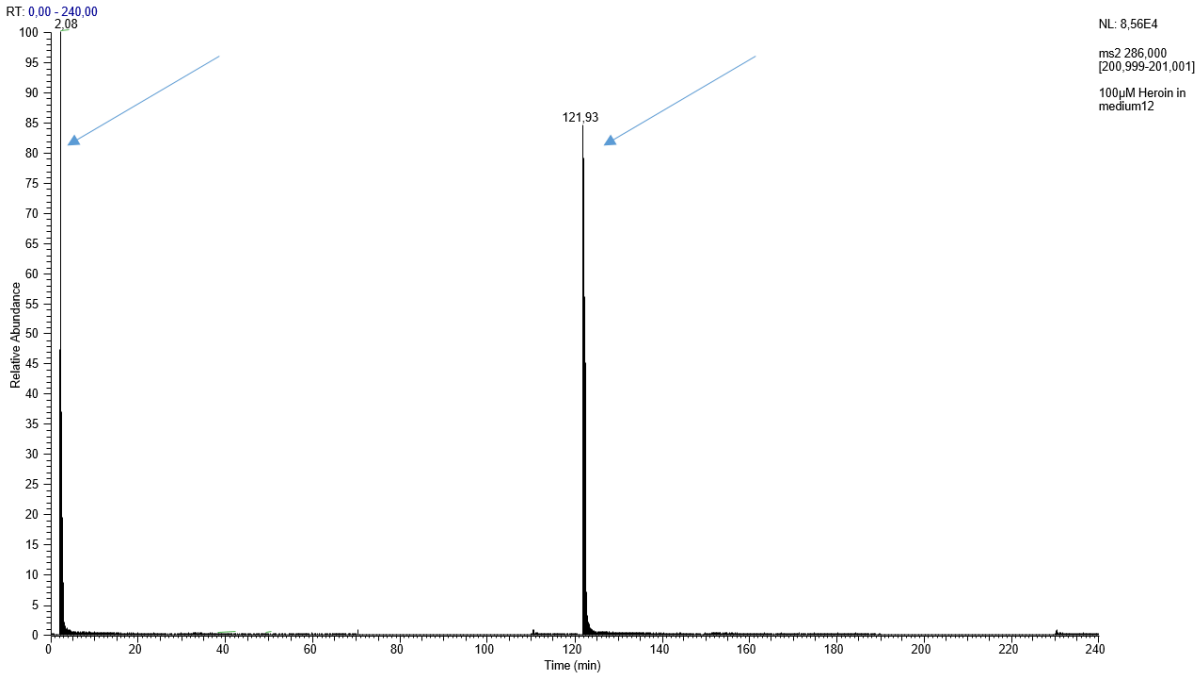

Figure 50 – MRM chromatogram of two injections of medium containing 100 µM heroin exposed to organoids. Peaks of morphine at 2.08 min and 121.93 min. Injections were performed at 0 and 120 min.

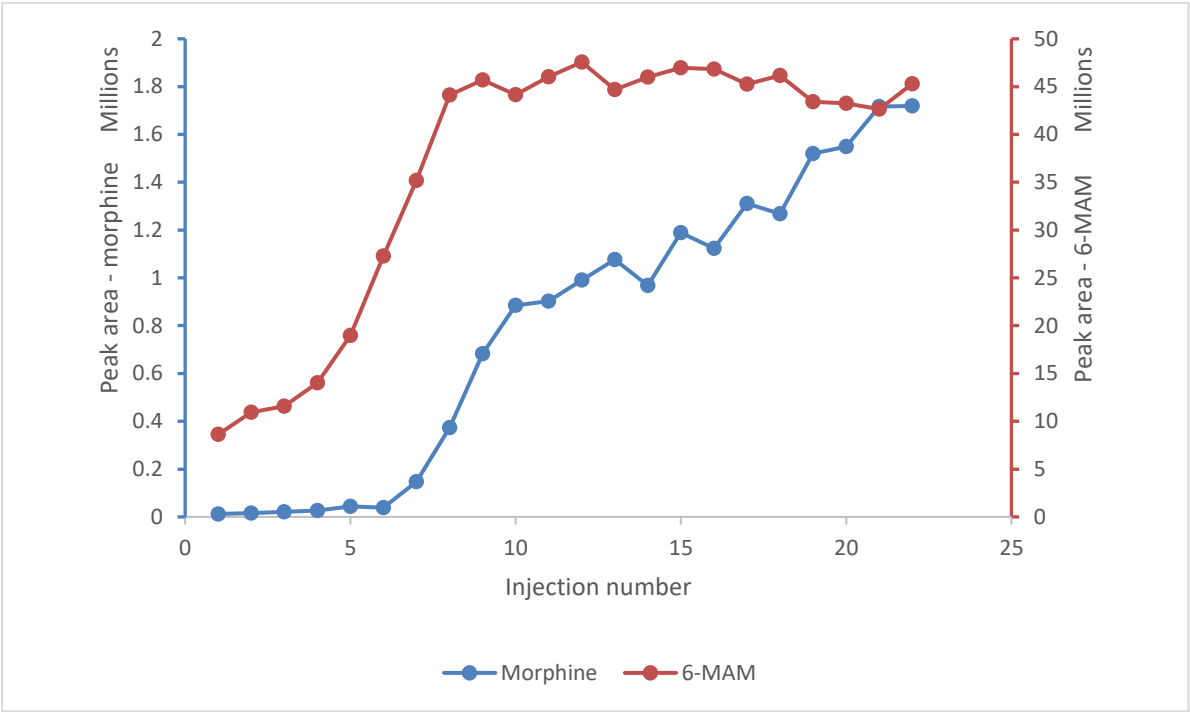

Figure 51 – Peak area as a plot of injection number. Peak area of morphine and 6-MAM is increasing substantially throughout 22 injections.

The retention time of remained quite stable throughout the experiment. The same zigzag pattern as earlier was observed during experiment as well because of varying length from the two-loop to the MS. A plot of the retention time is shown in **figure 52**.

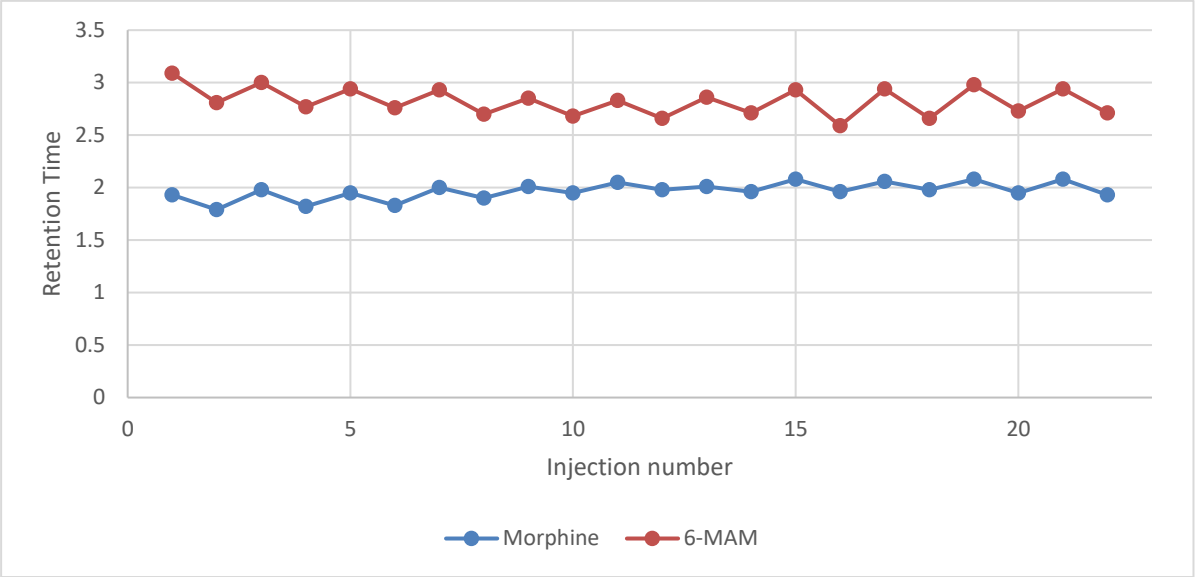

Figure 52 – Plot of retention times for morphine and 6-MAM from the 22 injections made.

Activity and kinetics

The size, age, and number of organoids used for making an OiC should be examined. Larger organoids are usually older, as cells and organoids aggregate over time. These larger organoids should have the possibility of metabolizing larger quantities of compounds, but the transfer of both nutrients and substrates may be limited into the center, and slow kinetics could affect metabolism experiments. On the other hand, large, old organoids may exhibit a more mature human-phenotype, more closely mimicking primary tissue.

By using small organoids in large numbers, kinetic issues may be overcome, and cells are more likely to be exposed to substrates, possibly speeding up the metabolism. However, the small organoids may still be in their infancy.

4.6.4 Live/dead staining for insight into organoid well being

Six days after the on-line measurement of heroin metabolism, discussed in section 4.6.3, the OiC was taken apart and its contents collected for staining. A live/dead staining kit was used to stain live and dead cells. A brief explanation of the functionality of the live/dead-staining kit is given in **appendix section 7.2.4**.

The stained organoids were then examined in a fluorescence microscope. The microscopy work was carried out by PhD Kulbhushan Sharma. In **figure 53**, three images of organoids are shown.

Ideally, this experiment should have been carried out immediately after the heroin exposure ended so that damages, either through hepatoxicity or through hypoxia due to the lack of oxygenation of medium, would be visible. Unfortunately, the OiC had to be left under perfusion of pure organoid medium for six days until the staining was carried out due to no available microscope. In the meantime, dead cells might have been flushed away, and living cells most likely have died as no oxygenation of media was possible combined with a syringe pump. This problem could easily be addressed using a peristaltic pump where oxygen could be bubbled through a reservoir. Another option would be to suck a few milliliters of air into the syringe in addition to the media. This would have allowed a thorough daily shake of the syringe to dissolve air in the medium.

Surprisingly, many of the organoids that were examined were still mostly alive, indicating that the developed system may work for long-term cultivation as long as a way of oxygenation is added.

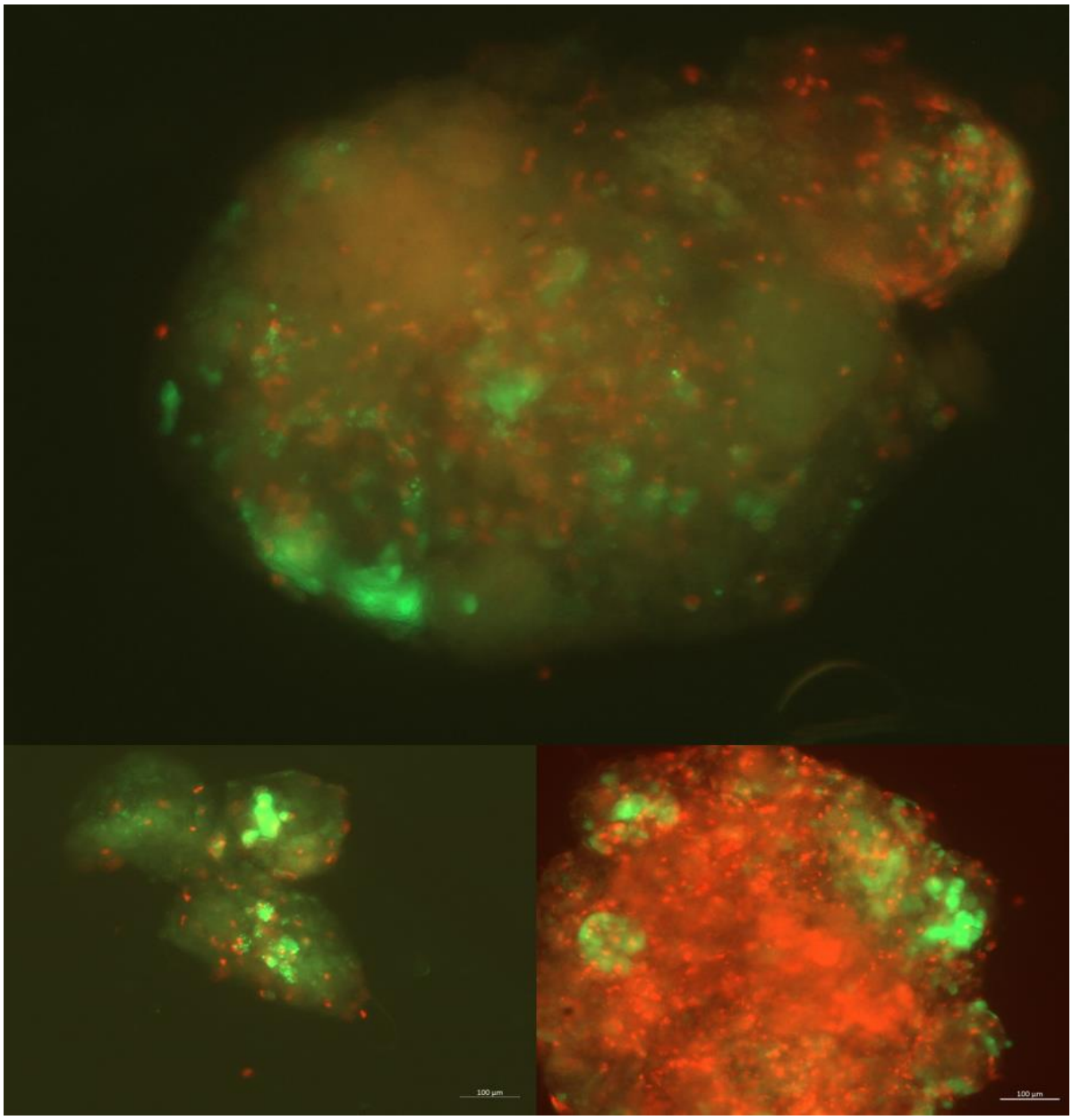

Figure 53 – Fluorescence microscopy image of organoids stained with live dead/kit. Dead cells are stained red. Viable cells are stained green.

5 Concluding remarks

The aim of this study was divided into two parts: First, to make emitter suitable for very narrow ID columns, which can be used to study the metabolism of small organoid populations. Second, to develop an on-line OoC-LC-MS system to prepare the ground for metabolism studies.

ALD-coated fused silica emitters with a coating of SnO_2 for nanoLC-ESI-MS have successfully been developed. Tin oxide has excellent chemical stability and is a long-lasting, robust material. The emitters exhibited slightly lower, but similar, signal to noise ratios as commercially available SS emitters (SS: 48 ± 6, fused silica: 36 ± 3), but have not been tested with sub 30 µm columns for which they are originally intended.

With regard to the on-line OoC-LC-MS system, a fluidic on-line system, similar to traditional 2D-LC systems, has been developed where metabolized medium can be sampled without subjecting the biological material to high pressure. Because the chips that initially were going to be used in this work did not function as intended, an OiC was developed that would house the hepatic organoids. The system was able to show successful phase 1 metabolism of heroin and 6-MAM to morphine, and the system has potential to be downscaled to utilize more narrow ID LC columns in the future.

Since a 1 mm ID column was used for the separation in this study, the developed emitters were not compatible with the rest of the system. Thus, two objectives have been achieved, but were not hyphenated as initially planned. **Figure 54** gives an overview of the conducted work in this study.

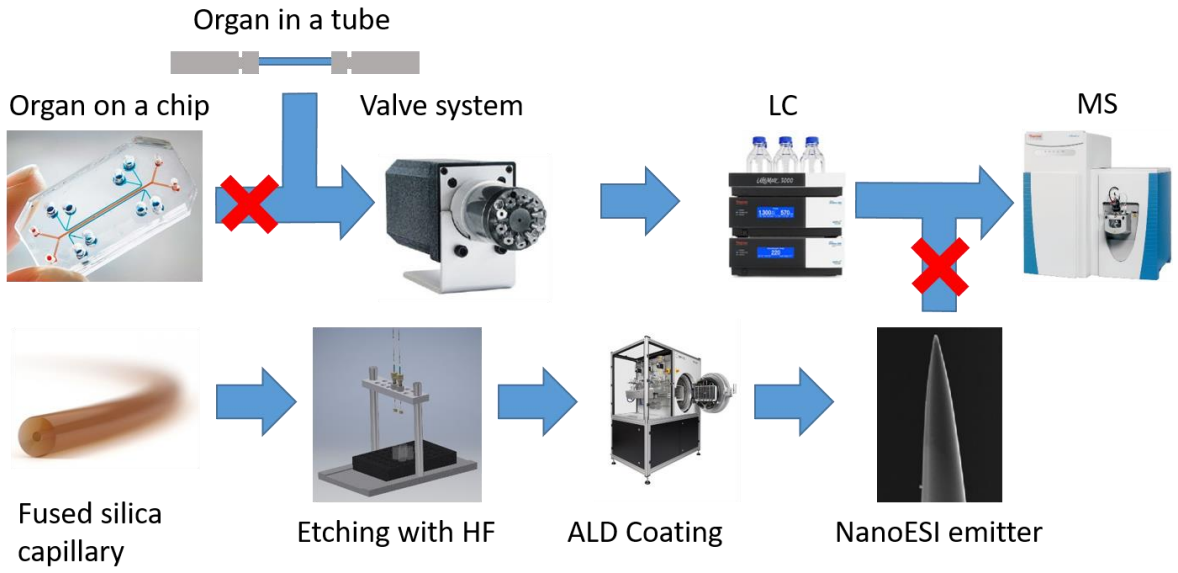

Figure 54 – A final overview of the achievements of this study. New emitters have been manufactured, and an on-line system for OiC has been developed, but these were not hyphenated.

Further work

The reproducibility of deposition on emitters should be tested. Further work to eliminate especially radial gradients in the reactor chamber should be performed. A comparison of commercially available fused silica emitters and SS emitters and in-house fabricated emitters with both gold and tin oxide coating should be conducted. This test should include the use of adequate chromatographic columns, and samples of both proteins and metabolites should be used.

The on-line analysis system for OiC should be further improved by changing the chromatographic column to a longer column with a stronger stationary phase to improve the chromatographic ability. The addition of a size exclusion column and a valve before the chromatographic column could eliminate proteins for metabolomics. An on-line sample preparation step should be added. For instance, the AFFL-system [102] could work as an on-line extraction system that works for many injections. This ensures high throughput.

Various flow rates over the organoids should be examined to achieve the full metabolizing potential of the organoids. A peristaltic pump would allow pump programs and oxygenation of medium. This would be useful, especially for long-term studies of drug exposure or disease modeling.

As soon as more intricate chip designs become available, co-culture of various tissues could give new insights. A first step in this direction would be the addition of islets, insulin-producing organoids. They would hyphenate well with liver organoids, and energy metabolism studies could be conducted. The OiC could also be downscaled by decreasing the ID, but this has to be done in accordance to the selection of organoids for packing, as larger organoids would need a larger ID. The packing of OiC should also be improved by quantifying the number of cells and organoids before packing so that the same amount is packed every time.

6 References

[1] L. Pecorino, *Molecular biology of cancer : mechanisms, targets, and therapeutics*, 4th ed., Oxford University Press (**2016)**

[2] J. McKim, M. James, *Building a tiered approach to in vitro predictive toxicity screening: a focus on assays with in vivo relevance*, Combinatorial Chemistry & High Throughput Screening, 13 **(2010)** 188-206

[3] E.-M. Materne, A.G. Tonevitsky, U. Marx, *Chip-based liver equivalents for toxicity testing–organotypicalness versus cost-efficient high throughput*, Lab on a Chip, 13 **(2013)** 3481-3495

[4] E. Kuntz, H.-D. Kuntz, *Hepatology : Textbook and Atlas*, 3rd ed., Springer Berlin Heidelberg : Imprint: Springer, Berlin, Heidelberg **(2008)**

[5] J.G. Betts, D. Peter, J. Eddie, E.J. Jody, K. Oksana, H.K. Dean, P. Brandon, A.W. James, W. Mark, A.Y. Kelly, Openstax, *Anatomy and Physiology*, 1st ed., Openstax, **(2013)**

[6] J. Sear, *Anatomy and physiology of the liver*, Baillière's Clinical Anaesthesiology, 6 **(1992)** 697-727

[7] M. Rowland, *Influence of route of administration on drug availability*, Journal of Pharmaceutical Sciences, 61 **(1972)** 70-74

[8] S.M. Pond, T.N. Tozer, *First-pass elimination basic concepts and clinical consequences*, Clinical Pharmacokinetics, 9 **(1984)** 1-25

[9] R.G. Harrison, *The outgrowth of the nerve fiber as a mode of protoplasmic movement*, Journal of Experimental Zoology, 9 **(1910)** 787-846

[10] B.M. Baker, C.S. Chen, *Deconstructing the third dimension–how 3D culture microenvironments alter cellular cues*, Journal of Cell Science, 125 **(2012)** 3015-3024

[11] R.L. Ehrmann, G.O. Gey, *The growth of cells on a transparent gel of reconstituted rat-tail collagen*, Journal of the National Cancer Institute, 16 **(1956)** 1375-1403

[12] R. Mroue, M.J. Bissell, *Three-dimensional cultures of mouse mammary epithelial cells*, in: Epithelial Cell Culture Protocols, Springer, (**2012)**, pp. 221-250

[13] T. Sato, H. Clevers, *Growing self-organizing mini-guts from a single intestinal stem cell: mechanism and applications*, Science, 340 **(2013)** 1190-1194

[14] M.A. Lancaster, M. Renner, C.-A. Martin, D. Wenzel, L.S. Bicknell, M.E. Hurles, T. Homfray, J.M. Penninger, A.P. Jackson, J.A. Knoblich, *Cerebral organoids model human brain development and microcephaly*, Nature, 501 **(2013)** 373

[15] D. Huh, G.A. Hamilton, D.E. Ingber, *From 3D cell culture to organs-on-chips*, Trends in Cell Biology, 21 **(2011)** 745-754

[16] D. Ingber, *Mechanobiology and diseases of mechanotransduction*, Annals of Medicine, 35 **(2003)** 564-577

[17] R. Greek, A. Menache, *Systematic reviews of animal models: methodology versus epistemology*, International Journal of Medical Sciences, 10 **(2013)** 206

[18] P. McGonigle, B. Ruggeri, *Animal models of human disease: challenges in enabling translation*, Biochemical Pharmacology, 87 **(2014)** 162-171

[19] M.A. Lancaster, J.A. Knoblich, *Organogenesis in a dish: modeling development and disease using organoid technologies*, Science, 345 **(2014)** 1247125

[20] P. Weiss, A. Taylor, *Reconstitution of complete organs from single-cell suspensions of chick embryos in advanced stages of differentiation*, Proceedings of the National Academy of Sciences of the United States of America, 46 **(1960)** 1177

[21] S.H. Au, M.D. Chamberlain, S. Mahesh, M.V. Sefton, A.R. Wheeler, *Hepatic organoids for microfluidic drug screening*, Lab on a Chip, 14 **(2014)** 3290-3299

[22] T. Takebe, K. Sekine, M. Enomura, H. Koike, M. Kimura, T. Ogaeri, R.-R. Zhang, Y. Ueno, Y.-W. Zheng, N. Koike, *Vascularized and functional human liver from an iPSC-derived organ bud transplant*, Nature, 499 **(2013)** 481

[23] M.D. Binder, N. Hirokawa, U. Windhorst, *Encyclopedia of Neuroscience*, 1st ed., Springer Berlin Heidelberg : Imprint: Springer, Berlin, Heidelberg,**(2009)**
[24] K. Takahashi, S. Yamanaka, *Induction of pluripotent stem cells from mouse embryonic and adult fibroblast cultures by defined factors*, Cell, 126 **(2006)** 663-676
[25] K. Takahashi, K. Tanabe, M. Ohnuki, M. Narita, T. Ichisaka, K. Tomoda, S. Yamanaka, *Induction of pluripotent stem cells from adult human fibroblasts by defined factors*, Cell, 131 **(2007)** 861-872
[26] A. Abbott, *Cell rewind wins medicine nobel*, Nature News, 490 **(2018)** 151
[27] D. Huh, B.D. Matthews, A. Mammoto, M. Montoya-Zavala, H.Y. Hsin, D.E. Ingber, *Reconstituting organ-level lung functions on a chip*, Science, 328 **(2010)** 1662-1668
[28] L. Griep, F. Wolbers, B. De Wagenaar, P.M. ter Braak, B. Weksler, I.A. Romero, P. Couraud, I. Vermes, A.D. van der Meer, A. van den Berg, *BBB on chip: microfluidic platform to mechanically and biochemically modulate blood-brain barrier function*, Biomedical Microdevices, 15 **(2013)** 145-150
[29] M. Kasendra, A. Tovaglieri, A. Sontheimer-Phelps, S. Jalili-Firoozinezhad, A. Bein, A. Chalkiadaki, W. Scholl, C. Zhang, H. Rickner, C.A. Richmond, *Development of a primary human small intestine-on-a-chip using biopsy-derived organoids*, Scientific Reports, 8 **(2018)** 2871
[30] A. Grosberg, A.P. Nesmith, J.A. Goss, M.D. Brigham, M.L. McCain, K.K. Parker, *Muscle on a chip: in vitro contractility assays for smooth and striated muscle*, Journal of Pharmacological and Toxicological Methods, 65 **(2012)** 126-135
[31] I. Wagner, E.-M. Materne, S. Brincker, U. Süßbier, C. Frädrich, M. Busek, F. Sonntag, D.A. Sakharov, E.V. Trushkin, A.G. Tonevitsky, *A dynamic multi-organ-chip for long-term cultivation and substance testing proven by 3D human liver and skin tissue co-culture*, Lab on a Chip, 13 **(2013)** 3538-3547
[32] Bernard Meyerson, Mariette DiChristina, Noubar Afeyan, Nayef Al-Rodhan, Jeffrey Carbeck, George Chen Guodiang, Liam Condon, Lee Sang Yup, Geoffrey Ling, Henry Markram, Kiyoshi Matsuda, Andrew D. Maynard, Apruv Mishra, Robert Pepper, Francoise Roure, L. Takayama, *Top 10 Emerging Technologies of 2016*, (**2016)**
[33] A. Skardal, T. Shupe, A. Atala, *Organoid-on-a-chip and body-on-a-chip systems for drug screening and disease modeling*, Drug Discovery Today, 21 **(2016)** 1399-1411
[34] R.T. Kelly, Y. Zhu, *Ultrasmall sample biochemical analysis*, Analytical and Bioanalytical Chemistry, 411 **(2019)**
[35] X. Li, T. Tian, *Recent advances in an organ-on-a-chip: biomarker analysis and applications*, Anlytical Methods, 10 **(2018)** 3122-3130
[36] J. Dang, S.K. Tiwari, G. Lichinchi, Y. Qin, V.S. Patil, A.M. Eroshkin, T.M. Rana, *Zika virus depletes neural progenitors in human cerebral organoids through activation of the innate immune receptor TLR3*, Cell Stem Cell, 19 **(2016)** 258-265
[37] Y.G. Zhang, S. Wu, Y. Xia, J. Sun, *Salmonella-infected crypt-derived intestinal organoid culture system for host–bacterial interactions*, Physiological Reports, 2 **(2014)**
[38] J.F. Dekkers, C.L. Wiegerinck, H.R. De Jonge, I. Bronsveld, H.M. Janssens, K.M. De Winter-de Groot, A.M. Brandsma, N.W. De Jong, M.J. Bijvelds, B.J. Scholte, *A functional CFTR assay using primary cystic fibrosis intestinal organoids*, Nature Medicine, 19 **(2013)** 939
[39] G. Schwank, A. Andersson-Rolf, B.-K. Koo, N. Sasaki, H. Clevers, *Generation of BAC transgenic epithelial organoids*, PLOS ONE, 8 **(2013)** e76871
[40] Y. Li, J. Muffat, A. Omer, I. Bosch, M.A. Lancaster, M. Sur, L. Gehrke, J.A. Knoblich, R. Jaenisch, *Induction of expansion and folding in human cerebral organoids*, Cell Stem Cell, 20 **(2017)** 385-396. e383
[41] M.C. Poznansky, R.H. Evans, R.B. Foxall, I.T. Olszak, A.H. Piascik, K.E. Hartman, C. Brander, T.H. Meyer, M.J. Pykett, K.T. Chabner, *Efficient generation of human T cells from a tissue-engineered thymic organoid*, Nature Biotechnology, 18 **(2000)** 729
[42] A.A. Akhtar, S. Sances, R. Barrett, J.J. Breunig, *Organoid and organ-on-a-chip systems: new paradigms for modeling neurological and gastrointestinal disease*, Current Stem Cell Reports, 3 **(2017)** 98-111

[43] S.F. Boj, C.-I. Hwang, L.A. Baker, I.I.C. Chio, D.D. Engle, V. Corbo, M. Jager, M. Ponz-Sarvise, H. Tiriac, M.S. Spector, *Organoid models of human and mouse ductal pancreatic cancer*, Cell, 160 **(2015)** 324-338
[44] C. Dorrell, B. Tarlow, Y. Wang, P.S. Canaday, A. Haft, J. Schug, P.R. Streeter, M.J. Finegold, L.T. Shenje, K.H. Kaestner, *The organoid-initiating cells in mouse pancreas and liver are phenotypically and functionally similar*, Stem Cell Research, 13 **(2014)** 275-283
[45] B.J. Tauro, D.W. Greening, R.A. Mathias, S. Mathivanan, H. Ji, R.J. Simpson, *Two distinct populations of exosomes are released from LIM1863 colon carcinoma cell-derived organoids*, Molecular & Cellular Proteomics, 12 **(2013)** 587-598
[46] P.M. van Midwoud, J. Janssen, M.T. Merema, I.A. de Graaf, G.M. Groothuis, E. Verpoorte, *On-line HPLC analysis system for metabolism and inhibition studies in precision-cut liver slices*, Analytical Chemistry, 83 **(2010)** 84-91
[47] M. Rogeberg, H. Malerod, H. Roberg-Larsen, C. Aass, S.R. Wilson, *On-line solid phase extraction–liquid chromatography, with emphasis on modern bioanalysis and miniaturized systems*, Journal of Pharmaceutical and Biomedical Analysis, 87 **(2014)** 120-129
[48] K.O. Svendsen, H.R. Larsen, S.A. Pedersen, I. Brenna, E. Lundanes, S.R. Wilson, *Automatic filtration and filter flush for robust online solid-phase extraction liquid chromatography*, Journal of Separation Science, 34 **(2011)** 3020-3022
[49] E. Lundanes, L. Reubsaet, T. Greibrokk, *Chromatography : basic principles, sample preparations and related methods*, Wiley-VCH, (**2014)**
[50] B. Domon, R. Aebersold, *Mass spectrometry and protein analysis*, Science, 312 **(2006)** 212-217
[51] G.L. Glish, D.J. Burinsky, *Hybrid mass spectrometers for tandem mass spectrometry*, Journal of the American Society for Mass Spectrometry, 19 **(2008)** 161-172
[52] A. Michalski, E. Damoc, J.-P. Hauschild, O. Lange, A. Wieghaus, A. Makarov, N. Nagaraj, J. Cox, M. Mann, S. Horning, *Mass spectrometry-based proteomics using Q Exactive, a high-performance benchtop quadrupole Orbitrap mass spectrometer*, Molecular & Cellular Proteomics, 10 **(2011)** M111. 011015
[53] K.K. Murray, R.K. Boyd, M.N. Eberlin, G.J. Langley, L. Li, Y. Naito, *Definitions of terms relating to mass spectrometry (IUPAC Recommendations 2013)*, Pure and Applied Chemistry, 85 **(2013)** 1515-1609
[54] K.K. Murray, *The term" multiple reaction monitoring" is recommended*, Rapid Communications in Mass Spectrometry, 29 **(2015)** 1926-1928
[55] K. Dettmer, P.A. Aronov, B.D. Hammock, *Mass spectrometry-based metabolomics*, Mass Spectrometry Reviews, 26 **(2007)** 51-78
[56] Y. Saito, K. Jinno, T. Greibrokk, *Capillary columns in liquid chromatography: between conventional columns and microchips*, Journal of Separation Science, 27 **(2004)** 1379-1390
[57] S.R. Wilson, T. Vehus, H.S. Berg, E. Lundanes, *Nano-LC in proteomics: recent advances and approaches*, Bioanalysis, 7 **(2015)** 1799-1815
[58] J. Vial, A. Jardy, *Experimental comparison of the different approaches to estimate LOD and LOQ of an HPLC method*, Analytical Chemistry, 71 **(1999)** 2672-2677
[59] D.C. Harris, C.A. Lucy, *Quantitative chemical analysis*, 9th ed., Freeman, (**2016)**
[60] X. Wang, L. Liu, Q. Pu, Z. Zhu, G. Guo, H. Zhong, S. Liu, *Pressure-induced transport of DNA confined in narrow capillary channels*, Journal of the American Chemical Society, 134 **(2012)** 7400-7405
[61] P. Feist, A.B. Hummon, *Proteomic challenges: sample preparation techniques for microgram-quantity protein analysis from biological samples*, International journal of molecular sciences, 16 **(2015)** 3537-3563
[62] R. Li, Y. Shao, Y. Yu, X. Wang, G. Guo, *Pico-HPLC system integrating an equal inner diameter femtopipette into a 900 nm ID porous layer open tubular column*, Chemical Communications, 53 **(2017)** 4104-4107

[63] M. Rogeberg, S.R. Wilson, T. Greibrokk, E. Lundanes, *Separation of intact proteins on porous layer open tubular (PLOT) columns*, Journal of Chromatography A, 1217 **(2010)** 2782-2786
[64] G. Hopfgartner, K. Bean, J. Henion, R. Henry, *Ion spray mass spectrometric detection for liquid chromatography: A concentration-or a mass-flow-sensitive device?*, Journal of Chromatography A, 647 **(1993)** 51-61
[65] S.C. Gad, *Handbook of pharmaceutical biotechnology*, John Wiley & Sons, (**2007)**
[66] A. Prüß, C. Kempter, J. Gysler, T. Jira, *Extracolumn band broadening in capillary liquid chromatography*, Journal of Chromatography A, 1016 **(2003)** 129-141
[67] A. El-Aneed, A. Cohen, J. Banoub, *Mass spectrometry, review of the basics: electrospray, MALDI, and commonly used mass analyzers*, Applied Spectroscopy Reviews, 44 **(2009)** 210-230
[68] R.B. Cole, *Electrospray ionization mass spectrometry : fundamentals, instrumentation, and applications*, Wiley, (**1997)**
[69] K.-Y. Li, H. Tu, A.K. Ray, *Charge limits on droplets during evaporation*, Langmuir, 21 **(2005)** 3786-3794
[70] P. Kebarle, U.H. Verkerk, *Electrospray: from ions in solution to ions in the gas phase, what we know now*, Mass Spectrometry Reviews, 28 **(2009)** 898-917
[71] *Thermo Scientific SS Emitters*, **19.09.2019**
[72] *SilicaTip™ Emitter Specifications*, http://www.newobjective.com/products/emitters/fs-2.shtml, **11.09.2019**
[73] *TaperTip™ Emitter Specifications*, http://www.newobjective.com/products/emitters/tt-2.shtml#MT, **11.09.2019**
[74] G.T. Gibson, S.M. Mugo, R.D. Oleschuk, *Nanoelectrospray emitters: trends and perspective*, Mass Spectrometry Reviews, 28 **(2009)** 918-936
[75] S. Kogler, *Evaluation of methods for etching and coating of nanoelctrospray emitters*, **(2017)**, Thesis, Unpublished
[76] X. Zhu, Y. Liang, Y. Weng, Y. Chen, H. Jiang, L. Zhang, Z. Liang, Y. Zhang, *Gold-coated nanoelectrospray emitters fabricated by gravity-assisted etching self-termination and electroless deposition*, Analytical Chemistry, 88 **(2016)** 11347-11351
[77] K.G. Arnesen, *Preparation of electrical conductive etched open emitters for nano electrospray ionization mass spectrometry*, **(2015)**, Thesis, Unpublished
[78] J. Aigueperse, P. Mollard, D. Devilliers, M. Chemla, R. Faron, R. Romano, J.P. Cuer, *Fluorine compounds, inorganic*, Ullmann's Encyclopedia of Industrial Chemistry, **(2005)**
[79] K. Selte, *Lærebok i Uorganisk Kjemi*, Tanum-Norli, Oslo, (**1982)**, pp. 121
[80] P. Kofstad, *Uorganisk kjemi : en innføring i grunnstoffenes kjemi*, TANO, Oslo, (**1992)**, pp. 204
[81] R.T. Kelly, J.S. Page, Q. Luo, R.J. Moore, D.J. Orton, K. Tang, R.D. Smith, *Chemically etched open tubular and monolithic emitters for nanoelectrospray ionization mass spectrometry*, Analytical Chemistry, 78 **(2006)** 7796-7801
[82] U. Schubert, N. Hüsing, *Synthesis of inorganic materials*, 3rd ed., Wiley, (**2012)**
[83] Y. Furubayashi, T. Hitosugi, Y. Yamamoto, K. Inaba, G. Kinoda, Y. Hirose, T. Shimada, T. Hasegawa, *A transparent metal: Nb-doped anatase TiO2*, Applied Physics Letters, 86 **(2005)** 252101
[84] J.-P. Niemelä, H. Yamauchi, M. Karppinen, *Conducting Nb-doped TiO2 thin films fabricated with an atomic layer deposition technique*, Thin Solid Films, 551 **(2014)** 19-22
[85] V. Pore, M. Ritala, M. Leskelä, T. Saukkonen, M. Järn, *Explosive crystallization in atomic layer deposited mixed titanium oxides*, Crystal Growth and Design, 9 **(2009)** 2974-2978
[86] R.G. Gordon, *Criteria for choosing transparent conductors*, MRS bulletin, 25 **(2000)** 52-57
[87] T. Minami, *Transparent conducting oxide semiconductors for transparent electrodes*, Semiconductor Science and Technology, 20 **(2005)** S35
[88] D. Nazarov, N. Bobrysheva, O. Osmolovskaya, M. Osmolovsky, V. Smirnov, *Atomic layer deposition of tin dioxide nanofilms: A review*, Reviews on Advanced Materials Science, 40 **(2015)** 262-275

[89] H.-E. Cheng, D.-C. Tian, K.-C. Huang, *Properties of SnO2 Films Grown by Atomic Layer Deposition*, Procedia Engineering, 36 **(2012)** 510-515
[90] C. Lu, A.W. Czanderna, *Applications of piezoelectric quartz crystal microbalances*, Elsevier, Amsterdam/New York, **(1984)**
[91] G. Sauerbrey, *Verwendung von Schwingquarzen zur Wägung dünner Schichten und zur Mikrowägung*, Zeitschrift für Physik, 155 **(1959)** 206-222
[92] U. Boerner, S. Abbott, R.L. Roe, *The metabolism of morphine and heroin in man*, Drug Metabolism Reviews, 4 **(1975)** 39-73
[93] E.J. Rook, A.D. Huitema, J.M.v. Ree, J.H. Beijnen, *Pharmacokinetics and pharmacokinetic variability of heroin and its metabolites: review of the literature*, Current Clinical Pharmacology, 1 **(2006)** 109-118
[94] L.M. Kamendulis, M.R. Brzezinski, E.V. Pindel, W.F. Bosron, R.A. Dean, *Metabolism of cocaine and heroin is catalyzed by the same human liver carboxylesterases*, Journal of Pharmacology and Experimental Therapeutics, 279 **(1996)** 713-717
[95] D.A. Barrett, A.L. Dyssegaard, P.N. Shaw, *The effect of temperature and pH on the deacetylation of diamorphine in aqueous solution and in human plasma*, Journal of Pharmacy and Pharmacology, 44 **(1992)** 606-608
[96] S. De Gregori, M. De Gregori, G.N. Ranzani, M. Allegri, C. Minella, M. Regazzi, *Morphine metabolism, transport and brain disposition*, Metabolic Brain Disease, 27 **(2012)** 1-5
[97] S. Mathapati, R. Siller, A.A. Impellizzeri, M. Lycke, K. Vegheim, R. Almaas, G.J. Sullivan, *Small-molecule-directed hepatocyte-like cell differentiation of human pluripotent stem cells*, Current Protocols in Stem Cell Biology, 38 **(2016)** 1G. 6.1-1G. 6.18
[98] *Chuck*, https://en.wikipedia.org/wiki/Chuck_(engineering), **19.09.2018**
[99] F.A. Jenkins, H.E. White, *Fundamentals of optics*, 4th ed., McGraw-Hill Higher Education, (**1976)**
[100] C.P. Desilets, M.A. Rounds, F.E. Regnier, *Semipermeable-surface reversed-phase media for high-performance liquid chromatography*, Journal of Chromatography A, 544 **(1991)** 25-39
[101] I.H. Hagestam, T.C. Pinkerton, *Internal surface reversed-phase silica supports for liquid chromatography*, Analytical Chemistry, 57 **(1985)** 1757-1763
[102] E. Johnsen, S. Leknes, S.R. Wilson, E. Lundanes, *Liquid chromatography-mass spectrometry platform for both small neurotransmitters and neuropeptides in blood, with automatic and robust solid phase extraction*, Scientific Reports, 5 **(2015)** 9308
[103] *Live/Dead Cell Double Staining Kit*, https://www.sigmaaldrich.com/catalog/product/sigma/04511?lang=en&region=NO&gclid=EAIaIQobChMInrzztJiP5QIVU6qaCh00fAMNEAAYASAAEgIylfD_BwE, **09.10.2019**

7 Appendix

7.1 Experimental conditions

7.1.1 Deposition on the Beneq TSF500-reactor

The different parameters used for deposition on substrates are shown in **Appendix Table 1 and 2**.

Appendix Table 1 - Deposition parameters for deposition of Nb2O5, TiO2 and Ti-NB-O on substrates.

Deposition number	Material	Repeats	Nb-source temperat-ure, °C	$Nb(OEt)_5$, s	Purge, s	$TiCl_4$, s	Purge, s	Line-purge, s	Purge, s
2018041001	Nb_2O_5	750	110	4	1			0.25	3
2018041601	Ti-Nb-O	250	105			0.5	2	0.5	3
2018041601	Ti-Nb-O	250	105			0.5	2	0.5	3
2018041601	Ti-Nb-O	250	105	4	1			0.25	3
2018041601	Ti-Nb-O	250	105			0.5	2	0.5	3
2018041601	Ti-Nb-O	250	105			0.5	2	0.5	3
2018041601	Ti-Nb-O	250	105	4	1			0.25	3
2018041601	Ti-Nb-O	250	105			0.5	2	0.5	3
2018052901	TiO_2	750				0.5	2	0.5	3

Appendix table 2 - Deposition parameters for deposition of SnO_2 on substrates.

Deposition number	Material	Cycles	$SnCl_4$, s	Purge	H_2O, s	Line purge, s	Purge, s
2018060401	SnO_2	750	0.5	2	2	0.5	3

Growth rates of TiO_2 are shown as functions of purging times of water in **Appendix Figures 1 and 2**, while **Appendix Figure 3** shows growth rates of TiO_2 as a function of purge times after $TiCl_4$-pulse.

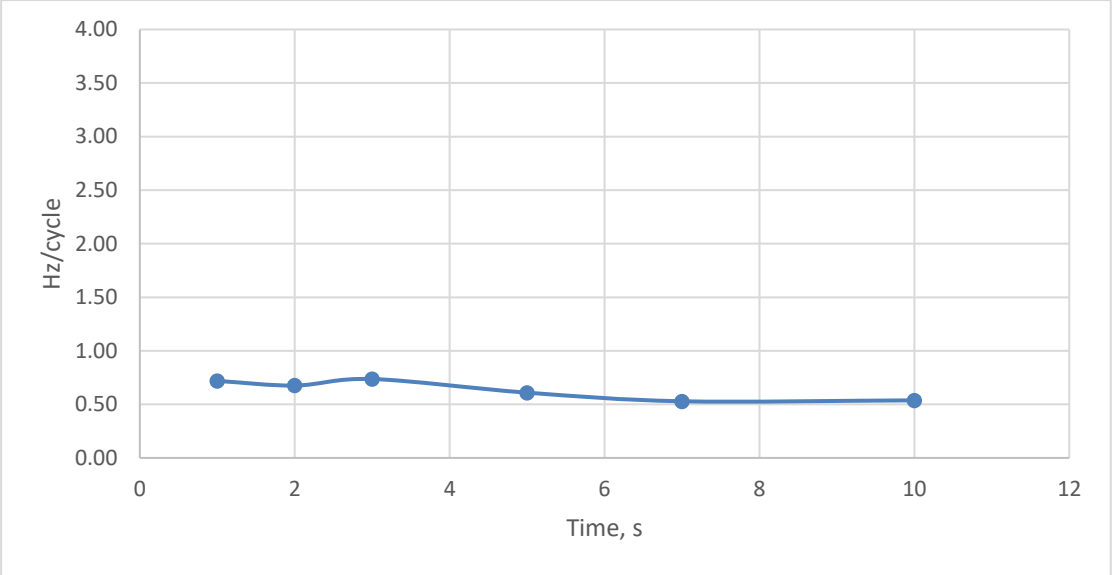

Appendix Figure 1 – Growth rate shown as a function of purge time after H2O-pulse

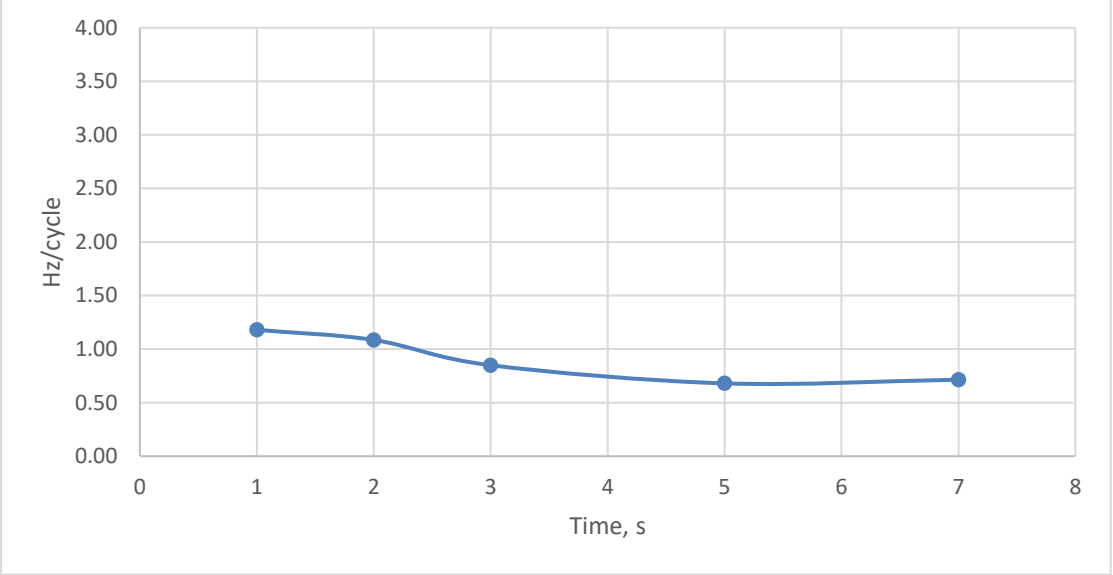

Appendix Figure 2 – Growth rate shown as a function of purge time after H2O-pulse

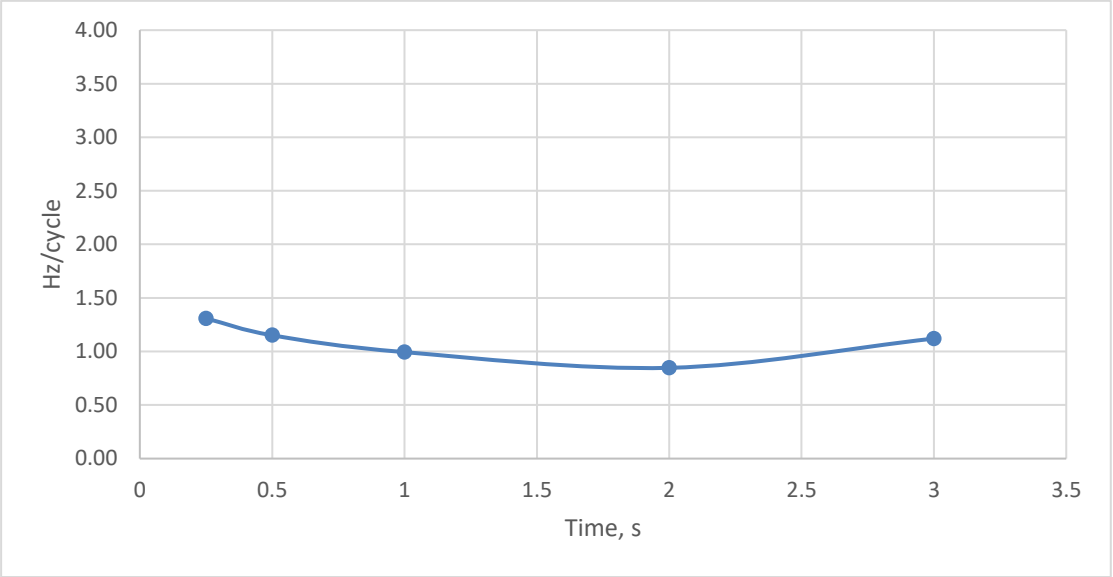

Appendix Figure 3 – Growth rate shown as a function of purge time after TiCl4-pulse

As different parameters were examined, significant growth rates of TiO_2 were observed even when water pulses went towards zero. These findings can be seen in **Appendix Figures 4-6**.

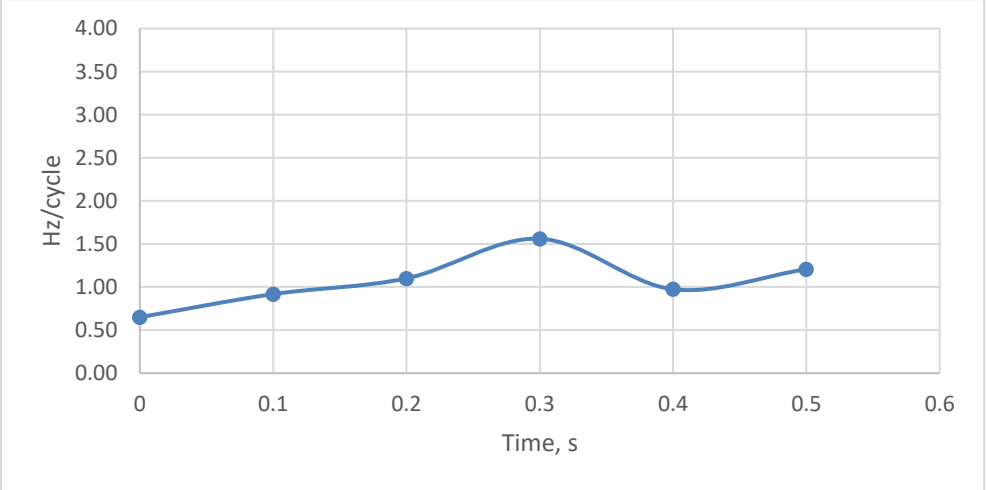

Appendix Figure 4 – Growth rate shown as a function of water pulse without line purge

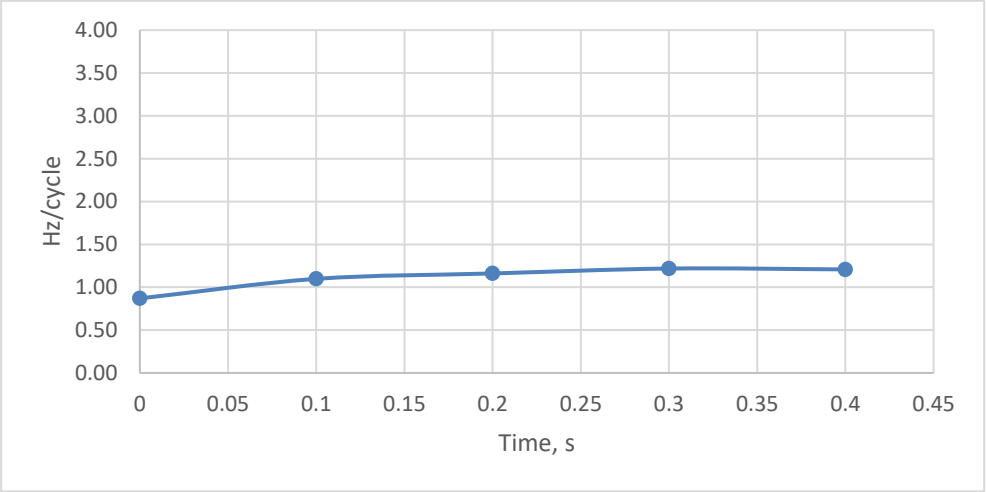

Appendix Figure 5 – Growth rate shown as a function of water pulse with 5-second purge

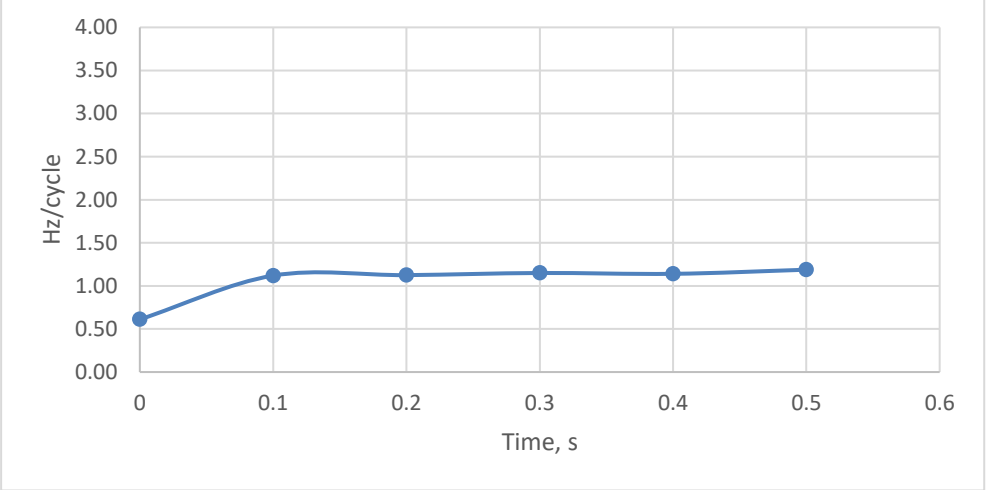

Appendix Figure 6 – Growth rate shown as a function of water pulse with 3-second purge.

7.1.2 Deposition on the in-house built ALD reactor

Deposition numbers and all parameters concerning the deposition of Al_2O_3 are shown in **appendix table 3**.

Appendix table 3 - Parameters for deposition of Al_2O_3.

Deposition number	˚C	In-line flow, SCCM	Flow around, SCCM	Cycles	TMA pulse	Line Purge	Purge	H_2O pulse	Line purge	Purge	Film F, nm	Film C, nm	Film B, nm
2018090701	200	150	50	300	300	500	2000	300	500	2000	65.57	29.30	15.95
2018090702	200	150	150	300	300	500	2000	300	500	2000	21.82	6.07	3.75
2018091101*	200	150	150	300	300	500	2000	300	500	2000	21.00	13.38	4.67
2018091201	200	150	150	300	600	500	2000	300	500	2000	76.22	33.39	5.58

* new vacuum pump

Deposition parameters, including deposition numbers, for deposition of SnO_2, are shown in **appendix table 4**.

Appendix table 4 - Deposition parameters for deposition of SnO_2.

Deposition number	˚C	In-line flow, SCCM	flow around, SCCM	Valve opening	Cycles	$SnCl_4$ pulse	Line purge	Purge	H_2O pulse	Line purge	Purge	Film F, nm	Film C, nm	Film B, nm
2018092001	400	150	150	1 round	300	600	500	2000	300	500	2000	8.47	3.35	1.22
2018092501	400	150	150	1 round	300	600	500	2000	300	500	2000	9.29	2.88	1.63
2018092601	400	150	150	1 round	300	1000	500	2000	300	500	2000	5.87	1.87	1.88
2018092701	400	150	150	1 round	300	2000	500	2000	2000	500	2000	24.70	14.60	1.80
2018101801	400	150	150	2 rounds	300	500	500	2000	2000	500	2000	42.45	12.72	2.30
2018101201	400	300	150	2 rounds	300	500	500	2000	2000	500	2000	15.08	16.41	2.26
2018101202	400	150	300	2 rounds	300	500	500	2000	2000	500	2000	13.47	12.44	2.20

7.2 Supplementary results and discussion

7.2.1 In depth description of optimization of tin dioxide deposition

To begin with growth rates of only 0.3 nm/cycle were obtained (2018092001 and 2018092501). Growth rates on the middle and back substrate were even lower. It was clear that more $SnCl_4$ was needed for satisfactory growth rates. It was believed that the pulsing time was insufficient, but increasing it to 1000 ms (2018092601) and then 2000 ms (2018092701), resulting in growth rates/cycle of only 0.02 and 0.08 nm/cycle, respectively. The low growth rates obtained, were likely due to to little access to the Sn-precursor.

In the subsequent deposition, the needle valve was opened two full rounds, and the Sn-precursor pulse was decreased to 500 ms (2018101801). This resulted in growth rates of 0.14 nm/cycle on the front substrate, but only 0.04 nm/cycle on the middle one. To push the pulsed precursors further into the chamber gas flows were increased.

First, the flow over the lines was doubled to 300 SCCM, while the flow around was left at 150 SCCM (2018101201). Then, the opposite was tried, setting the flow over the lines at 150 SCCM and the flow around at 300 SCCM (2018101202). These experiments yielded growth

rates/cycle of 0.05 nm and 0.05 nm for the first test (increased flow over lines), and 0.04 nm and 0.04 nm on the second test (increased flow around the chamber). Most notably, growth rates on the front and center substrate were equal, showing a larger area where the growth was the largest, optimal for deposition on emitters. Because of the 20% difference in growth rate, increasing the flow over the lines was chosen for deposition on emitters.

7.2.2 Emitter testing

TIC of two emitters tested with 5% MP B at 300 nL/min with 3 kV are shown in **appendix figure 7**. Emitters were placed in the middle (M) and bottom middle (BM) in the deposition stand.

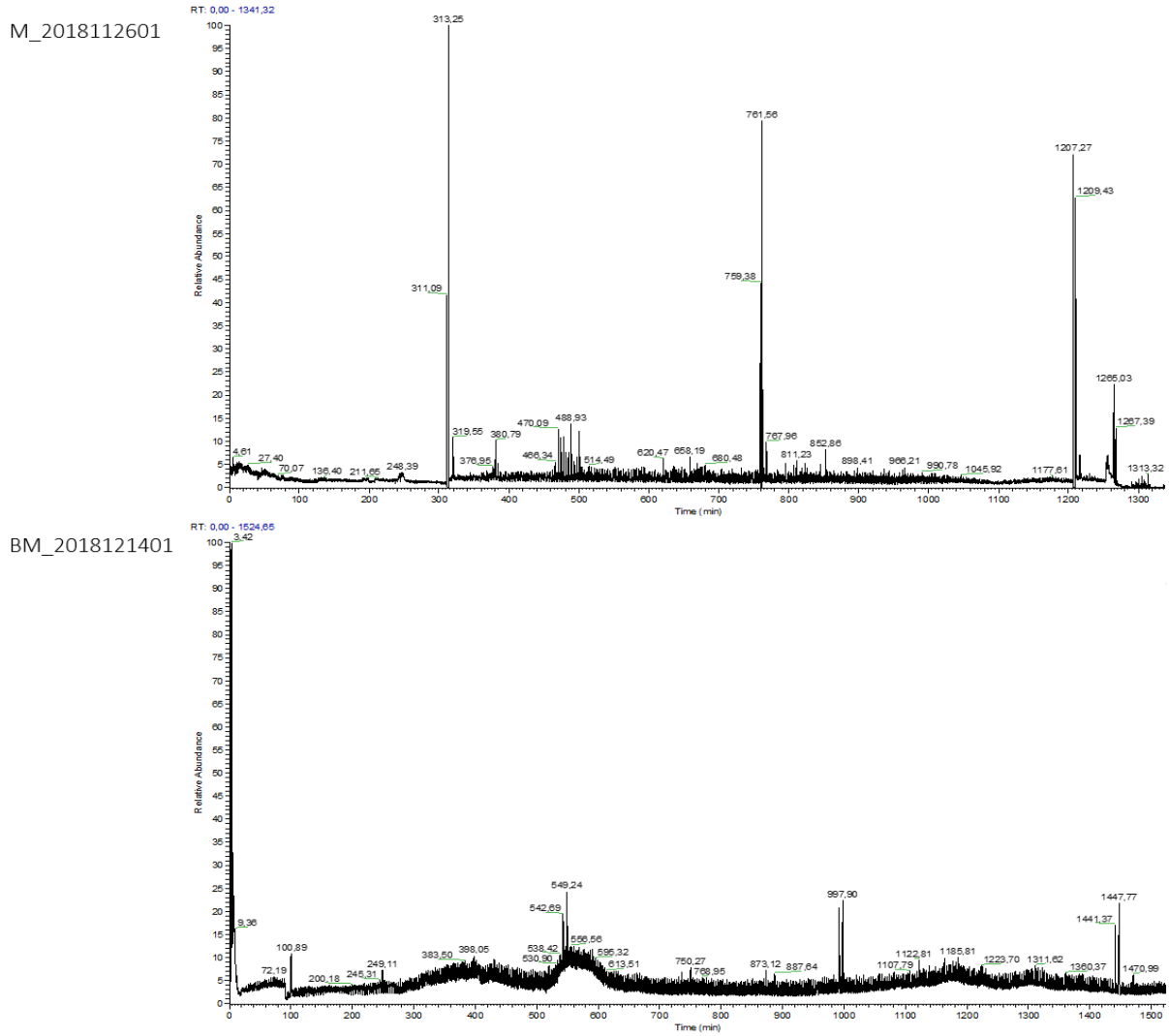

Appendix figure 7 - Top: Emitter coated in the middle of the deposition stand, showing stable spray for 1300 min. Bottom: Emitter coated in the bottom middle of the deposition stand, showing stable spray for 1500 min. Spikes in the TIC are due to the pump stopping to refill the syringe.

In **appendix table 5**, raw data measured in the chromatograms and calculations for signal to noise ratio is shown.

Appendix table 5 – Signal and noise raw-data including calculations made to determine the signal to noise ration.

Stainless Steel									
Noise before peak			**Noise after peak**			**Calculations**			
min	**max**	**AVG**	**min**	**max**	**AVG**	**AVG noise**	**Signal**	**Signal-AVG noise**	**Signal to noise ratio**
0	7	3.5	3	8	5.5	4.5	186	181.5	40.33
0	4.2	2.1	7.4	1.3	4.35	3.225	163	159.775	49.54
0	2.5	1.25	0.5	10	5.25	3.25	177	173.75	53.46
								AVG	47.78
Fused Silica									
Noise before peak			**Noise after peak**			**Calculations**			
min	**max**	**AVG**	**min**	**max**	**AVG**	**AVG noise**	**Signal**	**Signal-AVG noise**	**Signal to noise ratio**
13	26	19.5	23	36	29.5	24.5	817	792.5	32.35
13	27	20	20	35	27.5	23.75	934	910.25	38.33
13	25	19	19	35	27	23	903	880	38.26
								AVG	36.31

7.2.3 LC-UV

A chromatogram of 18 µM heroin, 6-MAM, M3G and M6G is shown in **appendix figure 8**. The solution was injected on the chip-LC-UV system shown in **figure 27**.

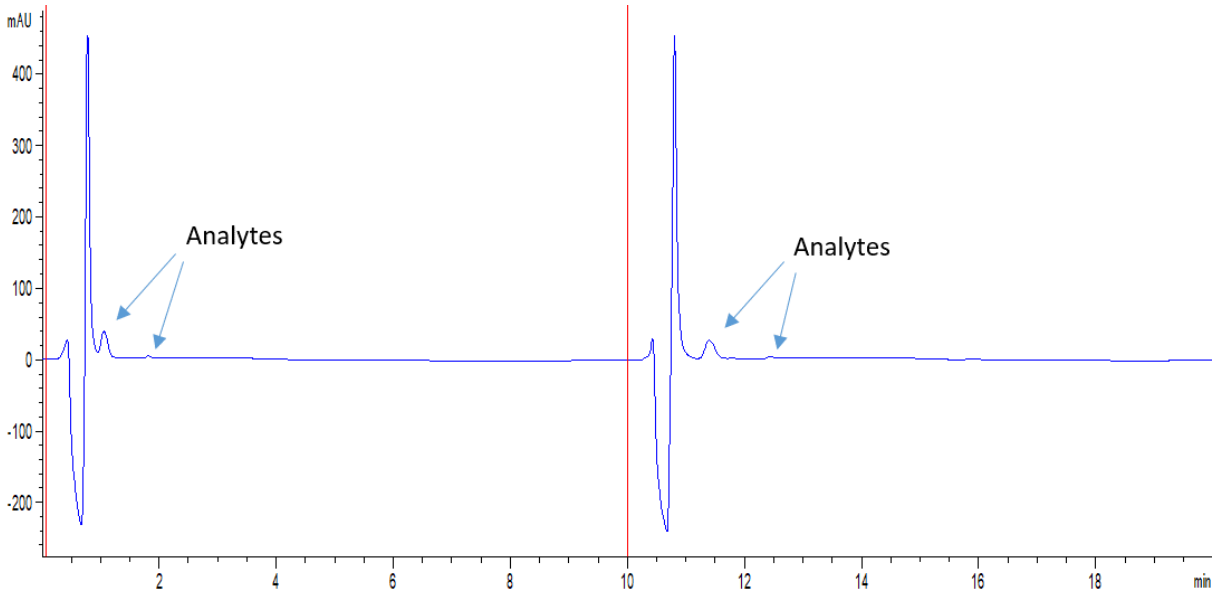

Appendix figure 8 – Chromatograms of 2 injections of 18 µM heroin, 6-MAM, M3G, and M6G. The wavelength on the UV-detector was only optimized for heroin is likely the reason why only two peaks show up. Another reason might be co-elution. The second peak is incredibly low, indicating that multiple wavelengths should have been used. The red lines indicate injection.

7.2.4 Live/dead staining

Calcein acetoxymethyl (Calcein-AM) was used for staining live cells, as the molecule quickly permeates the cell membrane. After metabolism to calcein through esterases in viable cells, the calcein emits strong green fluorescence. In this way, only cells that are alive are stained. Propidium iodide (PI) is used for staining dead cells red. The molecule cannot permeate cell membranes, but passes through broken membranes of dead cells and binds to the nuclei and emits red fluorescence. Through this mechanism only dead cells are stained [103].